INFORMATION TO USERS

This manuscript has been reproduced from the microfilm master. UMI films the text directly from the original or copy submitted. Thus, some thesis and dissertation copies are in typewriter face, while others may be from any type of computer printer.

The quality of this reproduction is dependent upon the quality of the copy submitted. Broken or indistinct print, colored or poor quality illustrations and photographs, print bleedthrough, substandard margins, and improper alignment can adversely affect reproduction.

In the unlikely event that the author did not send UMI a complete manuscript and there are missing pages, these will be noted. Also, if unauthorized copyright material had to be removed, a note will indicate the deletion.

Oversize materials (e.g., maps, drawings, charts) are reproduced by sectioning the original, beginning at the upper left-hand corner and continuing from left to right in equal sections with small overlaps.

ProQuest Information and Learning
300 North Zeeb Road, Ann Arbor, MI 48106-1346 USA
800-521-0600

Université d'Ottawa • University of Ottawa

Abstract

Although highly varied, all of the work in this thesis involves studying acid in photolithographically relevant systems. The objectives of the individual projects never stray far from the central goal of acquiring mechanistic insight into both the photoacid generation process as well as acid mobility in polymer films. It is the ultimate goal of this work to gain a fundamental understanding of chemical processes and reaction mechanisms, in order to apply this knowledge to the evaluation and design of materials for use in photolithography.

Techniques for quantifying and locating photogenerated acid in solution and in polymer films were both developed and extensively employed. These techniques are based on the protonation of acid-sensitive dyes and were used for the purposes of studying acid diffusion as well as evaluating photoacid generating efficiencies of photoacid generators (PAGs).

A novel technique for monitoring acid desorption from polymer films was developed in order to study the behaviour of acid in polymer films under processing conditions similar to those employed industrially. The kinetics for acid desorption were measured and the factors which control acid mobility were identified.

Much of the work presented in this thesis is focused on determining the mechanisms by which PAGs generate acid as well as designing and testing new molecules for use as PAGs. Among the molecules studied in these contexts were sulfones, N-heteroaromatic salts and sulfonium salts tethered to ketones. The key steps towards photoacid generation for these molecules include homolytic bond cleavage, photoinduced electron transfer and triplet energy transfer, respectively.

Acknowledgments

To thank my supervisor, Tito Scaiano, for giving me the opportunity to work in his lab and for useful discussions, while certainly appropriate, barely scratches the surface of what I am really indebted to him for. Tito showed me, intentionally or not, that a successful researcher must be equal parts scientist and used-car salesman. His generosity, both of spirit and with his research grants are, in my experience, unique qualities for a supervisor. I have long since thought that I would not have been as successful and as happy with any other supervisor; the more I hear about other students experiences and the more I interact with Tito, the more this idea is reinforced.

Other than Tito, the only two people who have had to deal with high doses of me for the entire time I have been in Ottawa are Gonzalo Cosa and Anne Vinette. Gonzalo's work habits and progress have always served as a benchmark for my own and I greatly appreciate the influence he has had on me. More than anyone else, Anne has made my time in the group and in Ottawa, special. She deserves a medal for her continuing efforts to get me out of the lab; realizing that left to my own devices I would rarely leave time for anything else. I can't imagine having done this without her.

I was lucky enough to share an office with Gerd Pohlers during my formative years in the group. Gerd answered a lot of questions for me, most of them more than once, and showed me both how to conduct experiments and direct my research. He also demonstrated for me that, despite labels which may say otherwise, dairy products need not be refrigerated and a full workday can start at noon.

Two post-docs from Italy, Fausto Ortica and Salvo Sortino were both important sounding boards for new ideas as well as good friends and hosts. Salvo's lust for life and desserts as well as his introduction of the term 'mind-masturbation' to describe the study of photochemical reaction pathways, are the stuff of legend. His inability to distinguish between the words, 'horse' and 'whores' as well as his mangled song lyrics, remain the source of much amusement.

Interaction with the above mentioned group members as well as fellow workers on various Shipley projects, Elena Bejan, Pam Arnold, Mariette Brandao and Carolina Aliaga have shaped me into the chemist I am today and continue to reveal the shortcomings of the chemist I am today. Over the course of my research I have had the opportunity to supervise a number of undergraduate students: Nicole Deschamps, Priscilla Brastianos, Matthew Haigh, Anne-Marie Boulanger and Larisa Mickelsons. Their contribution to my research was substantial and working with them was rewarding on many levels. I have been lucky enough to collaborate with a number of people from Shipley Co. Inc and St. Jean Photochemicals, Inc., all of whom have lent me their expertise in some way or another and have given me a peek into life outside of academics.

The work of the support staff in Tito's group was greatly appreciated. I thank Gerry Charette and André Simard for keeping all the instruments running smoothly. I thank Tito's secretaries, Anita Bowman, Cheryl Cole and Betty Yakimenko for their help in dealing with the giant network of red tape that is the University of Ottawa.

I would like to thank all of my friends and family for putting up with me over the years and for their understanding in the future when I ignore them unless they refer to me as Dr. Coenjarts. I especially want to thank Pat Forgione for his friendship and for setting a standard for Ph.D. chemists from Brantford which I should have no problem exceeding.

Table of Contents

List of Figures

List of Schemes

List of Tables

List of Abbreviations

A	pre-exponential factor
ACN	acetonitrile
$Ar^{\bullet}$	aryl radical
$Ar^{\bullet+}$	aromatic radical cation
ArH	polyalkylbenzene
$Ar_2S^{\bullet+}$	diarylsulfide radical cation
AZAX	1-azaxanthone
AZAX(H)$^{\bullet}$	1-azaxanthone ketyl radical
$AZAX^{\bullet-}$	1-azaxanthone radical anion
$^3AZAX^*$	1-azaxanthone triplet excited state
C	coulomb energy of an ion-pair
C1	coumarin 1
C6	coumarin 6
CAR	chemically amplified resist
ClSOH	chlorobenzenesulfonic acid
CPHS	camphorsulfonate
CSA	camphorsulfonic acid
CT	charge transfer
$\Delta E_{0,0}$	singlet excited state energy
ΔO.D.	change in absorbance of sample
DUR	durene
DTB	*di-t*-butylbenzene
DTT	*di-t*-butyltoluene
ε	molar absorptivity
E^*	excited state energy
Ea	activation energy
EL	ethyl lactate
E_{ox}	oxidation potential
E_{red}	reduction potential
ET	electron transfer
E_T	triplet excited state energy
ϕ	quantum efficiency
f	fraction of triplets
Φ	quantum yield
H	hydrogen abstraction
HP	2-heptanone
HT	hydrogen atom transfer
IC	internal conversion
IPET	indirect photoinduced electron transfer
ISC	intersystem crossing
λ	wavelength
LFP	laser flash photolysis
MEE	2-methoxyethyl ether

MES	mesitylene
MPA	1-methoxy-2-propanol acetate
MSA	methanesulfonic acid
MTT	2,4-bis(trichloromethyl)-6-methyl-5-triazine
PAA	poly(acrylic acid)
PAC	photoactive compound
PAG	photoacid generator
PEB	post-exposure bake
PET	photoinduced electron transfer
PFOS	perfluorooctanesulfonic acid
$Ph^{\bullet}$	phenyl radical
Ph^{+}	phenyl cation
$Ph_2S^{+\bullet}$	diphenylsulfide radical cation
Ph_2S	diphenylsulfide
PMMA	poly(methyl methacrylate)
PT	proton transfer
PVP	poly(vinylphenol)
Rb	rhodamine B base
S_0	ground state
S_1	lowest singlet excited state
SCE	saturated calomel electrode
SOC	spin-orbit coupling
S_n	singlet excited state
T_1	lowest triplet excited state
$\tau_{1/2}$	half-life
TAS	triarylsulfonium
tBOC	poly(4-*t*-butoxycarbonyloxystyrene)
TET	triplet energy transfer
TFA	trifluoromethanesulfonic acid
Tg	glass-transition temperature
T_n	triplet excited state
TOL	toluene
TPS	triphenylsulfonium
TSA	*p*-toluenesulfonic acid monohydrate
VR	vibrational relaxation
XAN	xanthone
XAN(H)$^{\bullet}$	xanthone ketyl radical
$XAN^{-\bullet}$	xanthone radical anion
$^3XAN^{*}$	xanthone triplet excited state
o,m,p -XYL	*o,m,p*-xylene

1. Introduction

1.1 The Photolithographic Process

Lithography is a technique used by the microelectronics industry in the fabrication of integrated circuits. In this context, the lithographic process involves using an exposure technique to transfer a pattern from a mask to a polymer film and finally to a semiconducting substrate. A variety of modes of exposure can be employed for this purpose including UV or X-ray radiation and electron- or ion-beams. The photolithographic process,[1,2] whose main features appear in Figure 1-1, employs UV radiation and is the primary technique currently used in industrial applications. Briefly, a thin film (0.5 -10 μm) of a photosensitive polymer, termed a resist, which has been spin-coated onto a semiconducting substrate is exposed to light through a mask. The mask is composed of a pattern which prevents light from reaching certain regions of the resist and allows it to reach others. Interaction of light with the resist induces a chemical change, creating a latent image of the pattern from the mask, in the resist. This photoinduced chemical change causes a difference in the dissolution rate between exposed and unexposed regions. Development of the resist with an appropriate solvent selectively dissolves the exposed or unexposed regions, producing positive or negative tone images, respectively. After the development step, regions of the substrate are left exposed, allowing them to be etched, thereby transferring the pattern to the substrate. Finally, the remaining resist is washed away to leave the bare, patterned substrate. Repetition of these steps with different masks and resists allows for the construction of detailed 3-dimensional circuit patterns. A discussion of design and processing aspects of semiconductor devices and integrated circuit technology is outside the scope of this thesis as it is primarily concerned with the chemical processes which allow for the creation of a latent image in a polymer film. For such a discussion the reader is directed to an excellent text with many leading references.[2]

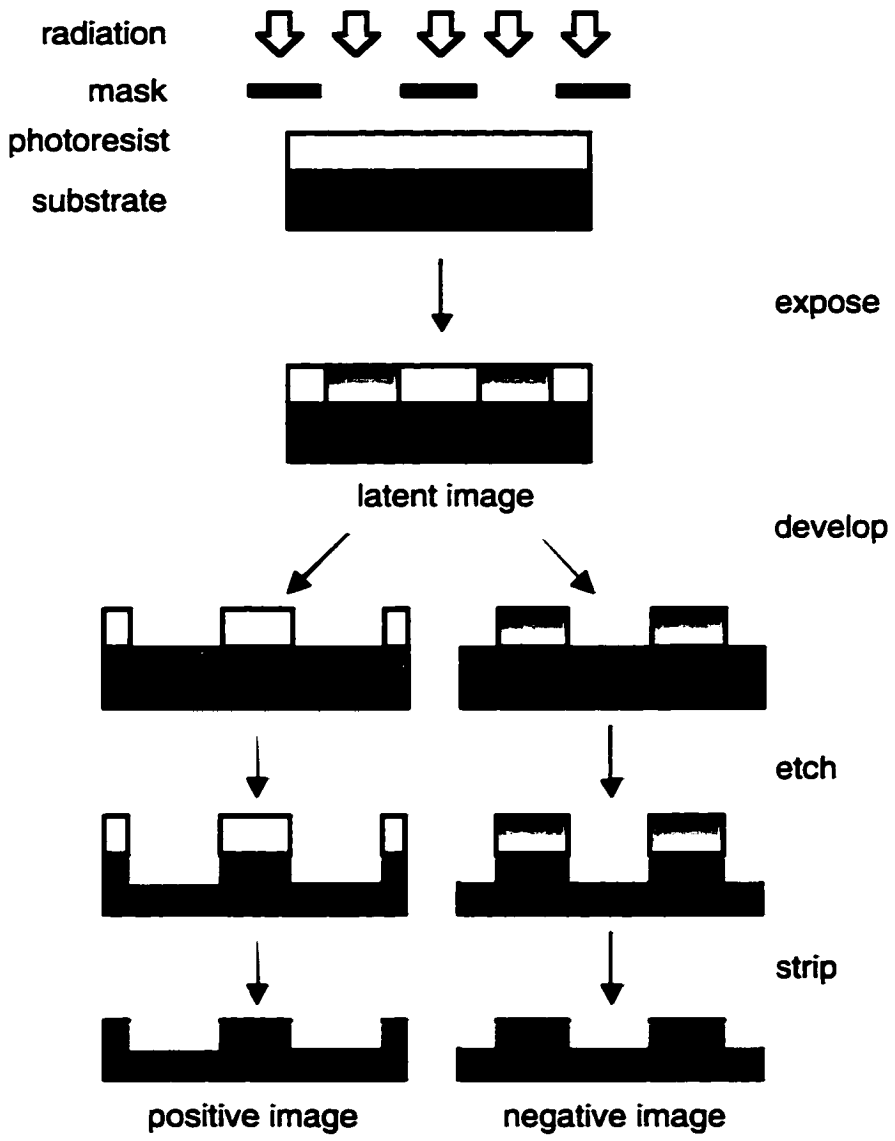

Figure 1-1. Schematic representation of the photolithographic process.

1.2 Resist Materials

The basic resist material used in photolithography is usually a two-component system in which a polymer is the film-forming material and a monomeric photoactive compound (PAC) serves as the sensitizer.

1.2.1 Classical Optical Resist Systems

1.2.1.1 A Two-Component Negative Resist

For most negative resists, photoinduced cross-linking of the polymer is the means by which regions exposed to light are made less soluble relative to unexposed regions. Generally, the resist is composed of a bis(arylazide) sensitizer as the PAC and a partially cyclized poly(*cis*-isoprene) as the polymer resin. Upon absorption of a photon the bis(arylazide) loses nitrogen to form a nitrene intermediate.[3] Although this nitrene can undergo a variety of different reactions with the polymer, the primary reaction is addition to sites of unsaturation to form aziridine linkages (Scheme 1-1).[4] A polymer cross-link is formed when the remaining azide functionality of the molecule absorbs another photon, thereby initiating the same set of reactions.

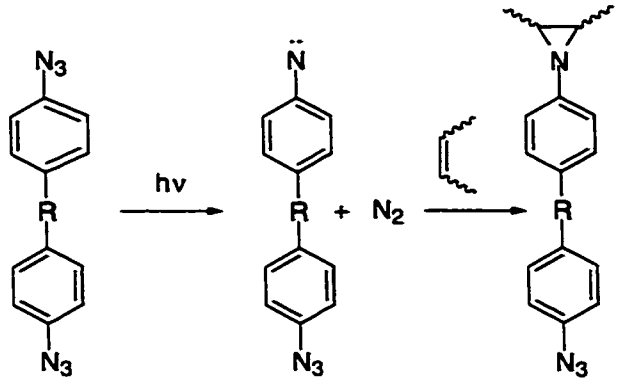

Scheme 1-1. Reactions involved in the photochemically induced cross-linking of a bis(arylazide)-rubber resist.

1.2.1.2 Two-Component Positive Resists

Although the bis(arylazide)-rubber resist was the first 'workhorse' of the microelectronics industry, it has been replaced almost entirely by positive resists due to their increased resolution and thermal stability.[4] The first positive resists were composed of a diazonaphthoquinone sensitizer as the PAC and a copolymer of variously substituted phenols with aldehydes, termed novolacs, as the polymer resin.[1,5] In these positive resists, the exposed regions of the film become more soluble to an aqueous base developer than the unexposed regions. The solubility difference is derived from the fact that while novolacs are soluble in aqueous base, diazonaphthoquinones are not, and their presence in sufficient amounts inhibits solubilization of the resist prior to exposure. However, the main photoproduct of the diazonaphthoquinone is base soluble, thereby allowing solubilization of the resist after exposure to light. Upon absorption of a photon, the diazonaphthoquinone loses nitrogen to form a carbene which undergoes Wolff rearrangement to a ketene. The ketene is attacked by water to form an indenecarboxylic acid (Scheme 1-2).[6]

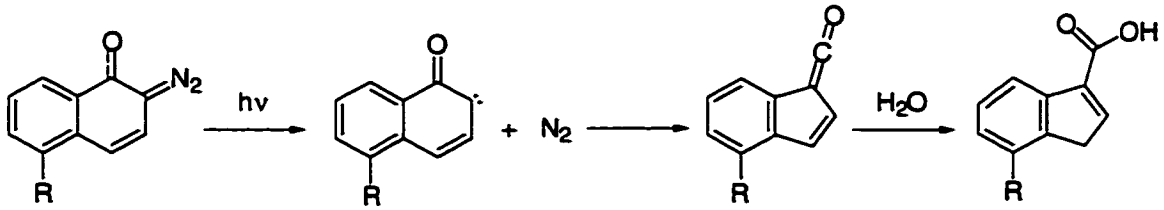

Scheme 1-2. Photochemical rearrangement of a diazonaphthoquinone (aqueous base insoluble) to an indenecarboxylic acid (aqueous base soluble).

1.2.1.3 Limitations of Classical Optical Resist Systems

In response to the demand for higher performance semiconductor devices, the microelectronics industry is constantly striving to increase circuit density by reducing the size of lithographically imaged features. One of the ways to improve lithographic resolution is to reduce the wavelength of light employed for the imaging.[7] The aforementioned resists are imaged primarily with high pressure

mercury arc lamps which have output from 250-600 nm, although the main emission lines used for photolithography occur at 436, 404 and 365 nm.[8] Continued improvement of resolution requires use of radiation in the deep UV (≤ 254 nm). The use of these shorter wavelengths required the development of new resist materials because of inappropriate absorbance properties of the classical resists as well as issues with the output of available light sources.

Although most of the polymers used in the classical resists are reasonably transparent above 300 nm, they have a sufficiently high absorbance at shorter wavelengths such that they filter light away from the intended target, i.e., the PAC. A resist which has an absorbance which is too high (> 50% of incident light absorbed over a resist film) does not provide well-defined images because of large gradients in the intensity of light as it penetrates the film. An additional roadblock to deep UV resists is that the high pressure mercury arc lamps traditionally used for photolithography have much lower output in the deep UV than at longer wavelengths. Even the use of alternate light sources, such as excimer lasers does not entirely solve the problem of low photon flux.[8] From a practical standpoint, a system with lower photon flux requires longer exposure times to induce the same number of photochemical events. In order to counteract the accompanying decrease in product throughput that this would entail, the resist materials for deep UV need to be more photosensitive than the classical resists. This increased sensitivity is accomplished via a process known as chemical amplification.

1.2.2 Chemically Amplified Resists

In photolithography, chemical amplification is achieved by photogeneration of a catalyst and subsequent action of that catalyst on labile side-chains of the polymer, thereby altering the solubility of the resist.[8] In this way, a single photochemical event is responsible for multiple chemical reactions in the film, as

controlled by the chain length for the catalytic process. A typical example of a chemically amplified resist (CAR) contains a triphenylsulfonium (TPS) salt as a photoacid generator (PAG) and poly(4-*t*-butoxycarbonyloxystyrene) as an acid-labile polymer.[9-12] Upon absorption of a photon, the TPS salt decomposes to generate a strong acid. Acid catalyzes the thermal decomposition of the *t*-butoxycarbonate groups in the polymer during a post-exposure bake (PEB, 90-150 °C, 60-90 s); a process known as deprotection. The thermolysis products are a phenolic polymer, carbon dioxide and a tertiary carbocation, which undergoes β-elimination to regenerate acid (Scheme 1-3).[13] This system behaves as a positive resist when developed with polar solvents, which solubilize the photoproducts, and as a negative resist with non-polar solvents, which favour solubilization of the initial polymer. Many variations on the chemical amplification process, including different PAGs and polymers are currently being employed successfully by the microelectronics industry as resist materials.[8,14]

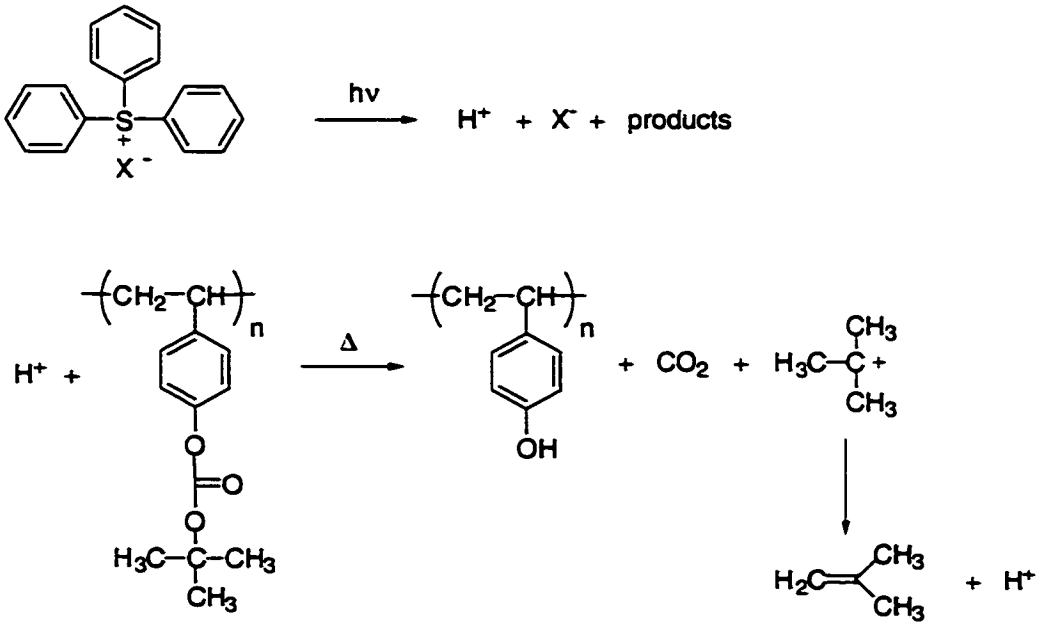

Scheme 1-3. Photogenerated acid from a triphenylsulfonium salt catalyzes the deprotection of poly(4-*t*-butoxycarbonyloxystyrene).

The photosensitivity of a CAR is ultimately a function of both the efficiency with which the PAG converts photons to acid as well as resist chemistry, in particular the chain length of the acid-catalyzed steps. The catalytic chain length in a CAR can range from one to several thousands of steps long,[15,16] while typical PAG efficiencies vary over a factor of less than 5 (a reasonable value, *vide infra*). It is therefore tempting to suggest that the efficiency with which photoacid generation occurs is of minor importance when compared to the impact of polymer chemistry on CAR photosensitivity. Certainly, polymer design is key to the performance of a CAR, but the importance of PAG photochemistry should not be underestimated. In the highly competive marketplace facing the current microelectronics industry, the factor of ~5 in photosensitivity of the CAR which is controlled by PAG efficiency, and its concomitant impact on product throughput, demands that close attention be paid to PAG photochemistry.

1.3 Photoacid Generators

1.3.1 General Photophysics/Photochemistry

As previously noted, PAGs are molecules which decompose to generate acid upon absorption of a photon. The more efficiently a PAG converts absorbed photons into acid, the higher its quantum yield of acid generation (Φ_{acid}).

Φ_{acid} = number of acid molecules generated / number of photons absorbed

Values of Φ_{acid} are always less than unity due to the presence of other deactivation pathways available to the PAG which compete with acid generation. An understanding of some basic photophysics, as described by a Jablonski diagram (Figure 1-2), is required in order to appreciate the role of these pathways in determining Φ_{acid}.

Absorption of a photon by a molecule excites it from its ground state (S_o) to an electronically excited singlet state. This transition is the result of an electron jump from a low energy orbital into a higher energy orbital with conservation of electron spin angular momentum. The singlet excited state (S_n) which is initially populated is not necessarily the lowest singlet excited state (S_1). S_1 is populated after vibrational relaxation (VR) and internal conversion (IC) of the first-formed S_n. The processes which lead to the formation of the lowest vibrational level of S_1 occur with unity efficiency for most molecules. It is from this state that most PAGs decompose, often via a bond-cleavage reaction, made possible due to the excess energy introduced by the photon. Other possible pathways from S_1 are fluorescence, IC back to S_0 and intersystem crossing (ISC) to a triplet excited state (T_n), which may be the lowest triplet excited state (T_1). ISC is an isoelectronic transition between states of differing multiplicities which involves flipping an electron's spin. A PAG can also decompose from the T_1, but must do so in competition with phosphorescence and ISC back to S_o. In order to favour acid

generation, chemical decomposition of the PAG from an excited state must dominate over these other relaxational processes. It is the behaviour of the reactive intermediates formed from decomposition of the PAG that ultimately leads to acid generation.

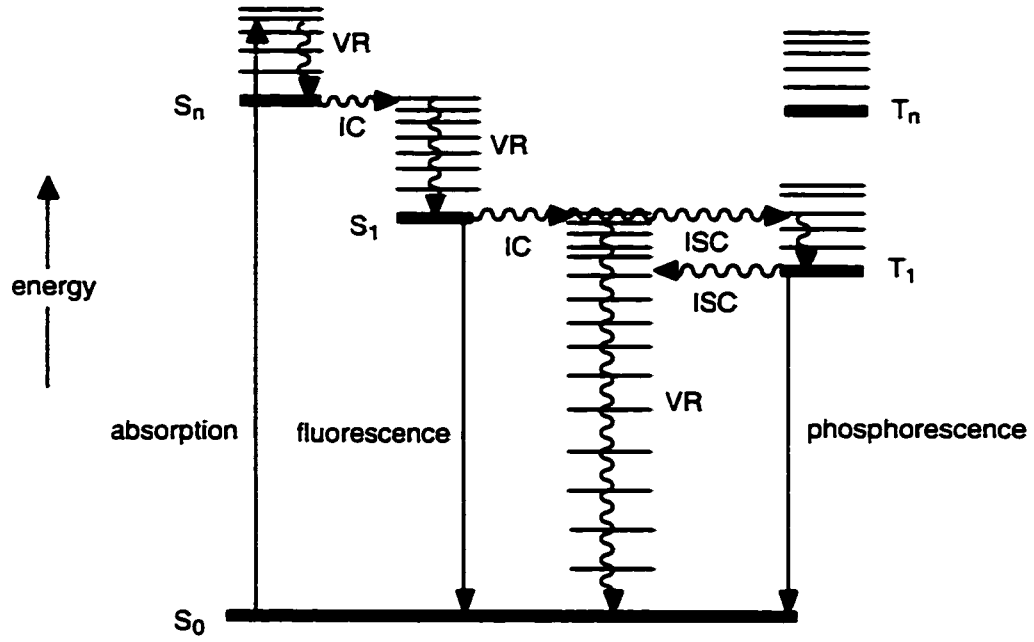

Figure 1-2. A Jablonski diagram.

Although most PAG studies are practical in nature, restricting themselves to some type of evaluation of acid generating efficiency, mechanistic studies, which consider the pathways in Figure 1-2, also exist for many classes of PAGs (*vide infra*). Reviews on PAG photochemistry and their lithographic performance, with many leading references are available.[14,17-21]

1.3.2 Mechanisms for Photoacid Generation

Many different classes of compounds can behave as PAGs; some representative examples, which have proven to be industrially useful, appear in Table 1-1.

Table 1-1. Φ_{acid} data for different classes of PAGs.

Class Name	Representative structure	Φ_{acid}
perhalomethyl triazines	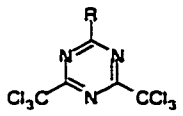	0.28 (ACN,[a] 266 nm, R=CH_3)[22] 0.31 (novolac, 365 nm, R=1-(4-ethoxynaphthyl))[23]
N-oxyimidosulfonates	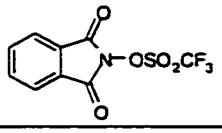	0.28 (ACN, 308 nm)[24] 0.069 (PMMA,[b] 193 nm)[25] 0.44 (acrylate,[c] 193 nm)[26]
o-nitrobenzyl esters	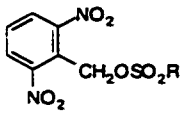	0.16 (PMMA, 248 nm, R=$C_6H_4CH_3$)[27] 0.15 (PMMA, 248 nm, R=$C_6H_4CF_3$)[16]
pyrogallolsulfonates	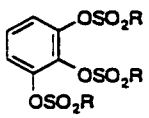	0.060 (PMMA, 193 nm, R=CH_3)[25] 0.014 (acrylate, 193 nm, R=CF_3)[26] 0.20 (novolac, 250 nm, R=CH_3)[28]
α-diazosulfonates	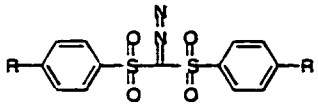	0.27 (PVP,[d] 248 nm, R=*t*-butyl)[29]
diaryliodonium salts	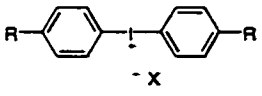	0.40 (ACN, 266 nm, R=*t*-butyl, X=SO_3CF_3)[30] 0.65 (ACN, 254 nm, R=H, X=AsF_6)[31] 0.032 (PMMA, 193 nm, R=H, X=SO_3CF_3)[25] 0.16 (acrylate, 193 nm, R=*t*-butyl, X=SO_3CF_3)[26] 0.46 (acrylate, 248 nm, R=*t*-butyl, X= CPHS[e])[32]
triarylsulfonium salts	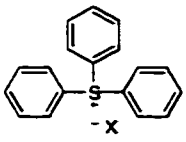	0.52 (ACN, 248 nm, X=SO_3CF_3)[33,34] 0.74 (ACN, 254 nm, X=AsF_6)[31] 0.037 (PMMA, 193 nm, X=SO_3CF_3)[25] 0.44 (PVP, 248 nm, X=AsF_6)[29] 0.26-0.4 (tBOC[f], 254 nm, X=SbF_6)[15] 0.23 (acrylate, 193 nm, X=SO_3CF_3)[26]

[a]ACN = acetonitrile, [b]PMMA = poly(methyl methacrylate) film, [c]acrylate = acrylate containing copolymer film, [d]PVP = poly(vinylphenol) film, [e]CPHS = camphorsulfonate, [f]tBOC = poly(4-*t*-butoxycarbonyloxystyrene) film

That all values for Φ_{acid} are less than unity indicates the involvement of quantum wasting and/or PAG wasting processes in their photochemistry. Quantum wasting processes are those which either allow the photoexcited PAG to relax down to S_0 without decomposition (Figure 1-2) or those which involve recombination of decomposition products to reform the initial PAG. In both cases the same PAG remains available for subsequent acid generation upon absorption of a second photon. Alternatively, a PAG wasting process is one which results in a decomposed PAG without the accompanying acid generation. A PAG wasting step occurs when the reactive intermediates generated by PAG photodecomposition are trapped by species via reactions which do not yield acid as a product. Such processes represent an irrecoverable loss of acid generating potential, i.e., the chemical yield of acid cannot equal the initial amount of PAG. Strictly speaking, a PAG wasting step is also a quantum wasting step. In order to be an effective PAG, a molecule should have both a high Φ_{acid} as well as a high chemical yield of acid.

The nature of PAG wasting reactions becomes more clear upon consideration of the specific mechanisms for photoacid generation by PAGs. Upon absorption of a photon, 2-methyl-4,6-bis(trichloromethyl)-1,3,5-triazine decomposes via homolytic carbon-chlorine bond cleavage from a singlet excited state.[23,35] Hydrogen abstraction from the media by the chlorine atom generates HCl. Potential quantum wasting steps are IC of S_1 back to S_0 or recombination of the initially formed radicals to reform the carbon-chlorine bond. Potential PAG wasting steps which compete with hydrogen abstraction by chlorine atoms are addition of chlorine atoms to sites of unsaturation in the polymer as well as recombination of chlorine atoms with any number of radical species which may be present. These competitive processes appear in Scheme 1-4.

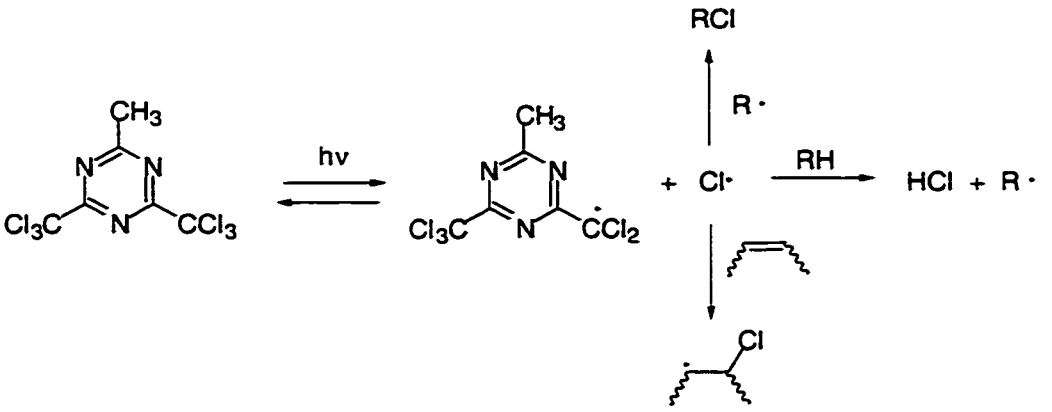

Scheme 1-4. Photodecomposition of 2-methyl-4,6-bis(trichloromethyl)-1,3,5-triazine to yield acid and other products.

The photodecomposition of N-trifluoromethylsulfonyloxyphthalimide occurs via heterolytic cleavage of its nitrogen-oxygen bond from a singlet excited state.[24] Acid generation occurs upon attack of the nitrogen centered cation by an appropriate nucleophile (Scheme 1-5), which is likely water in a properly designed resist.[4] After bond cleavage, there is little potential for interference from undesired reactions, apart from recombination of the initial fragments to reform starting material.

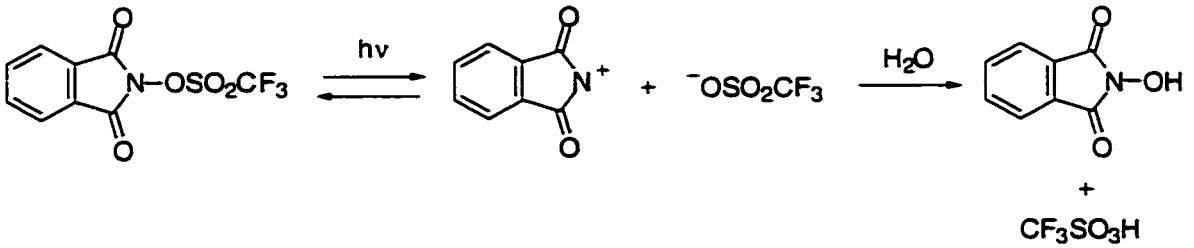

Scheme 1-5. Photodecomposition of N-trifluoromethylsulfonyloxyphthalimide to yield acid and N-hydroxyphthalimide.

The mechanism for photodecomposition of α–diazosulfonates[29,36,37] and presumably for pyrogallolsulfonates[28,38] also involve the formation of reactive intermediates which require the co-operation of an appropriate substrate in order to generate acid. Photodecomposition of *o*-nitrobenzyl esters involves a

rearrangement reaction which is self-sufficient in terms of acid generation because it does not require the involvement of another species to yield acid.[27] The mechanism for photoacid generation by onium salts is the subject of Chapter 6, but it should be noted here that they can behave both self-sufficiently and co-operatively, to generate acid. In addition to the mechanisms discussed here, PAG systems have also been designed which function via indirect routes, with the PAG participating in energy or electron transfer reactions, both intra- and intermolecularly, with a photochemically excited sensitizer.[39-41]

1.3.3 Other Photoacid Generator Considerations

Many factors other than Φ_{acid} are important in determining the effectiveness of a PAG in a photolithographic application. In order to appreciate these factors one is reminded that a CAR film is made from a solution containing, among other components, polymer and PAG, and that development involves a PEB in order to facilitate the action of the photogenerated acid on the polymer. As such, in order to be useful as a PAG, a molecule must be both chemically stable in solution and in films, as well as thermally stable. For obvious reasons, PAG decomposition via processes other than the desired photochemical pathway is detrimental to the performance of a CAR. The onium salts are thermally stable but their ionic nature can represent formulation difficulties due to their tendency to precipitate from organic solutions and films.[19] The use of many non-ionic PAGs raises concerns over their thermal stability, and the perhalomethyl triazines, *o*-nitrobenzyl esters, and N-oxyimidosulfonates are all susceptible to solvolysis.[19,27]

Even if a PAG is sufficiently stable and can be easily formulated, there are other issues, more closely related to the actual imaging process, which affect a PAG's utility. The absorbance properties of the PAG must be such that requirements for the amount of light absorbed and the amount of PAG that can be

dissolved in the film are compatible with one another. The type of acid generated by a PAG is also important because it affects the chain length of the acid-catalyzed reaction.[16] PAGs which generate stronger acids, such as trifluoromethanesulfonic acid, are the most effective. Also related to the nature of the photogenerated acid, is that PAGs which generate volatile acids, such as the perhalomethyl triazines, can encounter problems related to acid desorption from the CAR film during the PEB.[19] Finally, the presence of the PAG in the CAR can change the solubility properties of the entire film, with some PAGs serving as dissolution inhibitors, a property which has been used advantageously in certain lithographic strategies.[4] All of these factors combine with the Φ_{acid} to determine the lithographic performance of a PAG.

1.3.4 Photoacid Generation below 248 nm

Much of the current research in photolithography is directed towards developing CARs which function at 193 and 157 nm. This involves identifying and testing appropriate polymers as well as PAGs. In such cases that there are no satisfactory materials, new ones must be developed.

The low output of light sources for 193 and 157 nm as well as absorption of light by various optical components in imaging tools, necessitates the use of highly photosensitive CARs. The design of new polymer materials is considered to be essential because those employed in CARs designed for 248 nm are too highly absorbing at shorter wavelengths.[42,43] In fact, even the most promising polymer candidates for use at 193 nm are more absorbing at this wavelength than the polymers currently used at 248 nm are at that wavelength. In order to keep the overall absorbance of 193 nm CAR films at a reasonable level, the amount of PAG used must be lowered significantly relative to those used at longer wavelengths.[44] In order to compensate for the reduced photon flux as well as lower amounts of PAG in the CAR, PAGs with high Φ_{acid} are highly desirable.

Most, if not all of the polymer candidates for use at 193 and 157 nm are devoid of aromatic groups, which are too highly absorbing.[42,43] Without these groups the potential for photosensitization of the PAG by the polymer, a process which is important in some CARs,[28,45,46] is essentially eliminated. In light of this, it is very important to understand the mechanism by which any given PAG generates acid in order to ensure that it can function in the environment provided by any given CAR.

There are some schools of thought which suggest that existing PAGs are too highly absorbing at 193 and 157 nm, and that new PAGs, which absorb less are required.[47] This is a matter of some contention[48] and the subject of new PAGs for 193 and 157 nm has received much less attention than the subject of new polymers. It may seem counterintuitive to suggest that a PAG could absorb too much light; however, if the absorbance of the PAG is too high there are gradients in the amount of light as it penetrates the film, in the exact same manner as if the polymer absorbs too much. The result is that more acid is generated at the top of the film than at the bottom, and undesirable features may result upon development (Figure 1-3). A reduction in the PAG concentration, to reduce the absorbance, runs the risk of not having enough PAG to generate sufficient amounts of acid.

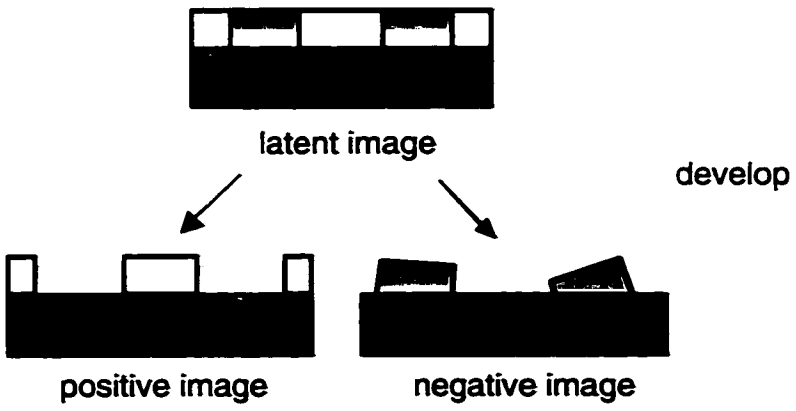

Figure 1-3. Schematic representation of resist development when the absorbance due to the PAG is too high.

This preceding discussion of the potential need for new PAGs and the definite need for mechanistic knowledge of all PAGs, is not meant to suggest that these issues are only relevant in terms of 193 and 157 nm lithography. The opportunity for new PAGs to find their way into an actual CAR formulation, for use at any wavelength, is only a matter of outperforming the PAGs currently in use. The introduction of a whole new set of CARs for 193 and 157 nm simply opens the window of opportunity for new PAGs a little wider. In the same way, fundamental PAG research has value in any context, though it seems to increase during periods in which new resist materials are being screened. The subject of PAG photochemistry is discussed extensively in Chapters 4, 5 and 6.

1.4 After Acid Generation

In order for photogenerated acid to be an effective catalyst it must diffuse within the CAR film, moving from one reactive site of the polymer to the next. In a typical CAR, a single molecule of acid diffuses to hundreds, even thousands of different reactive sites within the polymer.[15,16] This type of short-range diffusion is required for CAR functioning; however, long-range diffusion of acid can be very detrimental to CAR performance. Diffusion of acid into unexposed regions of the CAR and the accompanying acid-catalyzed reactions can severely compromise image definition.[49] The chemical amplification process, which is so crucial for creating very photosensitive CARs, is a hindrance when it comes to concerns about acid diffusion because even small amounts of acid can have a large impact on the developed image. Extensive diffusion of acid can potentially lead to acid desorption from the surface of the film.[50] Such a process negates the use of highly photosensitive CARs by removing the photogenerated acid from the system. Acid mobility, including both acid diffusion and acid desorption are discussed in more detail in Chapter 3 and to a lesser extent in Chapter 2.

1.5 Research Objectives

Although highly varied, all of the work in this thesis involves studying acid in photolithographically relevant systems. The objectives of the individual projects never stray far from the central goal of acquiring mechanistic insight into both the photoacid generation process as well as acid mobility in polymer films. This begins with the development and use of techniques for quantifying and locating photogenerated acid in solution and in films (Chapter 2) for the purposes of studying acid diffusion as well as evaluating photoacid generating efficiencies of PAGs. The behaviour of acid in polymer films was investigated by developing a novel technique for monitoring acid desorption from polymer films (Chapter 3) in order to determine the factors which control acid mobility in these environments. Much of the work presented here is focused on determining the mechanisms by which PAGs generate acid (Chapter 4) as well as designing and testing new molecules for use as PAGs (Chapter 5 and 6). It is the ultimate goal of this work to gain a fundamental understanding of chemical processes and reaction mechanisms, in order to apply this knowledge to the evaluation and design of materials for use in the photolithographic process.

1.6 References

(1) Reiser, A. *Photoreactive Polymers: The Science and Technology of Resists*; Wiley Interscience Publications: New York, 1989.

(2) Thompson, L. F.; Willson, C. G.; Bowden, M. J. *Introduction to Microlithography*; 2nd ed.; American Chemical Society: Washington, 1994.

(3) Abramovitch, R. A.; Kyba, E. D., *Decomposition of Organic Azides* in *The Chemistry of the Azido Group* ; Patai, S., Ed.; Interscience: New York, 1971, pp 221-329, and references therein.

(4) Willson, C. G., *Organic Resist Materials* in *Introduction to Microlithography* ; 2nd ed.; Thompson, L. F., Willson, C. G. and Bowden, M. J., Ed.; American Chemical Society: Washington, DC, 1994, pp 139-268.

(5) Suess, O. *Liebigs Ann. Chem.* **1944**, *556*, 65.

(6) Barra, M.; Fisher, T. A.; Cernigliaro, G. J.; Sinta, R.; Scaiano, J. C. *J. Am. Chem. Soc.* **1992**, *114*.

(7) Bowden, M. J., *The Lithographic Process: The Physics* in *Introduction to Microlithography* ; Thompson, L. F., Willson, C. G. and Bowden, M. J., Ed.; American Chemical Society: Washington, DC, 1994, pp 19-138.

(8) MacDonald, S. A.; Willson, C. G.; Frechet, J. M. *Acc. Chem. Res* **1994**, *27*, 151, and references therein.

(9) Frechet, J. M. J.; Ito, H.; Willson, C. G. *Proc. Microcircuit Eng.* **1982**, 260.

(10) Ito, H.; Willson, C. G. *Polym. Eng. Sci.* **1983**, *23*, 1012.

(11) Ito, H.; Willson, C. G., *Polymers in Electronics* in *ACS Symposium Series 242 American Chemical Society* ; Davidson, T., Ed.: Washington, DC, 1984, pp 11-23.

(12) Willson, C. G.; Ito, H.; Frechet, J. M. J.; Tessier, T. G.; Houlihan, F. M. *J. Electrochem. Soc.* **1986**, *133*, 181.

(13) Taylor, R., in *Chemistry of Carboxylic Acids and Derivatives* ; Patai, S., Ed.; J. Wiley and Sons: New York, 1979, pp 859-914.

(14) Reichmanis, E.; Houlihan, F. M.; Nalamasu, O.; Neenan, T. X. *Chem. Mater.* **1991**, *3*, 394.

(15) McKean, D. R.; Schaedeli, U.; McDonald, S. A. *J. Polym. Sci.: Part A: Polym. Chem.* **1989**, *27*, 3927.

(16) Houlihan, F. M.; Neenan, T. X.; Reichmanis, E.; Kometani, J. M.; Chin, T. *Chem. Mater.* **1991**, *3*, 462.

(17) Crivello, J. B. *Adv. Polym. Sci.* **1984**, *62*, 1.

(18) Pappas, S. P. *J. Imaging Technology* **1985**, *11*, 146.

(19) Pawlowski, G.; Dammel, R.; Przybilla, K.-J.; Roschert, H.; Spiess, W. *J. Photopolym. Sci. Technol.* **1991**, *4*, 389.

(20) Frechet, J. M. J. *Pure Appl. Chem.* **1992**, *64*, 1239.

(21) Shirai, M.; Tsunooka, M. *Bull. Chem. Soc. Jpn.* **1998**, *71*, 2483.

(22) Ortica, F.; Coenjarts, C.; Scaiano, J. C.; Liu, H.; Pohlers, G.; Cameron, J. F. *Chem. Mater.* **2001**, *13*, 2297.

(23) Buhr, G.; Dammel, R.; Lindley, C. R. *Polym. Mater. Sci. Eng.* **1989**, *61*, 269.

(24) Ortica, F.; Scaiano, J. C.; Pohlers, G.; Cameron, J. F.; Zampini, A. *Chem. Mater.* **2000**, *12*, 414.

(25) Naito, T.; Asakawa, K.; Shida, N.; Ushirogouchi, T.; Nakase, M. *Jpn. J. Appl. Phys.* **1994**, *33*, 7028.

(26) Szmanda, C. R.; Kavanagh, R.; Bohland, J.; Cameron, J.; Trefonas, P.; Blacksmith, R. *Proc. SPIE* **1999**, *3678*, 857.

(27) Houlihan, F. M.; Shugard, A.; Gooden, R.; Reichmanis, E. *Macromolecules* **1988**, *21*, 2001.

(28) Schlegel, L.; Ueno, T.; Shiraishi, H.; Hayashi, N.; Iwayanagi, T. *Chem. Mater.* **1990**, *2*, 299.

(29) Pawlowski, G.; Dammel, R.; Lindley, C. R.; Merrem, H. J.; Roeschert, H.; Lignau, J. *Proc. SPIE* **1990**, *1262*, 16.

(30) Unpublished results from our lab.

(31) Pappas, S. P.; Pappas, B. C.; Gatechair, L. R.; Schnabel, W. *J. Polym. Sci., Polym. Chem. Ed.* **1984**, *22*, 69.

(32) Cameron, J. F.; Fradkin, L.; Moore, K.; Pohlers, G. *Proc. SPIE* **2000**, *3999*, 190.

(33) Dektar, J. L.; Hacker, N. P. *J. Am. Chem. Soc.* **1990**, *112*, 6004.

(34) Tagawa, S.; Nagahara, S.; Iwamoto, T.; Wakita, M.; Kozawa, T.; Yamammoto, Y.; Werst, D.; Trifunac, A. D. *Proc. SPIE* **2000**, *3999*, 204.

(35) Pohlers, G.; Scaiano, J. C.; Sinta, R.; Brainard, R.; Pai, D. *Chem. Mater.* **1997**, *9*, 1353.

(36) Mulder, R. J.; van Leusen, A. M.; Strating, J. *Tetrahedron. Lett.* **1967**, 3057.

(37) King, J. F.; Lam, J. Y. L.; Skonieczny, S. *J. Am. Chem. Soc.* **1992**, *114*, 1743.

(38) Schlegel, L.; Ueno, T.; Shiraishi, H.; Hayashi, N.; Iwayanagi, T. *J. Photopolym. Sci. Technol.* **1990**, *3*, 385.

(39) Welsh, K. M.; Dektar, J. L.; Garcia-Garibaya, M. A.; Hacker, N. P.; Turro, N. J. *J. Org. Chem.* **1992**, *57*, 4179.

(40) Saeva, F. D. *J. Photochem. Photobiol. A: Chem.* **1995**, *86*, 149.

(41) Pohlers, G.; Scaiano, J. C.; Step, E.; Sinta, R. *J. Am. Chem. Soc.* **1999**, *121*, 6167.

(42) Ito, H. *Proc. SPIE* **1999**, *3678*, 2.

(43) Kunz, R. R.; Bloomstein, T. M.; Hardy, D. E.; Goodman, R. B.; Downs, D. K.; Curtin, J. E. *3678* **1999**, 13.

(44) Cameron, J. F.; Chan, N.; Moore, K.; Pohlers, G. *J. Photopolym. Sci. Technol* **2001**, *14*, 345.

(45) Hacker, N. P.; Welsh, K. M. *Proc. SPIE* **1991**, *1466*, 384.

(46) Hacker, N. P.; Welsh, K. M. *Adv. Chem. Ser.* **1993**, *236*, 557.

(47) Ishii, H.; Usui, S.; Douki, K.; Kajita, T.; Chawanya, H.; Shimokawa, T. *Proc. SPIE* **2000**, *3999*, 1120, and references therein.

(48) Reichmanis, E.; Nalamasu, F.; Houlihan, M. *Acc. Chem. Res.* **1999**, *32*, 659.

(49) Wallraff, G. M.; Hinsberg, W. D.; Houle, F. A.; Morrison, M.; Larson, C. E.; Sanchez, M.; Hoffnagle, J.; Brock, P. J.; Breyta, G. *Proc. SPIE* **1999**, *3678*, 138.

(50) Lamola, A. A.; Szmanda, C. R.; Thackeray, J. W. *Solid State Technol.* **1991**, *8*, 53.

2. Acid Detection in Non-Aqueous Systems

2.1 Introduction

The role of acid in the photolithographic process was discussed in Chapter 1. As noted there, the performance of a chemically amplified resist (CAR) is a function of many different components; the role of photogenerated acid being among the most important. The need to understand various aspects of photoacid generation and acid behaviour in CARs has driven the development of techniques which can both detect and quantify acid in non-aqueous systems, particularly polymer films. Ideally, these techniques should be both robust, so that they can be applied to a variety of systems, and convenient, to allow for their routine use. Most importantly, however, is that the data generated be accurate and unambiguous so that it can be used to gain insight into more complex processes, such as photoacid generator (PAG) photochemistry and acid diffusion kinetics.

This chapter serves as a record of the methods that have been employed in this lab for the sensing of acid in various non-aqueous environments. Some of these methods were significantly advanced as part of this thesis while others had reached a level of maturity such that they only required 'fine tuning' as part of this work. This chapter is intended to serve as a practical guide to performing these experiments. The utility of such a guide comes from the specific insights it contains which are not necessarily included in previous discussions of these techniques and the convenience associated with the collection of all of these details in one place. As such, much of the material presented here is experimental in nature with the inclusion of some representative results and a minimum amount of discussion.

Over the course of this thesis, techniques for sensing acid were employed in the context of various projects aimed at goals beyond simple acid detection, such as measuring acid mobility in polymer films and mechanistic studies of PAGs. This chapter is concerned primarily with the details relevant to actually performing acid-

sensing experiments. In cases in which acid sensing is the focus of the project, this will represent almost all of the work performed, while in others, in which acid sensing is employed as a tool as part of a larger project, there will be further discussion of results in subsequent chapters.

All of the techniques described here employ dyes as molecular probes for acid; made possible by changes in the optical properties of the dyes upon protonation. The most popular dye among workers in the photolithographic community is tetrabromophenol blue,[1-5] although more recently, monoazines,[6] xanthenes,[4,7-11] benzothiazoles,[7,12] and the rhodol derivative, Cl-Nerf,[13-15] have also proven useful. All of these dyes are similar in that protonation induces dramatic shifts in wavelengths of absorption and fluorescence as well as differences in quantum yields of fluorescence. A variety of different techniques have been used to monitor these changes including: fluorescence microscopy,[9,10,12-15] fluorescence spectroscopy,[6,8,11] steady-state absorption spectroscopy[1-5] and time-resolved absorption spectroscopy.[7]

All of the work with the aforementioned dyes and techniques employ one of two conditions: acid-detection is performed in polymer films or acid-detection is performed in solution. These are not just experimental differences but strategic ones. The work presented in this chapter explores a variety of different techniques and dyes and uses both of these strategies.

2.2 Acid Detection in Thin Polymer Films

2.2.1 Introduction

The ability to detect photogenerated acid within a polymer film is integral to the study of the chemistry of CARs. Experiments which are conducted entirely in actual resists or polymer films (which serve as reasonable models for resists) are practically ensured of providing relevant results whose interpretation is simplified over experiments performed in some other matrix. This fact becomes particularly clear in studies which investigate the issue of acid mobilities in CARs; studies which one is basically forced to conduct in polymer films.

2.2.2 Fluorescence Detection

Fluorescence detection is particularly well suited as a means to study acid mobility in CARs because of the high sensitivity of fluorescence techniques. This sensitivity allows the use of very small amounts of dye so as not to perturb acid diffusion. The popularity of this strategy is demonstrated by the fact that essentially all of the work currently in the literature on the subject of acid diffusion in CARs employs either exclusively, or in part, some type of fluorescence detection.[9,10,12-15]

Upon photoacid generation, the fluorescent properties of a dye-doped film change due to the different fluorescent characteristics of the various prototropic forms of the dye. These changes can be easily detected by standard fluorescent spectroscopy. If irradiation is performed through a mask, a latent image is created which can be easily resolved via fluorescence microscopy. The quality of the data obtained from fluorescence microscopy is highly dependent on the choice of dye. The dyes in current use are limited by the fact that significant fluorescence is observed for more than one of their prototropic forms, causing fluorescence to be observed in both exposed and unexposed regions of an imaged film.

Here is presented the use of coumarin 1 (C1) (Scheme 2-1) as a dye with fluorescent characteristics which make it ideally suited for this application. The absorption and fluorescence spectra of the two prototropic forms of C1 appear in Figure 2-1. The absorbance of the protonated form is blue-shifted with respect to the neutral, as is the fluorescence. In fact, the fluorescence of the neutral form can be monitored without any contribution from the protonated form, which has a much lower fluorescence intensity. This property allows for the creation of well-defined images with considerable fluorescence intensity in unexposed regions and practically none in exposed regions.

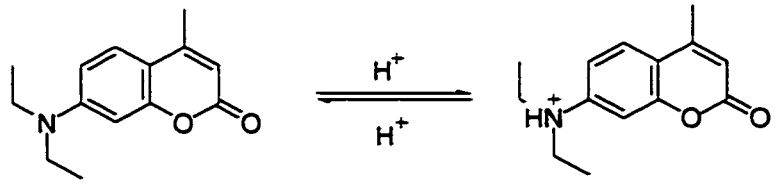

Scheme 2-1. The prototropic forms of C1.

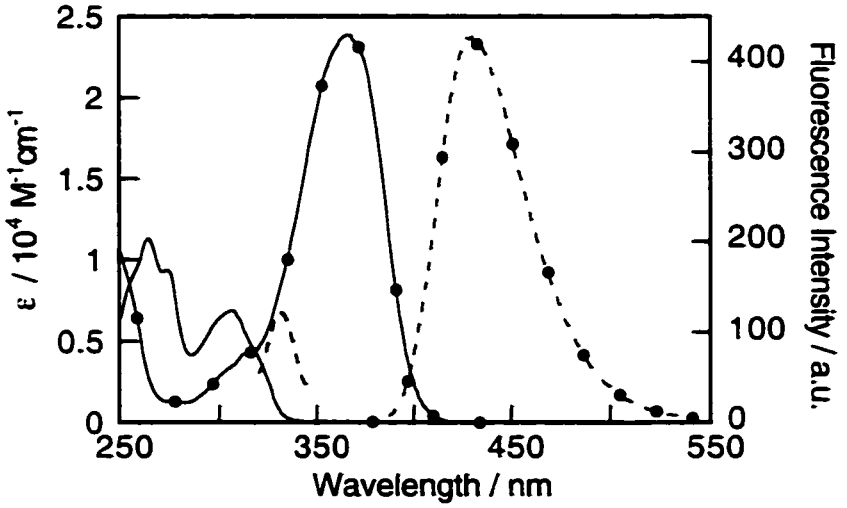

Figure 2-1. Absorption (—) and fluorescence (- -) spectra of neutral (•) and protonated C1 in acetonitrile.

Most acid sensitive dyes experience a red-shift in their fluorescence upon protonation. Consequently, they involve monitoring the protonated form of the dye

so as to minimize fluorescence contributions from the neutral form. By monitoring the species which has been exposed to high intensity irradiation one must be concerned with the possibility of photodegradation of the dye. C1 avoids this issue, as the neutral form of the dye, which is primarily in unexposed regions of the film is the species of interest. The main advantage of monitoring the neutral form, however, is in analysis of acid diffusion data. For C1, prior to acid generation, the maximum fluorescent signal is obtained as an experimental observable. This is accompanied by the knowledge that, with enough acid, the fluorescence will drop to zero, another easily measured quantity. Contrarily, for dyes which involve monitoring the protonated species, the fluorescence may or may not be zero in the absence of acid. As previously noted, many dyes do not have well-resolved fluorescences for both protropic forms. Additionally, upon acid generation the fluorescence intensity increases to a value which will vary with experimental conditions.

C1 was exploited in two different ways in order to monitor acid diffusion in polymer films, both of which were explored originally by Suzan Virdee as part of her Master's Thesis with a variety of different dyes.[16] Both adhere to the following basic strategy: generate an amount of acid in exposed regions of the film in excess of the amount required to completely protonate the dye. As the excess acid diffuses into unexposed regions the fluorescence properties of the film change.

2.2.2.1 Fluorescence Microscopy

A schematic representation of the manner in which fluorescence microscopy was employed to study acid diffusion appears in Figure 2-2a-d. A polymer film doped with C1 is highly fluorescent throughout (Figure 2-2a). Exposure through a grating reticle (a mask containing lines and spaces of equal width) creates a latent image in which the exposed regions do not fluoresce because they contain

protonated C1 (Figure 2-2b). As acid diffuses from exposed regions into unexposed regions, the fluorescence in the latter decreases (Figure 2-2c), and is eventually suppressed altogether (Figure 2-2d). An important aspect of this strategy is that enough acid be generated such that its diffusion out of exposed regions does not result in an increase in fluorescence from them.

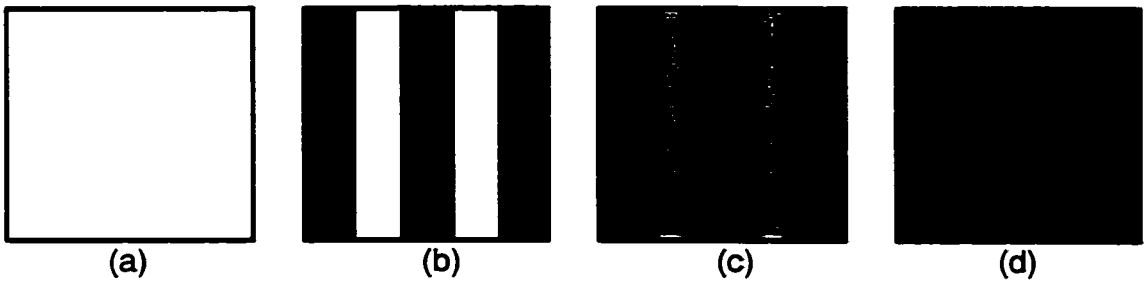

Figure 2-2. Schematic representation of the deterioration of a fluorescent image due to acid diffusion. White areas represent regions without acid and are highly fluorescent. Black regions represent areas in which acid is present and fluorescence is diminished. See text for further details.

In order to determine the ideal dose for generation of such images, calibration curves (Figure 2-3) were created using PAGs **2-1a** and **2-1b** (Scheme 2-2) in poly(vinylphenol) (PVP) films. The difference in the appearance of the curves is attributed to a difference in the acid generating efficiencies of the PAGs as opposed to differences in strength of the acids. These PAGs were chosen because they generate methanesulfonic acid (MSA), a very small and presumably mobile acid, and camphorsulfonic acid (CSA), an acid whose large size should restrict its movement in a polymer film.

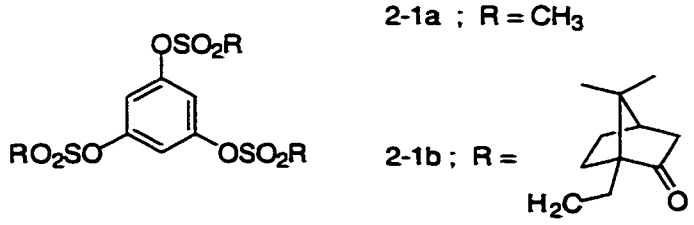

Scheme 2-2. PAGs used to generate acid in polymer films.

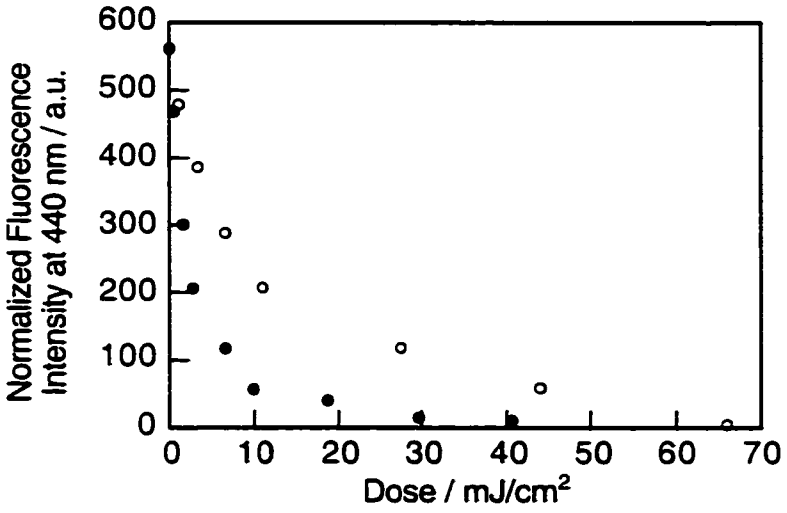

Figure 2-3. Fluorescence intensity of neutral C1 in PVP films upon photoacid generation with 2-1a (●) and 2-1b (○).

Images were created using PAG **2-1a** (Figure 2-4a and b) and observed via fluorescence microscopy. Although images with 1 μm features have been generated, those with 55 μm features are shown here in order to allow for careful examination of the images. The dose delivered to the film shown in Figure 2-4a was 1.1 mJ/cm^2; a well-defined image is obtained in which the average fluorescence intensity in unexposed regions is twice that of exposed regions, as expected based on Figure 2-3. The dose delivered in Figure 2-4b is 33 mJ/cm^2, which should generate enough acid to completely protonate all of the C1 in the exposed regions, thereby eliminating all fluorescence from these regions. Unexpectedly, the average fluorescence intensity in the exposed regions did not drop to zero, rather it only decreased to ~30% of the value observed in Figure 2-4a. Additionally, the boundaries between the exposed and unexposed regions are poorly defined and the regions in which acid is present have become noticeably wider. It appears that the quality of the image has deteriorated due to acid diffusion into the unexposed regions of the film. The time between acid generation and obtaining the fluorescent images was approximately one hour, during which time the film was kept at room

temperature and MSA appears to have moved at least 7 μm. Initially, this result may seem incompatible with the fact that resists with much higher resolution are routinely prepared by the microelectronics industry. However, one must consider that MSA is not used as an acid in high resolution applications and that the experiments described here were performed in polymer films as opposed to actual resists which contain basic additives which slow acid movement, thereby preserving the integrity of the image.

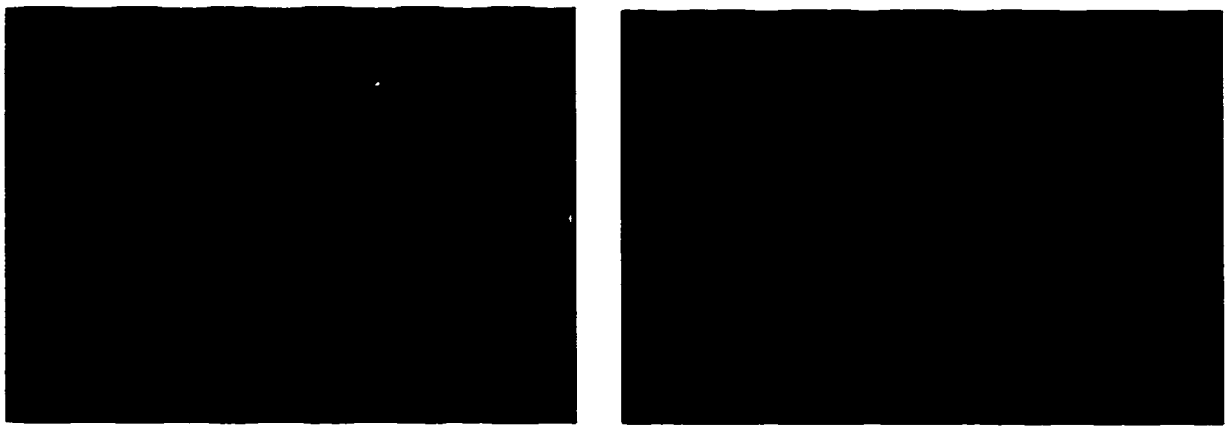

Figure 2-4 Fluoresence microscope images with 55 μm features of C1 in PVP films obtained upon photoacid generation with 2-1a at a dose of 1.1 mJ/cm² (a) and 33 mJ/cm² (b).

2.2.2.2 Fluorescence Spectroscopy

Diffusion of acid within imaged films can also be monitored by measuring the overall fluorescence of the film by standard fluorescence spectroscopy. Extraction of information about the image is possible because the fluorescence of the neutral form of C1 can be monitored without contribution from the fluorescence of the protonated form. As shown schematically in Figure 2-5, the fluorescence of a film exposed through a grating reticle is 1/2 that of an unimaged film, in which the entire film is fluorescent. As acid diffuses into unexposed regions, fluorescence from

these regions decreases so that the overall fluorescence of the film decreases. As in the case of the microscopy measurements, this experiment requires generating sufficient amounts of acid so that exposed regions do not experience an increase in fluorescence as acid diffusion occurs. This spectroscopic technique complements that of fluorescence microscopy because it allows for quick evaluation of image quality without requiring the effort of actually acquiring the image.

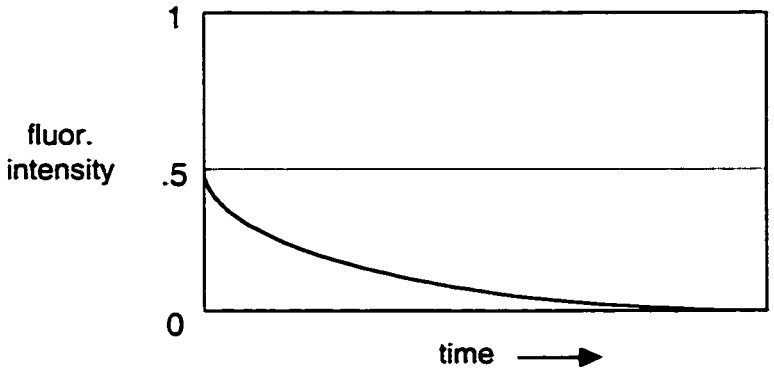

Figure 2-5. Schematic representation of the fluorescence intensity of an imaged film decreasing as acid diffuses into unexposed regions of the film.

From Figure 2-3, a dose above 20 mJ/cm^2 for PAG **2-1a** and above 60 mJ/cm^2 for PAG **2-1b**, should generate enough acid to completely quench the fluorescence of the neutral form of C1. However, films imaged using a grating reticle with 1 μm features with PAG **2-1a** at 22 mJ/cm^2 and **2-1b** at 66 mJ/cm^2 gave markedly different fluorescence intensities (Figure 2-6). When CSA was the acid generated, the fluorescence intensity was ~50% of an unirradiated sample, as expected, while the MSA sample had less than 10% of the intensity of the unirradiated sample. Apparently, when CSA is used to generate images in PVP films the diffusion of the acid is minimal at room temperature; thereby allowing sufficient amounts of acid to be generated to completely protonate all of the C1 in exposed regions without having acid migrate into unexposed regions. On the contrary, the diffusion of MSA is facile enough that a 1 μm image is severely

degraded over the 5 minute period between generation of acid and acquisition of the fluorescence spectrum. In fact, a film containing PAG **2-1a** which was exposed with a dose of 66 mJ/cm^2 was entirely non-fluorescent, indicating destruction of the image due to extensive MSA diffusion.

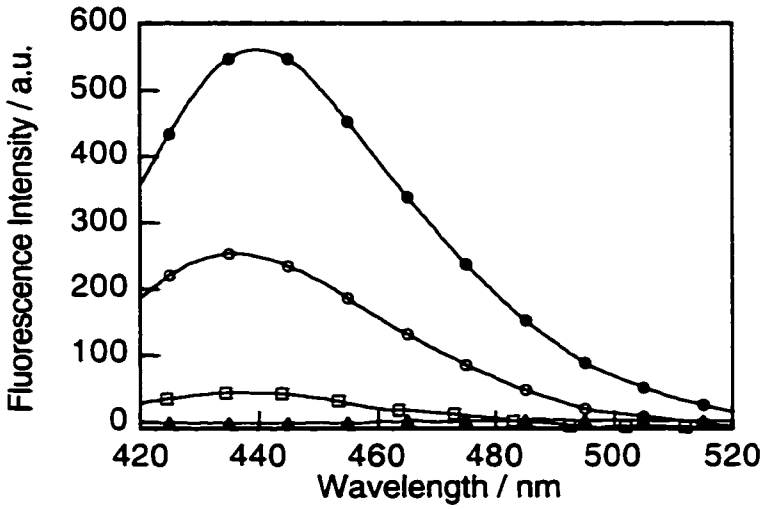

Figure 2-6. Fluorescence spectra of C1 in PVP films imaged using a grating reticle with 1 μm lines and spaces (baseline subtracted). Unirradiated (●); 2-1b, 66 mJ/cm^2 (○); 2-1a, 22 mJ/cm^2 (□) and 2-1a, 66 mJ/cm^2 (▲).

2.2.3 Conclusions

Although changes in fluorescence intensity associated with acid diffusion were observed, it was difficult to work under the conditions described in Figures 2-2 and 2-5. This study was not pursued further because this field became flooded with researchers more motivated and better equipped to create and analyze imaged films. However, these researchers would be well-advised to exploit the aforementioned properties of C1 in subsequent acid diffusion studies.

2.2.4 Absorption Detection

Although fluorescence measurements are the preferred method for sensing acid in polymer films due to their sensitivity, absorption spectroscopy has also been

used in this lab as a means to study acid diffusion. For this purpose rhodamine B base (Rb) and coumarin 6 (C6) are the dyes primarily used. A description of C6 and its use as an acid sensor for monitoring acid desorption from polymer films appears in Chapter 3.

Rb is a xanthene dye which undergoes an opening of its lactone ring upon protonation (Scheme 2-3) or dissolution in protic solvents.[17,18] The absorption spectrum of protonated Rb shows a dramatic red-shift relative to its lactone form (Figure 2-7). This property, coupled with its high molar absorptivity ($\varepsilon = 1.16 \times 10^5$ $M^{-1}cm^{-1}$) and sensitivity to acid, has prompted the use of Rb as an acid sensor in non-aqueous media.[4,7,16]

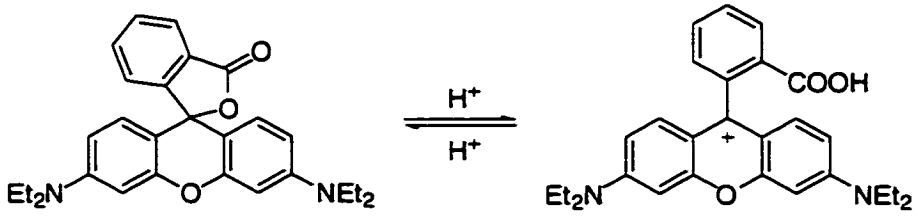

Scheme 2-3. The prototropic forms of Rb.

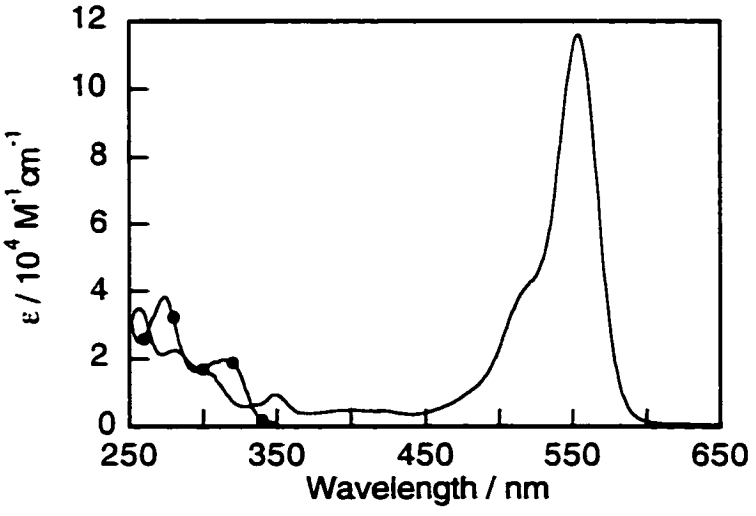

Figure 2-7. Absorption spectra of Rb in acetonitrile with and without (●) 10 mM MSA.

2.2.4.1 Laser Flash Photolysis[19]

Laser flash photolysis (LFP) is a technique that is used extensively in this lab and has been described many times over the years.[20-23] To avoid redundancy, only a brief overview is provided here. LFP involves using a pulsed laser to excite a sample, thereby generating an electronically excited state which sometimes behaves to yield other transient species. The duration of the laser pulse must be short (~10 ns) relative to the lifetime of these species in order to allow for their detection. Detection is accomplished by a monitoring light whose intensity is measured by a photomultiplier tube before and after the laser pulse. In this way, changes in absorptivity of the sample (ΔO.D.) due to depletion of the ground state and creation of transient species is measured. Both kinetic and spectral data are thus acquired. This technique is used as a tool for studying the mechanisms of photochemically initiated reactions.

LFP was employed here to study the reaction between a photogenerated acid and a basic dye, Rb, in a poly(methyl methacrylate) (PMMA) film. This was accomplished by generating acid via laser excitation of a PAG and monitoring the absorbance change due to the formation of protonated Rb. Several processes could potentially control the rate of the growth of this signal. The rate at which the PAG generates acid upon laser excitation, diffusion of the acid and dye molecules together as well as the actual protonation, all need to be considered as potential rate-determining steps. Ultimately, it is the slowest of the three processes that will be rate-determining, and hence, measured experimentally. If the reaction is diffusion-controlled, the kinetics observed will provide information about the diffusional properties of the photogenerated acid.

Preliminary experiments in solution were performed in order to gain insight into the reaction kinetics under conditions in which diffusion is considerably faster than in polymers. In acetonitrile, the rate of formation of protonated dye was found

to be ~2-3 x 10^9 $M^{-1}s^{-1}$ for a variety of different PAGs. These values indicate that the diffusion of the acid and the dye together is not the rate-limiting process as the diffusional limit in acetonitrile is 2 x 10^{10} $M^{-1}s^{-1}$. Hence, the rate-limiting process in solution is either generation of acid or protonation of the dye.

Work in PMMA films began with the assumption that in the more organized medium of the polymer film, the diffusion of the acid would be slowed to a greater extent than the other two processes, thereby allowing diffusion to take over as the rate-limiting process. PAGs **2-2**[24] and **2-3**[25] (Scheme 2-4) were used to generate trifluoromethanesulfonic acid and hydrochloric acid respectively. It was expected that these two acids would diffuse with differing rates and that this would be reflected in the kinetics measured. Briefly, the experiment involves preparing PMMA films with enough PAG to give an absorbance of ~0.1 at the excitation wavelength (308 nm) and a variety of different Rb concentrations. The film is mounted in the path of the laser and the growth of the signal due to protonated Rb is monitored at 520 nm after each laser pulse. Typical results from such an experiment appear in Figure 2-8.

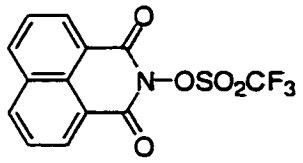

2-2

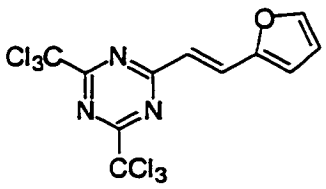

2-3

Scheme 2-4. PAGs used to generate acid in polymer films.

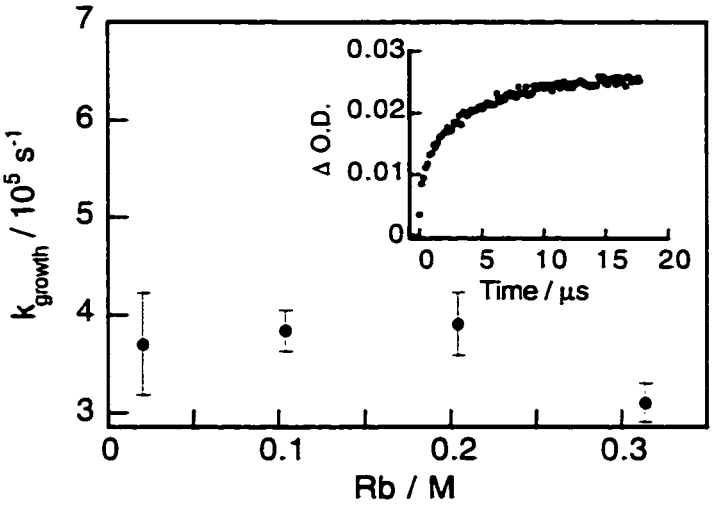

Figure 2-8. ***Pseudo*** **first-order rate constants for the growth of protonated Rb as a function of Rb concentration. Acid is generated from PAG 2-2 in PMMA films. Error bars represent the std. dev based on 3 separate measurements. Inset: Typical growth trace of protonated Rb at 520 nm.**

The most noteworthy aspect of these experiments is that bimolecular rate constants could not be obtained for the reaction between acid and Rb because the observed kinetics were unaffected by the concentration of Rb (Figure 2-8). It appears that under these experimental conditions the Rb concentration is so high relative to the acid concentration, even for the lowest Rb concentration sample, that acid is completely surrounded by Rb molecules immediately upon its generation. Increasing the Rb concentration does not change the amount of Rb immediately surrounding the acid and therefore cannot affect the rate of the reaction. Although lower Rb concentrations would alleviate this problem, it is not a practical option because of the accompanying decrease in signal strength which would occur.

In light of these limitations, one is forced to interpret the *pseudo* first-order rate constants obtained, 3.8 x 10^5 s^{-1} for PAG **2-2** and 2.1 x 10^6 s^{-1} for PAG **2-3**. The relative magnitudes of these rate constants are consistent with the expected diffusional properties of the acids generated, i.e., trifluoromethanesulfonic acid being slower than hydrochloric acid due to its greater bulk. Unfortunately, it is unclear

whether these numbers reflect a difference in diffusional behaviour of acid or in rates of acid generation.

2.2.4.2 Steady-State Absorption Spectroscopy

Acid detection in polymer films was also accomplished by steady-state absorption spectroscopy with C6 as the dye. This technique was used as a tool for measuring acid desorption from films. This is also an important parameter in resists because if extensive acid diffusion occurs, acid can escape the film. This technique was employed in an extensive study of the factors affecting acid desorption and the experimental details and results appear together in Chapter 3.

2.2.5 Conclusions

Acid diffusion studies using LFP were discontinued due to the aforementioned difficulties in extracting unambiguous kinetic data. However, the use of LFP in conjuction with Rb has proven useful for the detection of photogenerated acid in polymer films, if not acid diffusion itself. This technique could conceivably be used to study acid generating efficiencies of PAGs in polymer films. However, over the course of this work, the use of LFP with solution samples has been favoured (see Section 2.3.2) because of convenience in sample preparation and in performing the experiment.

2.2.6 Experimental

2.2.6.1 Materials

All PAGs and the PVP polymer were obtained from Shipley Co. and used as received. C1 was used as received from ACROS. Rb was obtained from Aldrich and purified by column chromatography on silica gel (230-400 mesh) using acetone as eluent. OmniSolv grade solvents were used for spectroscopic measurements

and were used as received from VWR. All other chemicals were used as received from Aldrich.

2.2.6.2 Preparation of Thin Polymer Films

Thin polymer films were spin coated at 3000 rpm for 20 s onto 2.5 cm diameter quartz disks using an Integrated Technologies Inc. P-6000 spin coater. A stock solution of 25 wt% PVP in 2-methoxyethyl ether was used to make all coating solutions. Coating solutions were 1 mM/0.12 wt% C1 and 55 mM/7.6 wt% of PAG **2-1a** or 55 mM/14.5 wt% PAG **2-1b** in the aforementioned stock solution. The concentration of dye and PAG are given as the concentrations in the solutions used for spin coating, not in the resulting polymer film. When wt% are also stated, they are given relative to the solids in the spin coating solution.

The quartz disks were cleaned with dichloromethane and dried with a heat-gun immediately prior to spin coating. This step is a very important final step in cleaning because dichloromethane evaporates to leave very little residue on the film and the moving air from the heat gun tends to remove dust and small particles from the disk. The actual spin coating involves placing a ~0.3 mL aliquot of the spin coating solution in the center of the quartz disk which has been placed in the spin coater. After spinning, the films were 'soft-baked' at 90 °C for 5 min to remove any remaining solvent.

2.2.6.3 Fluorescence Measurements in Thin Polymer Films

The thermal stability and photostability of C1 were established by heating PVP films containing dye at 150 °C for 60 s and exposing with a Hg/He arc lamp using a 250 nm interference filter at 250 mJ/cm^2, respectively. Fluorescence measurements using a Perkin-Elmer LS-50 luminescence spectrophotometer before and after confirmed lack of degradation.

Imaging of the films was done by placing a grating reticle with either 1 or 55 μm lines and spaces onto a spin coated film and exposing to the light from a Hg/He arc lamp using a 250 nm interference filter. Appropriate exposure times were determined by exposing unmasked samples and measuring the fluorescence intensity of the sample. A Zeiss Axiophot fluorescence microscope was used to observe the created image with a filter which allows excitation of C1 at ~365 nm and emission to be measured above 400 nm. Images were captured using a Hamamatsu digital camera and analyzed using MetaMorph from Universal Imaging Corp.

It should also be noted that it was found to be important to protect the film by placing another quartz disk on top of it and wrapping in teflon tape so as to prevent acid desorption from the film.

2.2.6.4 Laser Flash Photolysis in Thin Polymer Films

For the laser flash photolysis studies conducted on polymer films, a Lumonics EX-530 excimer laser (Xe/HCl, 308 nm, ~6 ns pulse width, 50-100 mJ/pulse) and the third harmonic of a Surelite Nd:YAG laser (355 nm, ~6 ns pulse width, ≤20 mJ/pulse) were used for the excitation. Other lasers available in this lab which are used in other LFP studies include: a Surelite Nd:YAG laser (266 nm, ~6 ns pulse width, ≤ 20 mJ/pulse) and a Molectron UV-24 nitrogen laser (337.1 nm, ~8 ns pulse width, 5 mJ/pulse). The system is controlled by a Power Macintosh computer running LabVIEW 3.1.1 software (National Instruments). A Tektronix 2440 digital oscilloscope is used to capture and digitize the signal from the photomultiplier tube. Further details of a similar laser system have been provided elsewhere.[20,21]

Polymer film preparation was done as described in Section 2.2.6.2 with the only change being that, quartz disks 10 cm in diameter which require ~5 mL of solution for coating, were used for these experiments. Spin coating solutions were

prepared from a stock solution of 15 wt% PMMA in 2-methoxyethyl ether. PAGs were added to the solution so as to give an absorbance of ~0.1 at the excitation wavelength. In order to perform measurements on thin polymer films the disks were mounted in a stepper-motor driven holder which moved the disk a determined distance between laser pulses. This ensured that each laser pulse reaches a fresh portion of the film. PAG/dye samples for the work in films and in solution were prepared in the dark so as to avoid premature formation of acid. During actual measurements, samples were protected from stray light from the monitoring beam so that no acid was photogenerated prior to the laser pulse.

2.3 Acid Detection in Solution

2.3.1 Introduction

Most mechanistic studies on PAGs performed in this lab begin, in some way or another, with an evaluation of a PAG's acid generating efficiency. Ideally, this takes the form of a quantum yield of acid generation (Φ_{acid}) determination, as defined by the following expression:

$$\Phi_{acid} = \text{number of acid molecules generated / number of photons absorbed}$$

Such an experiment is performed using relative actinometry with a standard PAG serving as a chemical actinometer. Alternatively, rapid screening of PAGs usually involves determination of a relative acid generating efficiency and employs a benchmark PAG for comparison. Both of these types of measurements are exclusively performed in solution both because of the ease of performing the experiments relative to measurements in polymer films and for comparison with other experiments such as product studies or LFP which are also performed in solution. For these types of experiments absorption is preferred over fluorescence detection because absorption measurements are more simple to perform and do not require an external calibration for quantification.

2.3.2 Laser Flash Photolysis

The Φ_{acid} experiments performed using LFP are similar to the acid diffusion studies described in the previous section in that they too are based on the protonation of Rb by a photogenerated acid. This technique was originally developed in this lab by Pohlers et al.[7] but was not used extensively by other workers in this lab until the beginning of the work described in this thesis. In the original work, laser irradiation was performed exclusively at 308 nm in which 2,4-

bis(trichloromethyl)-6-methyl-5-triazine (MTT) was used as an actinometer for which $\Phi_{acid} = 0.4$. In subsequent studies the use of 266 nm was required, necessitating a recalibration of MTT at this wavelength by a previously described technique.[25] This technique is based on the quantitative trapping of $Cl^{\bullet}$ radicals produced upon photolysis of MTT in the presence of Cl^- anions and subsequent detection of the $Cl_2^{\bullet-}$ complex.[26] Triplet benzophenone formation[27] in acetonitrile was used as an actinometer for this calibration with 266 nm laser excitation, quantum yield of triplet formation of 1.0.[28] The value obtained for Φ_{acid} of MTT at 266 nm was 0.28.[24]

Performing a Φ_{acid} experiment involves preparing optically matched solutions of the actinometer and the PAG to be studied in acetonitrile, with each solution containing 10 μM Rb. Laser excitation generates acid and the signal due to protonated Rb is monitored at 555 nm; the intensity of which is dependant on the amount of acid generated. A typical experiment is shown in Figure 2-9 in which the growth of the Rb signal is monitored at a variety of different laser powers. Measuring the power dependance on both samples allows for creation of a power dependance plot of ΔO.D. (inset: Figure 2-9) from which the Φ_{acid} of the PAG can be determined using the following expression:

$$\Phi_{acid(PAG)} = \Phi_{acid(actinometer)}(slope_{PAG} / slope_{actinometer})$$

This technique has been used repeatedly in this work to evaluate the Φ_{acid} of PAGs. Mechanistic insight from these experiments comes from comparisons of Φ_{acid} under a variety of different conditions such as: O_2 or N_2-saturated solution, in the presence of additives such as nucleophiles or hydrogen donors.

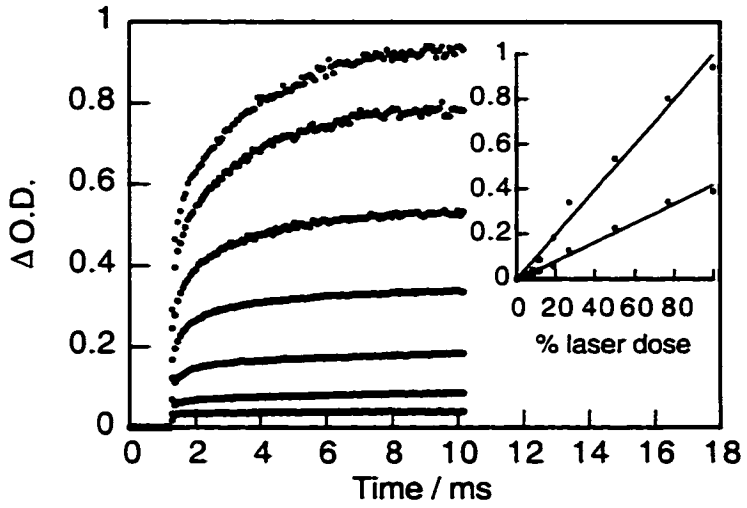

Figure 2-9. **ΔO.D. at 555 nm due to protonation of Rb in acetonitrile by acid photogenerated from MTT at 266 nm, measured at various laser powers. Inset: Power dependance of ΔO.D. for MTT (●) and *di-p*-toluene-α-disulfone (○).**

2.3.3 Steady-State Absorption Spectroscopy

Acid generating efficiencies of PAGs can also be determined via experiments in which Rb is not present during the irradiation but is added after acid generation and measurement occurs using a conventional spectrophotometer. This avoids concerns associated with Rb absorbing some of the incident light and does not involve such a labor-intensive and time-consuming technique as LFP. As such, this method is more suitable for quick screening of PAG behaviour, so the chemical actinometry is omitted in favour of simply comparing a series of PAGs.

A series of optically matched PAG solutions are prepared and irradiated using either low pressure mercury lamps or a laser source. In these experiments one is able to operate in any concentration range as long as appropriate care has been taken to optically match the samples at the excitation wavelength. Samples are still optically matched despite not using an actinometer and hence not determining the actual Φ_{acid}. This is done so that the acid generating efficiencies for

a series of PAGs will be 'relative Φ_{acid}' which are related to the 'absolute Φ_{acid}' (previously referred to only as Φ_{acid}), for the same series by some multiplier. Thus, if one is interested in the amount of photoacid generated by a certain PAG compared to another PAG as opposed to how efficiently a PAG converts photons into acid, these measurements are satisfactory.

After irradiation, two different approaches can be taken: add an aliquot of Rb directly to the irradiated sample or add an aliquot of the irradiated sample to a solution of Rb. The appropriateness of each procedure depends upon the amount of acid generated during PAG photolysis. The final Rb concentration in both samples must be 10-20 μM and acid concentrations in excess of that of Rb must be avoided. Thus, at low PAG conversions, the first method should be used and at higher PAG conversions, the latter is preferred. The latter method is slightly more cumbersome in that it involves using different cells for irradiation and measurement but it does allow for the irradiation of the same sample many times with removal of the appropriate aliquot after each time interval.

This technique was found to be quite general because the response of Rb absorbance at 555 nm to known quantities of acid was found to be linear at all acid concentrations and a variety of Rb concentrations used. Importantly, the Rb was found to react with *p*-toluenesulfonic acid (a sulfonic acid of intermediate acid strength) in a one to one ratio, suggesting that for a group of sulfonic acids of differing acid strengths, measurements can be compared because the extent of Rb protonation is the same.

Results of a typical experiment using laser irradiation at 193 nm appear in Table 2-1. Since these measurements involve irradiation of a variety of different types of PAGs (abs.> 2, 50-600 μM), cyclohexane (40 μM) and water (400 μM) were added to the acetonitrile solutions to serve as a hydrogen donor and nucleophile,

respectively, in case any of the photoacid generation mechanisms require reactions with these substrates. These results are singled out for inclusion here because the microelectronics industry is currently evaluating materials for the development of resists for use at 193 nm.

Table 2-1. Relative Φ_{acid} for a series of PAGs using 193 nm laser irradiation.

PAG	Relative Φ_{acid} at 193 nm
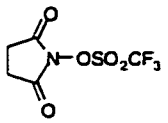	1.5
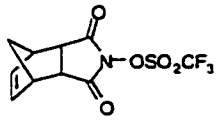	1.4
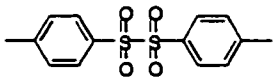	1.4
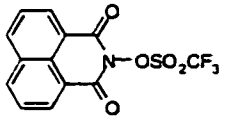	1.3
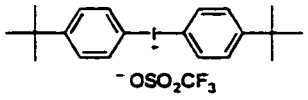	1.2
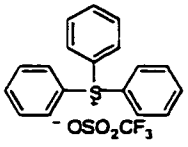	1.0[a]
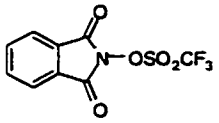	0.76
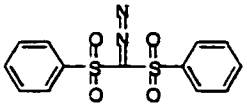	0.50
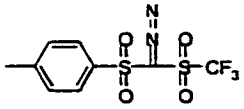	0.42

[a]all values normalized to this value

Under some circumstances it is desirable to perform the acid generation in a polymer film but actually measure the amount of acid in solution. This task is easily done by preparing PAG containing polymer films, as previously described, and irradiating them in a photoreactor. Dissolution of this film in acetone followed by addition of an aliquot of an Rb solution such that the final Rb concentration is 10-20 μM gives a solution that can be measured in the usual way.

2.3.4 Conclusions

The various methods for measuring the acid generating efficiency of a PAG using Rb are employed extensively throughout this thesis. Although these measurements are critical to mechanistic PAG studies one must try to avoid losing sight of the fact that they are merely the tools used to investigate the phenomenon of actual interest. As such, subsequent chapters lack lengthy discussions concerning the manner in which acid generation is measured in favour of focusing on the underlying PAG photochemistry.

2.3.5 Experimental

2.3.5.1 Materials

All PAGs, except MTT, were obtained from Shipley Co. and used as received. MTT was purchased from Panchim and purified by recrystallization from methanol (2 times) and subsequent sublimation. Potassium iodide (99%), potassium iodate (99.5%), sodium tetraborate decahydrate (≥ 99.5%) and *p*-toluenesulfonic acid monohydrate (98.5%) were obtained from Aldrich and used as received. OmniSolv grade solvents were used for spectroscopic measurements and were used as received from VWR.

2.3.5.2 Laser Flash Photolysis in Solution

Usage of the LFP system with polymer films was described in Section 2.2.6.4, here is provided details relevant to the use of solution samples. In order to perform a Φ_{acid} experiment, solutions of the PAG to be studied and the actinometer were optically matched to within 5 x 10^{-3} absorbance units at the excitation wavelength. Typically, acetonitrile solutions were matched at an absorbance of ~1 in a 7x7 mm cell. Each solution was diluted by a factor of 2 with a 20 μM Rb, 1 M 2-methoxyethyl ether, acetonitrile solution. Therefore, the actual solution used for the experiment contained 10 μM Rb with 0.5 M 2-methoxyethyl ether and gave an absorbance of ~0.5 at the excitation wavelength. The dilution factor was not critical to the experiment as long as all of the samples are diluted in the same manner. At least 250 mL of each solution was required to perform a thorough Φ_{acid} experiment.

The optical matching of samples was complicated by the fact that Rb absorbs some of the incident light when wavelengths below 355 nm are used. Generally, this was not a problem because both the sample and the actinometer contain the same amounts of Rb and are therefore 'filtered' to the same extent, and remained optically matched. Real concern came from samples which are contaminated by residual acid which protonates Rb prior to laser excitation and turns the solution slightly pink. Since this effect was likely not the same for both actinometer and sample, it was very important to avoid contamination by purifying the PAGs and using clean solvents and glassware. In actual practice, this effect was not as detrimental to an experiment as one might expect because at both 266 and 308 nm, the molar absorptivities of Rb and protonated Rb are very similar, so that solutions containing various ratios of both, do not greatly affect the amount of light available to the PAG.

Once the samples were prepared, they were degassed with N_2 for 30 minutes in a 500 mL reservoir connected by means of Teflon tubing to a 7x7 mm fused silica

flow cell. The flow technique was employed in order to allow irradiation of a fresh portion of the sample, thereby avoiding accumulation of photoproducts (mainly protonated Rb). While the flow technique is commonly used in LFP studies, it was never more important than in these experiments. The protonated Rb formed from each laser shot must be completely removed from the sample window prior to the next laser shot in order to obtain meaningful data. For this reason the tap which controls flow was completely opened to allow maximum flow of solution (>100 ml/min). In order to conserve solution, the flow was stopped during the delays in laser shots created by saving the data files on the computer.

2.3.5.3 Absorption Detection in Solution

Ground state absorption spectra were recorded using a Varian Cary 1E spectrophotometer. Typically, 7x7 mm quartz cells were employed in these experiments.

Irradiations were performed in a photoreactor equipped with either RPR-2540, RPR-3000 or RPR-3500 lamps and rotated by means of a "merry-go-round" apparatus to ensure that all the samples received the same irradiation dose. While these lamps are not monochromatic, the bulk of the light emitted from them is at 254, 300 and 350 nm, respectively. Irradiations ranged from 5 seconds to several minutes, depending on the absorbance of the sample and the number of lamps employed. Irradiations were also performed with 1-5 pulses from a EX-530 excimer laser (Ar/F 193 nm, 50-100 mJ/pulse). Limiting the number of shots taken eliminates much of the scatter associated with variations in the power of each laser shot which hampered earlier attempts to take these kinds of measurements

Absorbance values of each acetonitrile solution of PAG were carefully matched in order to have differences in absorbance within 5×10^{-3}. Normally, 2 mL of a PAG solution was irradiated followed by addition of 20-40 µl of a stock 1 mM Rb

solution and the absorbance measured in the same cell. Alternatively, a 100 μL aliquot of the irradiated sample was added to 2 mL of a 10-20 μM Rb solution. In these ways, Rb concentrations in the final solutions were kept at 10-20 μM so that the maximum absorbance in a 7x7 mm cell is less than 2, ensuring a linear response of the instrument.

Chemical actinometry was also used to determine Φ_{acid} using steady-state irradiations performed in a photoreactor equipped with RPR-2540 lamps. The actinometer consists of a solution of 0.5-0.6 M potassium iodide and 0.1 M iodate in 10 mM borate buffer, quantum yield = 0.75.[29] After irradiation, the formation of triiode was monitored at 472 nm (ε_{472}= 595 $cm^{-1}M^{-1}$) in a spectrophotometer. This actinometer was used extensively to evaluate the PAGs described in Chapter 4.

2.4 Conclusions

The use of a variety of different methods for the detection of acid in non-aqueous environments have been discussed. While all methods are similar in that they employ an acid-sensitive dye for acid detection, they differ greatly in their application to the study of photolithographic processes. Experiments in polymer films are performed in studies related to acid diffusion, while solution measurements are preferred for studying PAG photochemistry. The details of such experiments are presented in sufficient detail to allow future workers to conduct experiments in this area with only this chapter as a reference.

2.5 References

(1) Thackeray, J. W.; Denison, M. D.; Fedynyshyn, T. H.; Kang, D.; Sinta, R. *ACS Symposium. Series* **1995**, *614*, 110.

(2) Kim, J.-B.; Kwon, Y.-G.; Choi, J.-H.; Jung, M.-H. *Proc. SPIE* **1999**, *3678*, 546.

(3) Cameron, J. F.; Ablaza, S. L.; Xu, G.; Yueh, W. *Proc. SPIE* **1999**, *3678*, 785.

(4) Cameron, J. F.; Fradkin, L.; Moore, K.; Pohlers, G. *Proc. SPIE* **2000**, *3999*, 190.

(5) Houle, F. A.; Hinsberg, W. D.; Morrison, M.; Sanchez, M. I.; Wallraff, G.; Larson, C.; Hoffnagle, J. *J. Vac. Sci. Technol. B* **2000**, *18*, 1875.

(6) Pohlers, G.; Virdee, S.; Scaiano, J. C. *Chem. Mater.* **1996**, *8*, 2654.

(7) Pohlers, G.; Scaiano, J. C.; Sinta, R. *Chem. Mater.* **1997**, *9*, 3222.

(8) Zhang, P. L.; Eckert, A. R.; Willson, C. G.; Webber, S. E.; Byers, J. *Microlithography 1997: Advances in Resist Technology and Processing XIV, Proceedings of SPIE* **1997**, *3049*, 898.

(9) Zhang, P. L.; Webber, S.; Mendenhall, J.; Byers, J.; Chao, K. *Proc. SPIE.* **1998**, *3333*, 794.

(10) Lu, B.; Taylor, J. W.; Cerrina, F.; Soo, C. P.; Bourdillon, A. J. *J. Vac. Sci. Technol. B* **1999**, *17*, 3345.

(11) Jessop, J. L.; Goldie, S. N.; Scranton, A. B.; Blanchard, G. J.; Rangarajan, B.; Okoroananwu, U.; Subramanian, R.; Templeton, M. K. *Proc. SPIE* **2000**, *3999*, 161.

(12) Feke, G. D.; Grober, R. D.; Pohlers, G.; Moore, K.; Cameron, J. F. *Anal. Chem.* **2001**, *73*, 3472.

(13) Bukofsky, S. J.; Feke, G. D.; Wu, Q.; Grober, R. D.; Dentinger, P. M.; Taylor, J. W. *App. Phys. Lett.* **1998**, *73*.

(14) Dentinger, P. M.; Bing, L.; Taylor, J. W.; Bukofsky, S. J.; Feke, G. D.; Hessman, D.; Grober, R. D. *Triple Beam Conference* **1998**, 1.

(15) Feke, G. D.; Hessman, D.; Grober, R. D.; Lu, B.; Taylor, J. W. *J. Vac. Sci. Technol. B* **2000**, *18*, 136.

(16) Virdee, S. M.Sc. Thesis, University of Ottawa, 1998.

(17) Zanker, V.; Peter, W. *Ber.* **1958**, *91*, 572.

(18) Ramette, R. W.; Sandell, E. B. *J. Am. Chem. Soc.* **1956**, *78*, 4872.

(19) These experiments were performed with the aid of Nicole Deschamps, an undergraduate student at McMaster University, while she worked in our labs for 4 months as part of the Reactive Intermediates Student Exchance (RISE) program.

(20) Scaiano, J. C. *J. Am. Chem. Soc.* **1980**, *102*, 7747.

(21) Scaiano, J. C.; Tanner, M.; Weir, D. *J. Am. Chem. Soc.* **1985**, *107*, 4396.

(22) Scaiano, J. C. *Laser Photolysis in Polymer Chemistry*; Jellinik, H. H. G., Ed.; Elesevier: New York, 1989; Vol. 2, pp 1-41.

(23) Berinstain, A. Ph.D. Thesis, University of Ottawa, 1997.

(24) Ortica, F.; Scaiano, J. C.; Pohlers, G.; Cameron, J. F.; Zampini, A. *Chem. Mater.* **2000**, *12*, 414.

(25) Pohlers, G.; Scaiano, J. C.; Sinta, R.; Brainard, R.; Pai, D. *Chem. Mater.* **1997**, *9*, 1353.

(26) Nagarajan, V.; Fessenden, R. W. *J. Phys. Chem.* **1985**, *89*, 2330.

(27) Bensasson, R. V.; Gramain, J. C. *J. C. S. Faraday I* **1980**, *76*, 1801.

(28) Haselbach, E.; Vauthey, E.; Suppan, P. *Tetrahedron* **1988**, *44*, 7335.

(29) Rahn, R., O. *Photochemistry and Photobiology* **1997**, *66*, 450.

3. An *In Situ* Method for Measuring Acid Desorption from Polymer Films

3.1 Introduction

As the feature size in photolithography decreases in response to the demand for higher performance semiconductor devices, issues related to acid diffusion and acid desorption become more important. The role of photogenerated acid in the photolithographic process was discussed in Chapter 1 and will be mentioned only briefly here. Lateral diffusion of acid can compromise image definition as acid moves into unexposed regions of the chemically amplified resist (CAR).[1] Extensive diffusion of acid within a CAR can potentially lead to acid desorption from the surface of the resist. Loss of acid in this way not only lowers the amount of acid available to initiate the desired cross-linking or deprotection reactions, but also contributes to the formation of undesirable structures at the surface of CARs due to the formation of concentration gradients.[2-6] Thermal processing conditions, i.e., the post-exposure bake (PEB), for CARs must be carefully chosen to allow sufficient diffusion of the acid to catalyze the aforementioned reactions, while minimizing long-range diffusion and surface desorption.

Much work within the photolithographic community has been done to gain insight into the factors which control acid mobility in CARs as well as to quantify said mobility. Although a number of different strategies have been employed for these purposes, they can be loosely grouped into two categories: those which measure the abundance/location of acid directly and those which attempt to accomplish this indirectly. The former type includes techniques which determine the amount of acid in resists via ion-conductivity measurements,[7-9] or with an acid sensitive dye.[7,10-13] These dyes are also used to create latent images of photogenerated acid, from which one can obtain information about the location of acid within a resist.[11,14-16] The latter category involves extracting information after the development of a resist image, using scanning electron microscopy,[8,17-19] infrared red spectroscopy,[20,21] film thickness measurements[12,20] and dissolution rate monitoring.[22] This strategy is

described as 'indirect' because the appearance of developed CAR images is not only a function of acid mobility. Resist chemistry and development conditions also affect these images, and results must be interpreted accordingly.

Collectively, these techniques have allowed insight into many of the factors which control acid mobility in resist films. PEB temperature and duration,[9,10] acid structure[7,11,23] basic additives[12,22] as well as properties of the polymer including: residual casting solvent,[17] polydispersity,[19] phenolic groups,[8,18] and free volume,[13,24] have all been implicated in controlling acid diffusion.

Despite all of the work that has accumulated in the literature on this topic it is difficult to form a unified picture of acid mobility in CARs. The difficulty arises from the fact that most techniques are time-consuming and labor intensive so as to limit one's ability to perform a detailed study involving manipulation of many experimental parameters. The result is that most work involves studying acid mobility from a single photoresist or polymer under a certain set of conditions while perhaps varying a single experimental parameter such as PEB. If one wants to compare the effects of multiple factors on diffusional processes, one must compare results from different authors, using different techniques, obtained under different conditions. A more desirable situation is one in which a technique is simple enough to allow many experiments to be performed under a variety of conditions so that the effect of a variety of factors on diffusional processes can be compared in a more direct manner.

In an attempt to address the issue of acid desorption during PEB conditions, we have developed an *in situ* method for monitoring acid movement out of polymer films. The basis for this method is a dye, coumarin 6 (C6) whose acid-base properties[25] and utility as an acid sensor in polymer films have been demonstrated

previously.[26] The use of dyes for the purpose of detecting acid in polymer films is well established and was discussed extensively in Chapter 2.

The study of acid desorption from polymer films using acid sensitive dyes has been previously explored. Kim et al. measured acid desorption from one polymer film by trapping it with another dye-containing film.[12] The data obtained was interpreted qualitatively because only one measurement under a single set of PEB conditions was obtained. Thackeray et al. monitored acid desorption from polymer films by photogenerating acid in the films and extracting each film into a dye-containing solution after a PEB.[10] It is difficult and tedious to get detailed acid desorption data using this method because multiple extractions are required in order to obtain quality data. An adaptation of this method is described here, in which a dye and an acid are incorporated into a thin polymer film on a quartz disk and heated in an oven which is mounted in an absorption spectrophotometer, thereby allowing *in situ* absorption measurements. In this way, as acid leaves the film, the absorption of the film changes and well-defined acid desorption plots can be obtained. A schematic of the experiment is shown in Figure 3-1.

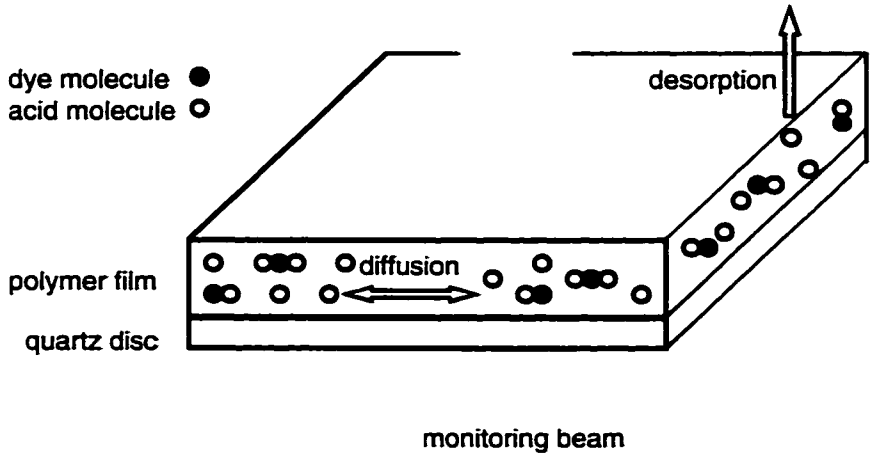

Figure 3-1. A schematic representation of the *in situ* technique used to study acid desorption from polymer films.

In order to determine the nature of the process which controls the rate of acid desorption from polymer films, the kinetics of acid desorption obtained using this *in situ* technique were compared to those obtained using the aforementioned spectrophotometric extraction method of Thackeray et al., as well as a technique designed to measure acid donation between two polymer films. For the most part, we adopt a phenomenological approach to our study of the acid desorption process. Simply put, the direct observation of acid escaping a polymer film allows us to measure the kinetics for this process and acquire predictive sets of data. However, we do indulge in some interpretation of these results; the quality of such speculations does not negate the validity of the data itself.

3.2 Results and Discussion

3.2.1 Suitability of Coumarin 6 as a Probe for Measuring Acid Desorption

The structure of the various prototropic forms of C6 and their absorption spectra are shown in Scheme 3-1 and Figure 3-2, respectively. The absorbance of the monoprotonated form is red-shifted relative to that of the neutral form and that of the diprotonated form is blue-shifted relative to that of the neutral form. The response of C6 to changes in acid concentration, as measured by the absorbance of the monoprotonated form at 533 nm in a poly(vinylphenol) (PVP) film, are shown in Figure 3-3. In the presence of excess acid, diprotonated C6 is the dominant species and the absorbance at 533 nm is low.

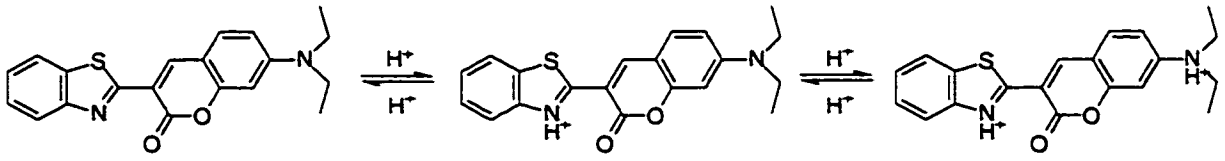

Scheme 3-1. The various prototropic forms of C6.

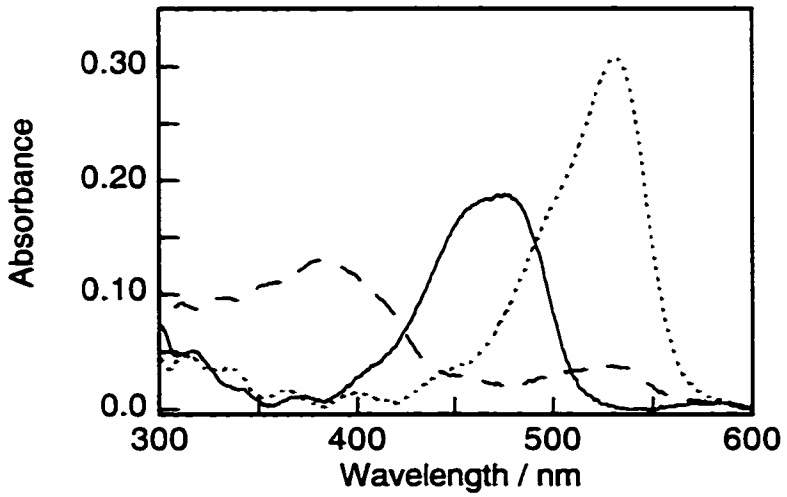

Figure 3-2. Absorption spectra of the prototropic forms of C6 (1 wt%) in PVP films: neutral (—), monoprotonated (---) and diprotonated (——).

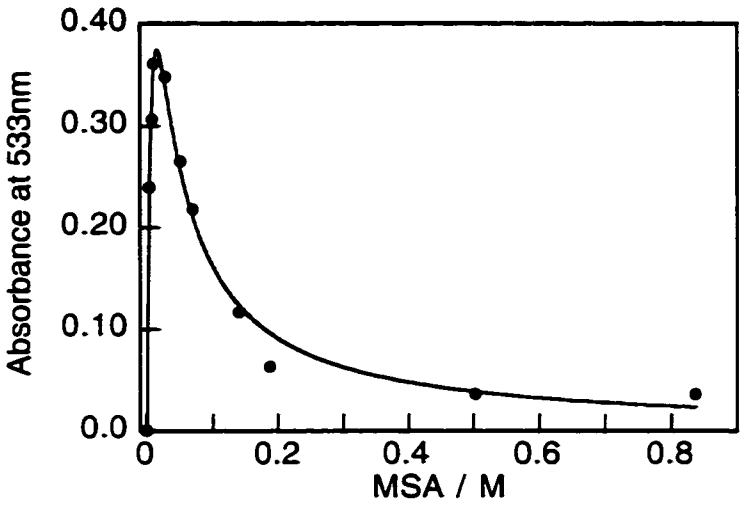

Figure 3-3. Absorbance of C6 (1 wt%) in PVP films with different concentrations of MSA.

In order to be useful in this application, a dye must not only be a thermally stable acid sensor, it must also be a sufficiently weak base so that it does not interfere with acid desorption from the film. A base which acts to anchor the acid in place is not a useful probe for studying acid mobility. C6 was used for these acid desorption studies because it has two protonation sites of different basicities. It was hypothesized that the monoprotonated form of C6 would be a sufficiently weak base that deprotonation of the diprotonated form should occur readily, so as not to anchor the acid. In order to prove this, the amounts of acid lost from dye-containing films were compared with the amounts lost from films without dye, using the aforementioned extraction method. Films containing C6 and methanesulfonic acid (MSA) were heated and, after cooling to room temperature, the absorbance measured and compared to the calibration curve (Figure 3-3), in order to determine the extent of acid desorption. Acid desorption from those films without C6 was measured via a spectrophotometric titration in which each film was heated and then extracted with a solution containing Rb. It was found that acid desorption from a film in which the monoprotonated form of C6 must be deprotonated is slowed down

because the dye is anchoring the acid within the film. However, when enough acid is present in the film to allow formation of diprotonated C6, acid desorption occurs much faster, and a close agreement was found for the amounts of acid lost from the films with and without dye. A direct comparison of MSA desorption from films of PVP2 (refer to Table 3-1 for description of the various PVP films employed) at 130 °C as measured by both methods is shown in Figure 3-4. The deprotonation of diprotonated C6 is facile enough that it does not control the rate of acid desorption and hence it serves as an innocuos probe. Figure 3-4 demonstrates an important point concerning the need for an *in situ* approach to measuring acid desorption; a critical kinetic analysis is impossible with so few data points.

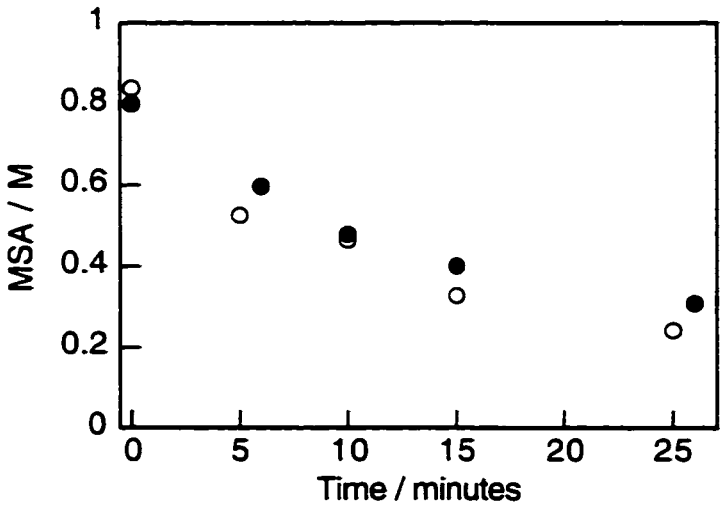

Figure 3-4. Comparison of the amount of MSA in films of PVP2 after heating at 130 °C via the extraction method (○) and the *in-situ* method (●).

3.2.2 Kinetic Treatment of Acid Desorption Data

In order for this method to be truly superior to the existing extraction method, the absorbance measurements must be performed *in situ*, while the film is being heated. In this way, many more measurements can be taken and at much shorter intervals, so that well-defined plots of acid desorption can be generated. The raw

data obtained when a film is heated inside the spectrophotometer cannot be directly converted into plots of acid desorption by comparison with Figure 3-3 due to absorbance changes which occur upon heating of the film which are due to factors other than acid desorption (see Experimental Section). Therefore, kinetic analysis of the data is performed over small changes in acid concentration in which the response of the absorbance of the dye to changes in acid concentration is assumed to be linear. Comparison with a calibration curve is not required because over such a small range, changes in the absorbance follow first-order kinetics, as described by the integrated first-order rate law: $A_t = A_i e^{-kt}$. Since acid concentration and absorbance are proportional over the region analyzed, acid desorption follows the same first-order kinetics. Typical kinetic fits for MSA at different temperatures are shown in Figure 3-5. Since the rate constants obtained are based on the data obtained over a small portion of an experiment a responsible interpretation involves acknowledging the assumption that the acid desorption behaviour in the first few moments of an experiment and at long time scales is well-described by the data at intermediate times.

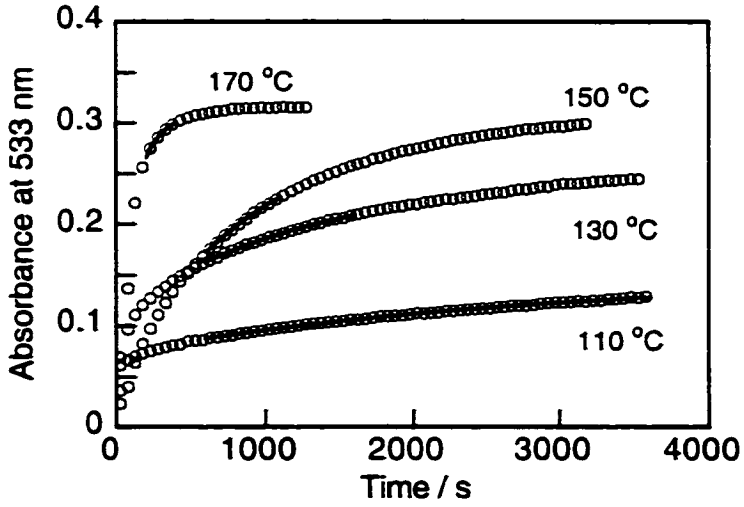

Figure 3-5. MSA desorption from films of PVP2 at different temperatures, as measured by the absorbance of C6 at 533 nm: 10% of the experimental data points (o) and first-order kinetic fits (—).

One of the implications of the fact that acid desorption obeys first-order kinetics is that the rate of acid desorption is described by the first-order rate law: rate = k[acid]. If required, the first-order rate law may be used to determine the rate of acid desorption at acid concentrations closer to those found in CARs.

3.2.3 Characterizing the Acid Desorption Process

In order to interpret the results of the acid desorption studies one must establish the nature of the acid desorption process. Clearly, diffusion of acid within the film and volatilization of the acid are both required for acid desorption to occur, but the extent to which either process is reflected in the observed kinetics is not obvious. Though the kinetics of sorption and desorption of gases and organic vapours in polymer films are controlled entirely by diffusion within the film,[27] it seems unreasonable to assume that evaporation of acids occurs without overcoming an additional activation barrier.

The fact that acid desorption is well described by first-order kinetics suggests that it is not controlled entirely by diffusion in the film because diffusion is typically described by more complicated kinetics.[27] Alternatively, the rate of acid evaporation from a polymer surface is a process which one might expect to have a simple dependance on acid concentration.[27]

Further evidence that acid desorption involves a surface phenomenon is provided by the results of acid donation experiments, which measure the rate of acid entering a PVP film. The data obtained using the acid donation technique results from acid entering a dye-containing PVP/acceptor film from a poly(acrylic acid) (PAA)/donor film and protonating the dye. This general strategy, i.e., using donor and acceptor films, has been used by others in acid diffusion studies.[12,22,28,29] The experiment and the kinetic analysis are performed in much the same manner as for an acid desorption experiment. However, for acid donation, the increase in the

absorbance of the monoprotonated form of C6 is monitored as acid enters the film and protonates the neutral form of the dye. Once again, the data follows first-order kinetics but gives much faster rate constants than those obtained in the acid desorption studies. That the acid movement again exhibits first-order kinetics suggests that it is controlled by a surface effect, either in exiting the donor or entering the acceptor film. This is consistent with the fact that if acid desorption is governed by some type of surface phenomenon, it should be faster for this approach than in the acid desorption studies because here volatilization of the acid is not required. In both studies, the rate of acid diffusion in the PVP films is the same because the composition of the films are the same as well as the temperature for the experiments. Given that the kinetics observed are not the same, at least one of the methods is not monitoring absorption changes due solely to acid diffusion. The expected relative magnitudes of any surface effects, coupled with the observation that the kinetics for acid desorption are slower than for acid donation, effectively eliminate the possibility that diffusion of acid within the film is the only process influencing the acid desorption data. In fact, it remains to be seen if diffusion influences the observed kinetics at all.

Experiments using MSA in various polymers were performed in order to probe the effect of polymer structure on acid desorption and thereby gain further insight into the nature of the acid desorption process. The results of experiments using MSA in a variety of different polymers are summarized in Table 3-1, where the acid desorption is reported as a half-life ($\tau_{1/2}$), which is the time required to lose half of the acid. This quantity is related to the unimolecular rate constant k for acid desorption by the expression: $\tau_{1/2} = 0.693/k$. The glass-transition temperatures (Tg) for all of the polymers employed are also given in Table 3-1 and the structures appear in Scheme 3-2.

Table 3-1. $\tau_{1/2}$ **of MSA in various thin polymer films.**

		$\tau_{1/2}$ (minutes)					
Polymer	**Tg (°C)**	**70 °C**	**90 °C**	**110 °C**	**130 °C**	**150 °C**	**170 °C**
PMMA[a]	**114**	58	10	1.4	<0.5	<0.5	<0.5
PVP1	**151**	>100	>100	34	14	9.6	1.4
PVP2[b]	**167**	>100	>100	41	16	8.9	4.4
PVP3	**182**	>100	>100	44	24	13	6.1
Novolac1	**80**	>100	>100	82	2.3	0.6	<0.5
Novolac2	**174**	>100	>100	37	18	12	2.6

[a]poly(methyl methacrylate)
[b]The experimental error on the half-lives was determined to be ±10% based on the standard deviation of four separate runs at each of the temperatures using MSA in PVP2.

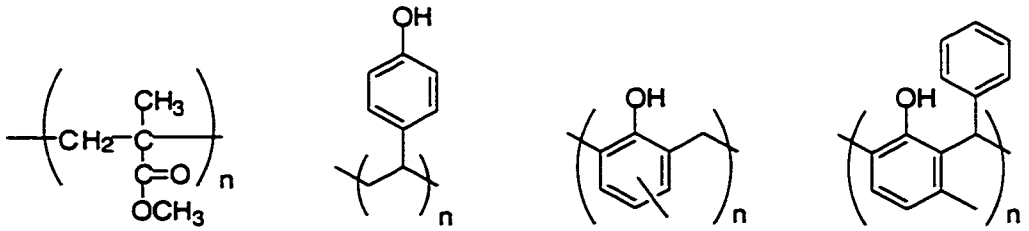

PMMA PVP Novolac1 Novolac2

Scheme 3-2. The polymers employed in acid desorption studies.

A consideration of the rate constants which can be extracted from the data in Table 3-1 allows for construction of the Arrhenius plot shown in Figure 3-6. The linearity of the plots obtained indicates that the kinetics for acid desorption can be described by the equation: $k = Ae^{-Ea/RT}$. The values for the activation energy (Ea) and pre-exponential factor (A) determined from this plot are shown in Table 3-2. Given the limited amount of data used to generate these values, they will be interpreted in a qualitative sense only.

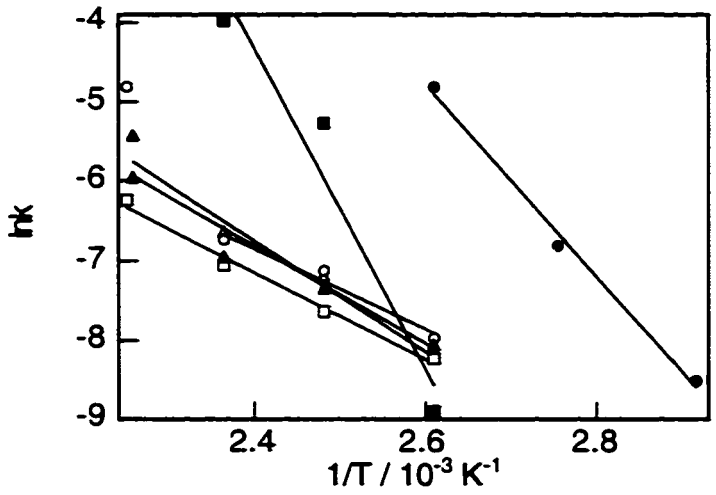

Figure 3-6. **Arrhenius plot for acid desorption from thin films of PMMA (●), PVP1 (○), PVP2 (△), PVP3 (□), Novolac1 (■) and Novolac2 (▲).**

Table 3-2. **The Arrhenius parameters for MSA desorption from various thin polymer films.**

	Arrhenius Parameters[a]	
Polymer	**Ea (kJ/mol)**	**A (s^{-1})**
PMMA	100	$> 10^{10}$
PVP1	42	10^2
PVP2	51	10^3
PVP3	46	10^2
Novolac1	170	$> 10^{10}$
Novolac2	58	10^4

[a]All values were determined from data obtained at temperatures below polymer Tg except for Novolac1 for which all measurements were performed above polymer Tg.

When a film of PVP1 is heated above its Tg of 151 °C, to 170 °C, the rate of acid desorption increases more than is predicted by a consideration of the Arrhenius equation. This is demonstrated both by a decrease in the $\tau_{1/2}$ by a factor of ~7 on going from 150 °C to 170 °C, as compared to the other PVP films for which 170 °C

is at or below Tg, which only drop by a factor of ~2 over the same range, as well as by an obvious break in the linearity of the Arrhenius plot (Figure 3-6) above the Tg. Analysis of the plot reveals that for all of the PVP polymers, the Ea for MSA desorption is 40-50 kJ/mol and the A is 10^2-10^3 s^{-1} when the temperature is below the Tg of the polymer. The observation that acid desorption is much faster above the Tg of the polymer demonstrates that acid desorption is not only a function of properties associated with the acid but also the polymer; specifically, the overall morphology of the polymer, below and above the Tg.

Consideration of results obtained in Novolac films with widely separated Tg's provides more information concerning the observed effect of Tg. Though the Novolac's are not structurally identical, the differences in observed rate constants are interpreted as being due, primarily to, the fact that experiments were performed well above the Tg of Novolac1 and below that of Novolac2. The impact of structural features on acid desorption will be discussed later. Acid desorption from Novolac1 gives an Ea of 170 kJ/mol and an A of > 10^{10} s^{-1} at temperatures above its Tg of 80 °C while that from Novolac2 gives an Ea of 58 kJ/mol and an A of ~10^4 s^{-1} at temperatures below its Tg of 174 °C. The increase in A by several orders of magnitude at temperatures above the polymer Tg dominates over the 3-fold increase in Ea and results in an overall increase in the $\tau_{1/2}$ values above Tg.

That acid desorption is dramatically affected by changes in properties of the polymer suggests that diffusional processes do impact the observed kinetics. Moreover, the increased A and Ea observed above Tg for the acid desorption process is in agreement with results obtained for the diffusion of small molecules within polymers in which diffusion is analyzed as an activated process which is also described by a variation on the Arrhenius equation.[27] However, given that results from donation experiments suggest that acid desorption is not entirely controlled by

acid diffusion, it is proposed that acid desorption from polymer films is a function of both diffusion within the polymer and volatilization of the acid from its surface.

This situation is expected if acid desorption from a polymer involves diffusion of acid into sites at the surface which permit escape and is followed by acid volatilization in competition with acid diffusion back into sites within the film. One can draw an analogy between the diffusion of acid into and out of sites at the surface followed by acid evaporation to the "steady-state hypothesis" of classical kinetics in which a pre-equilibrium is established prior to formation of the final product. Under such conditions, the experimentally observed rate constant is a function of all of the rate constants for the individual processes (Scheme 3-3).[30] Therefore, in acid desorption experiments the observed rate constants are functions of both diffusional processes and acid evaporation.

$$A \underset{k_{-1}}{\overset{k_1}{\rightleftharpoons}} B \xrightarrow{k_2} C$$

$$d[C]/dt = k_1 k_2 [A] / (k_2 + k_{-1})$$

Scheme 3-3. The 'Steady-State Hypothesis' as applied to acid desorption kinetics; where A is acid in the polymer, B is acid at a site in the polymer which allows for volatilization and C is an acid which has escaped the polymer. In this way, -d[C]/dt, the negative of the rate of formation of C is the experimentally measurable parameter which has contributions from all of the rate constants.

Diffusion can be described as a series of jumps of the diffusant into vacant sites in the polymer structure. Sites which permit escape are simply the free regions within a polymer film which are large enough to accomodate an acid molecule. In terms of the Arrhenius parameters introduced earlier: Ea is a function of the energy barriers required to diffuse within the film as well as that required to leave the polymer surface. More specifically, Ea is a reflection of factors affecting both the

ease of diffusion, such as solubility of diffusant and free volume within the polymer[27] as well as intrinsic properties of the acid which determine how easily it can be volatilized. The pre-exponential factor, A, represents the rate at which acid molecules are able to diffuse into sites at the polymer surface which permit escape.

3.2.4 Factors Controlling the Acid Desorption Process

Having established a framework for describing acid desorption, rationalization of the observed effects of different parameters on desorption rates can be undertaken. Differences in $\tau_{1/2}$ can now be discussed in terms of varying abilities to diffuse and/or volatilize.

The decrease in $\tau_{1/2}$ with increasing temperature is not surprising given that at higher temperatures a greater proportion of molecules have enough energy to overcome the energy barrier defined by Ea, as it relates to both volatilization and jumping into a vacant sites within the polymer. As such, the PEB temperatures for CAR development must be chosen carefully in order to avoid loss of acid.

The pronounced increase in acid desorption at temperatures above Tg can also be discussed in terms of the aforementioned framework. Below the Tg, a polymer is restricted to short-range motion, i.e., vibrations and rotations; while above the Tg it experiences more long range molecular motions and greater rotational freedom. Diffusional studies indicate that this results in larger and/or more abundant regions of free volume within a polymer which are available for occupation by acid molecules upon their diffusion.[27] The implication on acid desorption is obvious: the greater the number of these sites at the surface, the greater the rate at which acid can diffuse into these sites and the larger the pre-exponential factor expected for acid desorption.

The larger Ea shown for acid desorption from Novolac1 (at temperatures above its Tg) relative to Novolac2 (at temperatures below its Tg) can also be rationalized in terms of the free volume within a polymer. As previously noted, diffusion can be described as a series of jumps of the diffusant into vacant sites in the polymer structure. An increase in free volume tends to increase the distance between these sites and thereby increases the jump length required for diffusion; a larger jump involves a greater activation barrier. Above Tg, the rate of increase of free volume within a polymer with temperature changes and an increase in activation energy is the result.[27] The importance of polymer Tg on the rates of acid desorption is relevant to the choice of PEB conditions used for CARs as well as the choice of polymers. For example, a longer PEB at temperatures below Tg may prove more effective in reducing acid desorption than a shorter PEB at temperatures above Tg.

The differences in the kinetics of MSA desorption observed for the various PVP and PMMA films is interpreted to be due to structural differences because most of the data was obtained at temperatures below the Tg's of each polymer. The Ea and A for PMMA are 100 kJ/mol and $>10^{10}$ s^{-1}, respectively. These values are considerably larger than the values found for the PVP films. Upon switching the polymer from PVP to PMMA again the increase in A dominates the increase in Ea and results in an overall decrease in the $\tau_{1/2}$ values.

The bulk of the phenolic groups as well as the H-bonding interactions between phenolic groups on different polymer chains reduces the availability of free volume within PVP for acid occupation.[27] The less bulky PMMA and its weaker interaction between adjacent polymer chains may allow for more free volume available for acid occupation and a larger A value is the result.

The larger Ea found for PMMA relative to PVP is likely due to a variety of factors. These include the aforementioned effect of free volume on Ea values, which arises from the differing interactions between polymer chains, as well as the solubility of the acid, which is partly controlled by the basicity of the polymers. The basicity of the oxygens in the ester functionality of PMMA are higher than that of the phenolic oxygens in PVP's. More extensive protonation of PMMA than PVP by acid is demonstrated by the fact that higher concentrations of acid are required in order to fully protonate C6 in a PMMA film. The solvation of acid in PMMA is aided by an ionic interaction between the protonated ester group and the conjugate base of the acid. In phenolic polymers the interaction between acid and polymer is limited to dipole-dipole interactions and hydrogen bonding. Clearly, the stronger the interaction between acid and polymer the greater the Ea for diffusion. Based on these results, in addition to the lithographic requirements placed on polymers, one should consider the structure of the polymer as it pertains to its basicity as well as the bulk of, and interaction between functional groups in order to minimize acid desorption.

The $\tau_{1/2}$ values were determined for a variety of different acids in films of PVP2 in order to identify the role played by acid structure in acid desorption. In addition to MSA the acids studied were: trifluoromethanesulfonic acid (TFA), *p*-toluenesulfonic acid monohydrate (TSA), camphorsulfonic acid (CSA), and perfluorooctane sulfonic acid (PFOS). A thorough consideration of the behaviour of acid desorption at different temperatures for those acids other than MSA is not possible because most acids do not move appreciably at a wide enough range of temperatures. The most obvious conclusion one can draw from the data in Table 3-3 is that under the conditions commonly used for PEB's in industry (90-150 °C, 60-90 s), desorption of most acids is minimal. However, since most of the acid lost is presumably from regions near the surface of the film, even desorption of small

amounts result in formation of undesirable surface features in a developed resist, i.e., T-topping in a positive resist and rounding in a negative resist.

Table 3-3. **$\tau_{1/2}$ values for various acids in films of PVP2.**

	Half-life $\tau_{1/2}$(minutes)			
Acid	**110 °C**	**130 °C**	**150 °C**	**170 °C**
MSA	41	16	8.9	4.4
TFA	>100	55	20	8.9
TSA	>100	>100	>100	61
CSA	>100	>100	>100	41[a]
PFOS	>100	>100	40	19

[a]The half-life of CSA at 170 °C is controlled, in part, by its decomposition.

The data in Table 3-3 shows that the trend in $\tau_{1/2}$ values is MSA<TFA<PFOS<TSA<CSA. Upon further examination of the data, the most dominant trend is that low molecular weight acids leave the film more rapidly than heavier ones, with the exception of PFOS. MSA leaves the film 2-4x faster than does TFA despite their boiling points of 167 °C/10 mmHg and ~45 °C/10 mmHg, respectively. Under these conditions, molecular weight is a better measure of volatility than is boiling point since boiling points are, in part, a reflection of the strength of interactions between acid molecules, which is of limited relevance when they are dispersed throughout a polymer. Not surprisingly, the observed trend in $\tau_{1/2}$ values with molecular weights of acids has a coinciding trend for molecular volumes of acids. The size of a diffusant is very important to diffusional processes as it is relevant to the ease of occupation of vacant sites in the polymer.[27] In order to reduce the potential for acid desorption during PEB one should use a photoacid generator (PAG) which generates an acid that is both large and heavy.

Of all the acids studied, PFOS has by far the largest molecular weight yet its $\tau_{1/2}$ in a PVP film is intermediate to that of TFA and TSA. This result is attributed to weak solvation interactions between the organic polymer and the highly fluorinated acid molecule, which render them incompatible with one another. This interpretation is supported by the observation that the quality of the films obtained was poor when high PFOS concentrations were used in the spin-coating solution. Additional support for this conclusion comes from results of experiments aimed at determining the spatial distribution of PAGs within CARs which indicate significant aggregation of highly fluorinated PAGs.[31] This effect is presumably due to the same lack of strong interaction evident between the polymer and the PFOS which allows it to leave the film so rapidly. The desorption result is especially significant because highly fluorinated acids such as PFOS were, until recently, commonly used in photolithographic applications. The extensive fluorination increases the acid strength considerably and, in the case of PFOS, the large size was originally expected to reduce acid diffusion and desorption. This strategy may be misguided since it seems to result in an acid which is poorly solvated in a resist and may phase separate, allowing it to leave the film quickly. Interestingly, since the completion of this work, perfluorinated octanyl sulfonate compounds have been targeted by the EPA due to their persistence in the environment. One major supplier of these materials, 3M, are voluntarily removing them from all of their product lines and they are expected to be phased out of use in microelectronics applications.[32,33]

Given that the strength of the interaction between the acid and PVP plays a role in determining the rate at which acid leaves a film, one might suspect that the stronger acids will be retained by the film more strongly than weaker ones due to an increased potential for protonation of the phenolic functionality. Although it is difficult to extract this information from the data given the presence of the more dominant trends previously described, the strongest acids, TFA and PFOS are

among the fastest to leave the films. It would appear then that acid strength is not a significant issue in acid desorption from PVP films.

The results of the experiments discussed to this point seem to have identified the primary factors controlling the rate of acid desorption from a film, i.e., temperature and a variety of polymer/acid interactions. This technique can now be used to explore some of the other industrially relevant parameters to acid desorption: film thickness, casting solvent and basic additives.[34]

In order to probe the effect of film thickness on acid desorption, polymer films of different thicknesses were prepared. This can be accomplished in one of two ways: by varying the wt% of solids in the spin-coating solution, thereby changing its viscosity or by varying the spin speed. While both techniques work, the latter proved to be more successful in creating uniform films and was therefore preferred for acid desorption experiments. These experiments involved monitoring MSA desorption from a film of PVP2 casted from 1-methoxy-2-propanol-acetate. This is another common solvent employed by in photolithographic applications and was chosen here because among all of the solvents screened (2-methoxyethyl ether, ethyl lactate and 2-heptanone and 1-methoxy-2-propanol-acetate) it provided films of the most consistent thickness at a given spin speed. The solution was spin coated at a range of speeds and the various films obtained were subjected to thickness analysis followed by a kinetic run at 150 °C. The results (Table 3-4) indicate that within experimental error, the rate of acid desorption does not change with film thickness over the 1.6-2.3 μm range. Since this is not a large sampling of film thicknesses, it can only be concluded that over a narrow range, film thickness does not affect acid desorption.

Table 3-4. $\tau_{1/2}$ **for acid desorption as a function of film thickness.**

Spin speed (rpm)	Film thickness (μm)	$\tau_{1/2}$(min)
3000	2.26 ± 0.003	9.8
4000	1.97 ± 0.009	9.9
5000	1.77 ± 0.004	9.2
6000	1.61 ± 0.013	9.5

The presence of residual casting solvent in CARs has been shown to increase the rate of acid diffusion.[17] Usually, the amount of residual solvent in a CAR is primarily a function of soft-bake conditions. The soft-bake occurs immediately following preparation of the film by spin coating. However, in these experiments the soft-bake is followed by a prolonged period of heating (~600 s), at the chosen acid desorption temperature, during which time the bulk of the remaining solvent evaporates from the film. Therefore, this technique is not suitable for studies involving residual solvent. However, experiments using MSA on films of PVP2 casted from different solvents: 2-methoxyethyl ether (MEE), 1-methoxy-2-propanol acetate (MPA), ethyl lactate (EL) and 2-heptanone (HP) were performed. All of these are typical solvents for preparing CAR films and have boiling points of ~160 °C. Examination of the $\tau_{1/2}$ values obtained (Table 3-5) reveal that although the differences are outside of experimental error, they are not so strikingly different as to cause concern.

Table 3-5. $\tau_{1/2}$ **for acid desorption as a function of casting solvent**

	$\tau_{1/2}$ (minutes)		
Solvent	**130 °C**	**150 °C**	**170 °C**
MEE	16	8.9	4.4
MPA	12	---	2.9
EL	14	---	1.9
HP	14	7.3	2.1

The role of basic additives in diffusion has been previously studied[22] and as one would expect, they retard the diffusional process. Attempts to further describe the effect of base on acid mobility using this technique failed due to the formation of precipitates upon addition of the typical lithographic bases 1,8-diazabicyclo[5.4.0]undec-7-ene and trioctylamine to spin coating solutions.

3.3 Conclusions

Results from a new *in situ* technique for measuring acid desorption from polymer films have been presented. This technique allows for quick and convenient determination of $\tau_{1/2}$ values of acids and has proven useful for probing the effects of PEB conditions, as well as polymer and acid structure on acid desorption. While temperature has the most dominant effect on the rate of acid desorption, the size of the acid as well as both the acid and polymer structures, as they pertain to the interaction between the polymer and the acid, are also key factors in determining the $\tau_{1/2}$ values of acids in polymer films. The increased free volume generated in polymers above Tg acts to increase the rate of acid desorption. The bulk of and interaction between phenolic groups of PVP and Novolac polymers tends to slow acid desorption relative to PMMA films.

It is clear that in order to minimize acid desorption from resists during PEB's the choice of polymer and PAG must be made carefully. This technique may prove useful for screening polymer/PAG formulations as the industry introduces new resists for use at 193 and 157 nm.

3.4 Experimental

3.4.1 Materials

PMMA (avg. M_w~120 000) and PAA (avg. M_w~2000) were obtained from Aldrich and used as received. The various phenolic and Novolac polymer samples used: PVP1-3, and Novolac1-2, were obtained from Shipley Co and no characterization was attempted. The acids employed, with the exception of PFOS, were obtained from Aldrich and used as received. PFOS was obtained from TCI America and used as received. The casting solvents were obtained from Aldrich and used as received. The dyes, C6 and Rb, were obtained from Aldrich. C6 was recrystallized twice from methanol/dichloromethane. Rb was purified by column chromatography on silica gel (230-400 mesh) using acetone as eluent.

3.4.2 Preparation of Polymer Films

Thin polymer films were prepared as described in Chapter 2 Section 2.2.6.1. The stock coating solutions were: 15 wt% PMMA in MEE and 40 wt% PAA in water and all other polymers were 25 wt% in the various solvents employed. The films were baked at 90 °C for 5 min immediately after coating. No attempt was made to determine segregation of components in these films.

Film thickness measurements were performed on a Metricon PC-2000 prism coupler using a 633 nm He-Ne laser; films were placed in direct contact with the prism for measurement. All of the films employed had thicknesses of ~1-2 μm.

3.4.3 Acid Desorption Experiments

In acid desorption experiments, a stock solution of 7.5 mM/1.0 wt% C6 in PVP/MEE was used. Initial acid concentrations varied from 0.01-0.8 M. The thermal stability of C6 in a PVP film was established by heating at 170 °C for one

hour and noting no appreciable change in the absorption spectrum as measured using a Varian CARY 1E spectrophotometer. The response of the dye to known amounts of acid was determined and used as a calibration curve. Acid desorption studies were performed by placing a quartz disk with a spin coated film into a small oven which fits in the sample compartment of an absorption spectrophotometer. The oven has openings on either side to allow the sample beam of the spectrophotometer to enter the oven, pass through the sample and reach the detector. A temperature controller wired to the heaters in the oven maintains a constant temperature in the oven via feedback from a thermocouple. Photographs of the oven appear in Figure 3-7. An acid desorption experiment involves placing the disk in the pre-heated oven and acquiring absorption data every 5 s for 1 hour. When possible, kinetic analyses were performed on portions of the data obtained after the signal/system had completely stabilized (> 600 s). The stabilization period was required to allow the polymer film to reach thermal equilibrium and because of changes in the absorption of the polymer as well as a shift in the acid/base equilibrium between acid and dye which occur at elevated temperatures. The duration of the stabilization period required was determined based on data obtained with films containing either no acid or containing CSA, a relatively immobile acid (*vide infra*). The absorption changes observed in the initial moments of an experiment, which are unrelated to acid desorption, complicate the interpretion of data which is acquired at temperatures different than those used for the creation of calibration curves. In order to perform a meaningful analysis, only a small portion of the experimental data (Δabs. ~ 0.05) is used to extract kinetic information because the response of the dye to small changes in acid concentration is linear over much of the calibration curves.

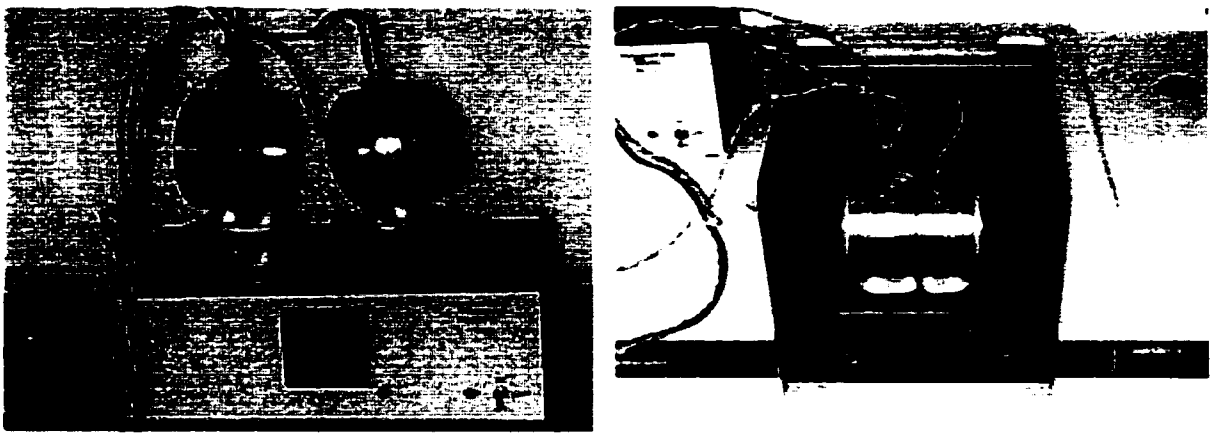

(a) (b)

Figure 3-7. The oven used for acid desorption measurements. (a) The oven sits open on top of the temperature controller. The quartz disk fits in the recessed area in the middle of the piece on the left. (b) The oven sits closed in the sample compartment of a CARY 1E spectrophotometer. The sample beam enters through a hole on the left of the oven and exits through a hole on the right.

3.4.4 Acid Donation Experiments

In acid donation experiments, a PVP film is spin coated onto a disk and heated in the usual manner. This is followed by the spin coating of a PAA film onto the PVP film. The two spin coating solutions must be mutually incompatible so that the acceptor film is not dissolved during the application of the donor film. A stock solution of 7.5 mM/1 wt% C6 in PVP/2-methoxyethyl ether was used for the acceptor film. The donor film was made from a solution of 0.2 M of the appropriate acid in PAA/water. An acid donation experiment is performed in the same way as an acid desorption experiment with the addition of a quartz disk on top of the sandwich, the edges of which are wrapped in teflon tape to ensure that acid cannot escape the films. Analysis of the data is also performed in the same manner as that used in the acid desorption experiments.

3.5 References

(1) Wallraff, G. M.; Hinsberg, W. D. *Chem. Rev.* **1999**, 1801.

(2) Lamola, A. A.; Szmanda, C. R.; Thackeray, J. W. *Solid State Technol.* **1991**, *8*, 53.

(3) Reichmanis, E.; Houlihan, F. M.; Nalamasu, O.; Neenan, T. X. *Chem. Mater.* **1992**, *5*, 348.

(4) Ito, H.; Willson, C. G. *Polym. Eng. Sci.* **1983**, *23*, 1012.

(5) Brunsvold, W.; Conley, W.; Gelorme, J.; Nunes, R.; Spinello, G.; Welsh, K. *Microlithography World* **1993**, *4*, 6.

(6) Thackeray, J. W.; Fedynyshyn, T. H.; Lamola, A. A.; Small, R. D. *J. Photopolymer Sci. Tech.* **1992**, *5*, 215.

(7) Fedynyshyn, T. H.; Thackeray, J. W.; Georger, J. H.; Denison, M. D. *J. Vac. Sci. Technol. B.* **1994**, *12*, 3888.

(8) Itani, T.; Yoshino, H.; Hashimoto, S.; Yamana, M.; Samoto, N.; Kasama, K. *Jpn. J. Appl. Phys.* **1996**, *35*, 6501.

(9) Itani, T.; Yoshino, H.; Hashimoto, S.; Yamana, M.; Samoto, N.; Kasama, K. *J. Vac. Sci. Technol. B* **1996**, *14*, 4226.

(10) Thackeray, J. W.; Denison, M. D.; Fedynyshyn, T. H.; Kang, D.; Sinta, R. *ACS Symposium. Series* **1995**, *614*, 110.

(11) Coenjarts, C.; Cameron, J.; Deschamps, N.; Hambly, D.; Pohlers, G.; Scaiano, J. C.; Sinta, R.; Virdee, S.; Zampini, A. *Proc. SPIE* **1999**, *3678*, 1062.

(12) Kim, J.-B.; Kwon, Y.-G.; Choi, J.-H.; Jung, M.-H. *Proc. SPIE* **1999**, *3678*, 536.

(13) Jessop, J. L.; Goldie, S. N.; Scranton, A. B.; Blanchard, G. J.; Rangarajan, B.; Okoroananwu, U.; Subramanian, R.; Templeton, M. K. *Proc. SPIE* **2000**, *3999*, 161.

(14) Zhang, P. L.; Eckert, A. R.; Willson, C. G.; Webber, S. E.; Byers, J. *Microlithography 1997: Advances in Resist Technology and Processing XIV, Proceedings of SPIE* **1997**, *3049*, 898.

(15) Zhang, P. L.; Webber, S.; Mendenhall, J.; Byers, J.; Chao, K. *Proc. SPIE.* **1998**, *3333*, 794.

(16) Lu, B.; Taylor, J. W.; Cerrina, F.; Soo, C. P.; Bourdillon, A. J. *J. Vac. Sci. Technol. B* **1999**, *17*, 3345.

(17) Schlegel, L.; Ueno, T.; Hayashi, N.; Iwayanagi, T. *J. Vac. Sci. Technol.* **1991**, *9*, 278.

(18) Yoshimura, T.; Shiraishi, H.; Terasawa, T.; Okazaki, S. *J. Vac. Sci. Technol. B* **1996**, *14*, 4216.

(19) Itani, T.; Yoshino, H.; Hashimoto, S.; Yamana, M.; Samoto, N.; Kasama, K. *J. Vac. Sci. Technol. B* **1997**, *15*, 2541.

(20) Wallraff, G. M.; Hinsberg, W. D.; Houle, F. A.; Morrison, M.; Larson, C. E.; Sanchez, M.; Hoffnagle, J.; Brock, P. J.; Breyta, G. *Proc. SPIE* **1999**, *3678*, 138.

(21) Houle, F. A.; Hinsberg, W. D.; Morrison, M.; Sanchez, M. I.; Wallraff, G.; Larson, C.; Hoffnagle, J. *J. Vac. Sci. Technol. B* **2000**, *18*, 1875.

(22) Asakawa, K.; Ushirogouchi, T.; Nakase, M. *Proc. SPIE* **1995**, *2438*, 563.

(23) Cameron, J. F.; Ablaza, S. L.; Xu, G.; Yueh, W. *Proc. SPIE* **1999**, *3678*, 785.

(24) Croffie, E.; Cheng, M.; Neureuther, A. *J. Vac. Sci. Technol. B* **1999**, *17*, 3339.

(25) Corrent, S.; Hahn, P.; Pohlers, G.; Connolly, T. J.; Scaiano, J. C.; Fornes, V.; Garcia, H. *J. Phys. Chem. B* **1998**, *102*, 5852.

(26) Pohlers, G.; Scaiano, J. C.; Sinta, R. *Chem. Mater.* **1997**, *9*, 3222.

(27) Crank, J.; Park, G. S. *Diffusion in Polymers*; Academic Press Inc.: London, 1968.

(28) Sakamizu, T.; Arai, T.; Yamaguchi, H.; Shiraishi, H. *Proc SPIE* **1997**, *3049*, 448.

(29) Uchino, S.; Yamamoto, J.; Migitaka, S.; Kojima, K.; Hashimoto, M.; Murai, F.; Shiraishi, J. *J. Photopolym. Sci. Technol.* **1998**, *11*, 555.

(30) Laidler, K. J. *Chemical Kinetics*; 3rd ed.; HarperCollins: New York, 1987.

(31) Barclay, G.; Sundarajan, N.; Xu, G.; Zhibido, M.; Paddock, C.; Ober, C. *manuscript in preparation* **1999**.

(32) Tullo, A. *Chem. Eng. News.* **2000**, *78*, 9.

(33) Tullo, A. *Chem. Eng. News.* **2000**, *78*, 12.

(34) These experiments were performed with the aid of Matthew Haigh, an undergraduate student at The University of Durham, while he worked in our labs for 4 months.

4. Photoacid Generation by Sulfones

4.1 Introduction

4.1.1 Diaryl-α-disulfones and 1,2-di(Arylsulfonyl)hydrazines

The role of photoacid generators (PAGs) in the photolithographic process was discussed extensively in Chapter 1. Knowledge of the transient species formed upon photoexcitation of a PAG, particulary those directly involved in acid generation, is necessary in order to gauge its potential for use in this process. In our lab, mechanistic insights into acid generation are acquired using laser flash photolysis (LFP) in conjunction with product studies. It is with these techniques that the behaviour of PAGs in solution is studied in order to allow for reasonable predictions about their behaviour in a chemically amplified resist (CAR). As noted in Chapter 1, photoacid generation often involves interaction of reaction intermediates with one of the many components in a CAR formulation. Typical acid generating mechanisms require the presence of nucleophiles, hydrogen donors, or electron donating species. This type of knowledge is becoming increasingly important as the microlithographic community shifts to 193 and 157 nm lithography for which the design of new PAGs may be required.

The PAGs under consideration here are *di-p*-toluene-α-disulfone (**4-1**) and the structurally similar 1,2-*di*(arylsulfonyl)hydrazines (**4-2a - 4-2d**) (Figure 4-1). These molecules represent a design strategy in which multiple acids can be formed from a single PAG molecule due to the presence of multiple sulfonyl moieties. Interestingly, sulfonyl groups account for most, if not all, of the molecular weight of these molecules. This is an advantageous property as industrial use of PAGs often involves loading by weight; a molecule whose entire weight is potential acid makes efficient use of this fact.

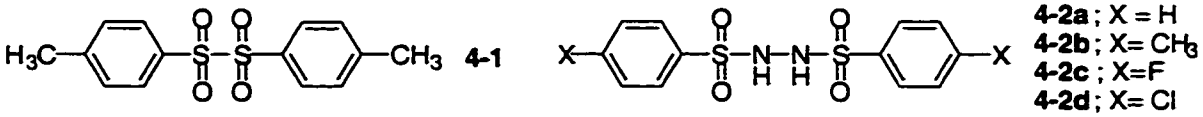

Figure 4-1. PAGs: *di-p*-toluene-α-disulfone (4-1) and 1,2-*di*(arylsulfonyl)hydrazines (4-2a - 4-2d).

The photochemistry of diaryl-α-disulfones has been previously studied and their potential for use as PAGs has been noted.[1-3] Product studies suggest the intermediacy of arylsulfonyl radicals.[4] In fact, these molecules have been employed as clean sources of arylsulfonyl radicals, in order to characterize their optical properties.[5,6] PAG **4-1** is studied here both in order to probe its usefulness as a PAG as well as characterize the behaviour of arylsulfonyl radicals under LFP conditions. The latter is of particular interest as these intermediates were shown to be involved in the photochemistry of another class of PAGs, the N-oxysuccinimidosulfonates (**4-3a - 4-3d**) studied in this lab (Figure 4-2).[7]

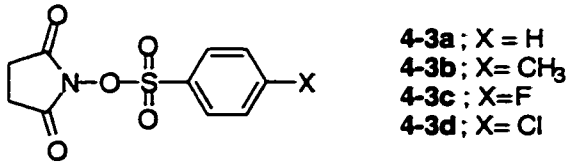

Figure 4-2. PAGs: N-oxysuccinimidosulfonates (4-3a - 4-3d).

The 1,2-*di*(arylsulfonyl)hydrazines are structurally similar to arylsulfonamides, whose photochemistry has been extensively described, in part owing to their utility as photolabile protecting groups for amines.[8] Product studies on arylsulfonamides suggest that the main pathway for photodecomposition is homolytic cleavage of the S-N bond to yield an arylsulfonyl radical.[9]

The 1,2-*di*(arylsulfonyl)hydrazines and *di-p*-toluene-α-disulfone are considered together here because of mechanistic similarites arising from the

intermediacy of arylsulfonyl radicals. For purposes of comparison, additional experiments were also performed with some N-oxysuccinimidosulfonates.

4.1.2 Arylsulfonyl Radicals

Arylsulfonyl radicals can be generated in a variety of different ways including: (a) addition of aryl radicals to SO_2,[10,11] (b) homolysis of arenesulfonyl halides,[5,6,12-14] azosulfones,[15-17] diarylsulfones[18] and diaryl-α-disulfones[1,4] via photolysis or thermolysis, and (c) oxidation of sulfinic acids[19] and 1,2-*di*(arylsulfonyl)hydrazines.[20]

ESR spectra and INDO calculations suggest that arylsulfonyl radicals have the unpaired electron localized predominantly in a sulfur σ-orbital in the plane of the aromatic ring.[13,19] Kinetic analysis of both ESR[14] and LFP[5,6] data reveal that self-reaction of these radicals is a diffusion-controlled process. Product studies have been used to characterize this self-reaction as a dimerization process which is followed by a disproportionation reaction that ultimately leads to anhydrides and thiolsulfonate esters as the photoproducts (Scheme 4-1).[11]

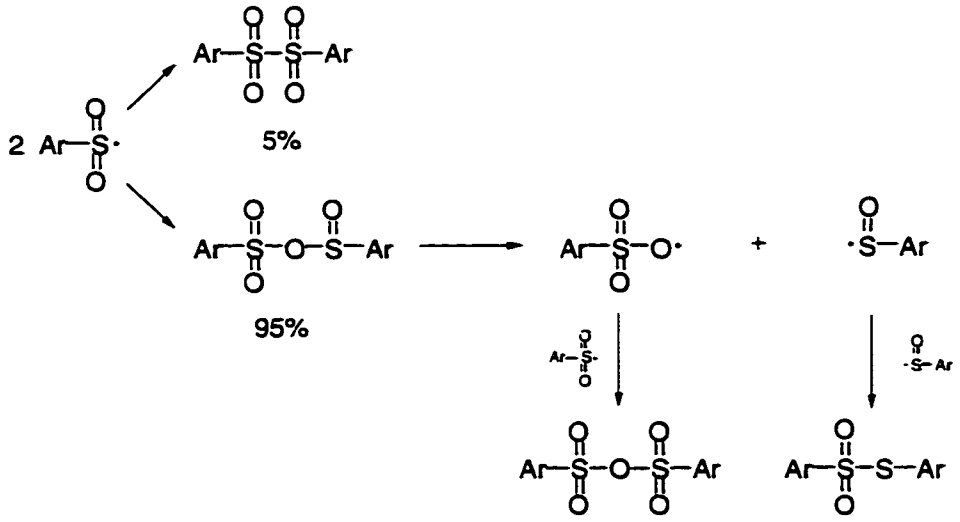

Scheme 4-1. Self-reaction of arylsulfonyl radicals.

Although arylsulfonyl radicals and their behaviour have been characterized to some extent in the aforementioned ways, little work has been done concerning their reactivity with other substrates. Apart from their low reactivity towards arenes[10,18,20] and their reactivity towards vinylic compounds,[21,22] little convincing information appears in the literature about their behaviour. Given that a typical CAR mixture contains many different components, it is important to study the reactions of arylsulfonyl radicals towards a variety of substrates in order to address issues of compatibility. Also, the high surface-to-volume ratio of polymer films suggests that O_2 is likely present in a CAR under typical photolithographic processing conditions, and its reactivity with any reaction intermediates must be probed.

The primary focus of this study is to determine the manner in which these PAGs generate acid. This is an interesting subject, not simply from a practical standpoint, but also a mechanistic one, because acids are not always indicated as products from reactions in which arylsulfonyl radicals are intermediates.

4.2 Results and Discussion

4.2.1 di-p-Toluene-α-disulfone[23]

The ground state absorption spectra of **4-1** in acetonitrile has a main peak < 200 nm ($\varepsilon = 5.2 \times 10^4$ $M^{-1}cm^{-1}$) and another band with a maximum at ~255 nm ($\varepsilon = 3 \times 10^4$ $M^{-1}cm^{-1}$) and extending to 300 nm.

The transient absorption spectra obtained upon LFP of **4-1** in N_2-saturated acetonitrile has a maximum in the UV at 300 nm and another band with a maximum at 450 nm (Figure 4-3). There is a residual absorption in the UV region of the spectrum, evident in the inset of Figure 4-3, which is presumably due to the formation of photoproducts. The appearance of this spectrum is very similar to those obtained in the LFP of arenesulfonylhalides and diaryl-α-disulfones,[5,6] and assigned to the corresponding arylsulfonyl radicals; it is tentatively assigned as such here.

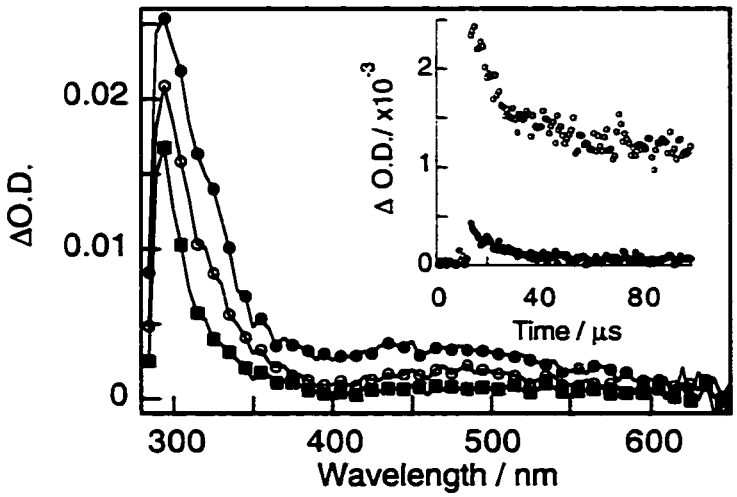

Figure 4-3. Transient absorption spectrum obtained upon LFP of 4-1 at 266 nm in N_2-saturated acetonitrile solutions, recorded 1.2 μs (●), 8.4 μs (○) and 54 μs (■) after the laser pulse. Inset: Kinetic decay traces monitored at 300 nm (○) and 470 nm (●).

The *p*-toluenesulfonyl radical likely results from homolytic cleavage of the S-S bond from an electronically excited state of **4-1** (Scheme 4-2).

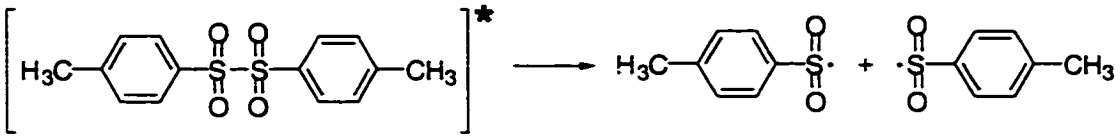

Scheme 4-2. Homolytic cleavage of the S-S bond from an electronically excited state of 4-1 to generate two *p*-toluenesulfonyl radicals.

The decay of the signal follows first-order kinetics and is the same at all wavelengths, indicating the presence of a single transient with a lifetime of < 20 us. It should be noted that in particularly well-purged samples this signal develops second-order contributions to its decay. This result is not unusual under these experimental conditions as some measurements are performed in a sample cell in which efficient removal of O_2 by degassing with N_2 is possible, and other measurements are performed in a larger 'flow apparatus' (see Chapter 2) in which this task is more difficult. The second-order kinetics are likely a result of radical recombination between *p*-toluenesulfonyl radicals which is not an important process in the presence of residual O_2 due to reactivity of these radicals with O_2 (*vide infra*).

In previous kinetic studies involving arylsulfonyl radicals it was determined that they recombine with diffusion-controlled[14] or nearly diffusion-controlled rate constants.[6] Determination of rate-constants from second-order kinetics obtained using LFP is complicated by the fact that the kinetic analysis does not yield the rate constant, k, directly, but a value which corresponds to $2k/\varepsilon l$: where ε is the molar absorptivity at the monitoring wavelength and l is the optical pathlength. The value for $2k/\varepsilon l$ obtained in the LFP of **4-1** while monitoring at 550 nm is 1.6×10^7 s^{-1}. Determining the ε of a transient species requires knowledge of its quantum yield of formation and was not attempted here for the *p*-toluenesulfonyl radical. However,

an ε of 1850 $M^{-1}cm^{-1}$ for the *p*-toluenesulfonyl radical at 420 nm in CCl_4 does appear in the literature[6] and using this value to analyze the data obtained here (despite the large error associated with this type of comparison) results in a $k = 1.0 \times 10^{10}\ M^{-1}s^{-1}$. This value is close to the diffusion-controlled limit in acetonitrile and, as such, is consistent with the results which appear in the literature.

In order to further confirm the identity of the observed transient as the *p*-toluenesulfonyl radical, its reactivites towards quenchers were studied by LFP. This confirmation is necessary because to this point its identification has been based primarily on spectral similarities to literature reports. Although its reactivity has not been extensively described, certain behaviour consistent with a radical centered on a heteroatom can be expected.

The signal presumed to be the *p*-toluenesulfonyl radical reacts with O_2 with a slightly below diffusion-controlled rate constant, $1.3 \times 10^9\ M^{-1}s^{-1}$. Such a rate constant is consistent for the reaction of O_2 with either radical or triplet species. In order to establish that in this case the reaction is due to radical addition as opposed to triplet energy transfer, anthracene was employed as a triplet quencher. Anthracene (0.5 mM) had no effect on the decay kinetics and there was no evidence of sensitization of the anthracene triplet. The reaction of the *p*-toluenesulfonyl radical with O_2 presumably generates the *p*-toluenesulfonylperoxy radical (Scheme 4-3), which is the likely precursor involved in acid generation (*vide infra*). The radical nature of the observed signal is further confirmed because it reacts with TEMPO, a known radical scavenger, with a rate constant of $1.0 \times 10^9\ M^{-1}s^{-1}$.

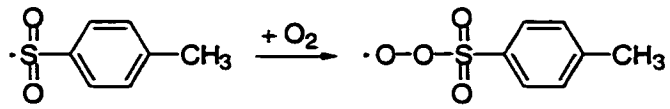

Scheme 4-3. Reaction between the *p*-toluenesulfonyl radical and O_2 to form the *p*-toluenesulfonylperoxy radical.

A heterolytic cleavage of the S-S bond in **4-1**, as opposed to the proposed homolytic pathway, would yield ionic intermediates. Such species are not responsible for the observed transient as it is unreactive towards tetrabutylammonium chloride (5 mM), an ion-pair reagent with nucleophilic activity due to the chloride ions.

These results are consistent with the expected behaviour of an arylsulfonyl radical and are considered to be confirmation of its responsibility for the signal observed in Figure 4-1. To further describe the behaviour of arylsulfonyl radicals, its reactivity towards a few more substrates was studied. The *p*-toluenesulfonyl radical reacts with copper chloride with a rate constant of $5.5 \times 10^9\ M^{-1}s^{-1}$, reflecting the oxidizing properties of Cu^{2+} ions. The *p*-toluenesulfonyl radical did not react with 2-propanol (6.5 M), demonstrating it has little tendency to abstract hydrogens.

As previously noted, in O_2-saturated acetonitrile the *p*-toluenesulfonyl radical is quenched so that its lifetime is reduced to ~100 ns (Figure 4-4: inset) from a value of 20 μs in N_2-saturated acetonitrile (Figure 4-4). In addition to this quenching behaviour, a new signal also forms in O_2-saturated acetonitrile with a rise time of ~10 μs (Figure 4-4). The fact that the kinetics for the decay of the *p*-toluenesulfonyl radical do not match the kinetics for the growth of the new signal indicates that the new signal is not the direct product of the *p*-toluenesulfonyl radical, i.e., it is not a *p*-toluenesulfonylperoxy radical.

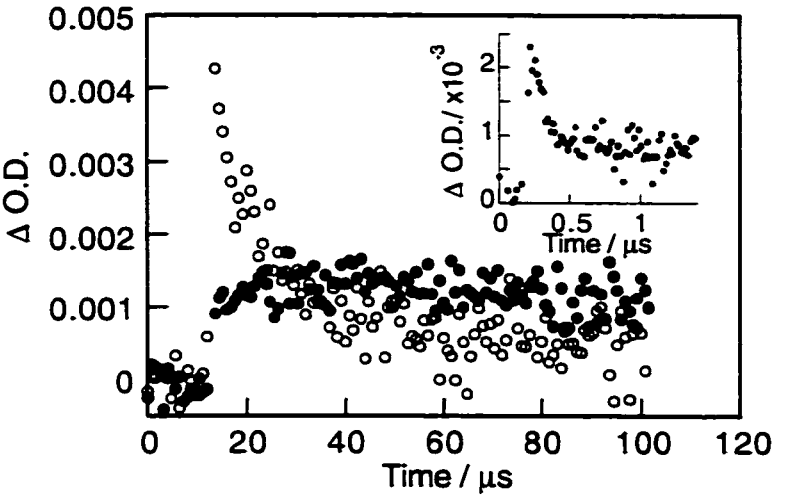

Figure 4-4. Kinetic decay traces obtained upon LFP of 4-1 at 266 nm in N_2-saturated (○) and O_2-saturated acetonitrile (●), monitored at 470 nm. Inset: Another kinetic decay trace in O_2-saturated acetonitrile obtained on shorter timescales to permit observation of the *p*-toluenesulfonyl radical decay.

In order to identify the species responsible for the new signal observed in the presence of O_2, one must consider additional behaviour of arylsulfonyl radicals previously observed in this lab; a desulfonylation reaction to yield SO_2 and aryl radicals.[7] In the literature, the kinetics of the desulfonylation process have been studied extensively in the case of benzylic sulfonyl radicals[24-26] which yield benzylic radicals and sulfur dioxide. The desulfonylation of arylsulfonyl radicals to yield the much less stable aryl radical has also been proposed on the basis of product studies.[4,27] Evidence for this process was detected in the LFP of **4-3a - 4-3d**[7] via the observation of signals assigned to arylperoxy radicals which are formed in the reaction of aryl radicals with O_2.[22,28-32] This signal consisted of an intense band in the UV, whose maximum is located below 300 nm, and a second broad band in the visible region, which was centered at 560 nm. The arylperoxyl radical was characterized, in part, by its kinetics of formation (rise time < 10 μs) and its subsequent decay on similar time scales. This description is consistent with the signal observed in the LFP of **4-1** (Figure 4-4) although it is very weak and detailed

kinetic analysis could not be performed. However, upon addition of 2-propanol (6.5 M) the formation of the signal is completely suppressed (Figure 4-5). This effect is interpreted as being due to quenching of the aryl radical via hydrogen abstraction in competition with reaction with O_2 so that the arylperoxyl radical formation is not observed.

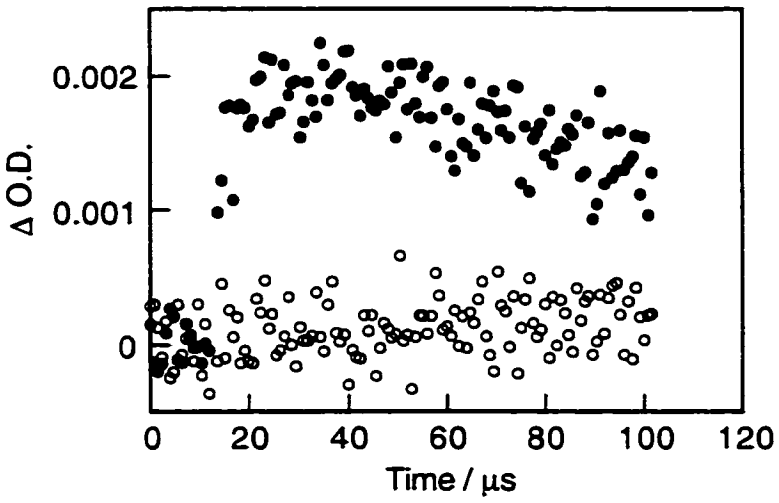

Figure 4-5. Kinetic decay traces at 560 nm obtained upon LFP of 4-1 at 266 nm in O_2-saturated acetonitrile with (○) and without (●) 6.5 M 2-propanol.

The desulfonylation of the arylsulfonyl radical and the subsequent reactions of the aryl radical appear in Scheme 4-4.

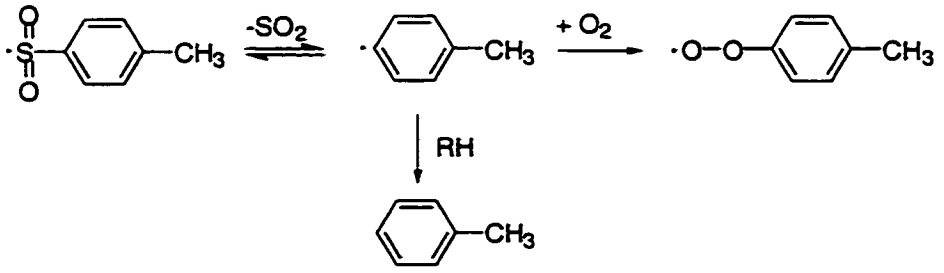

Scheme 4-4. Desulfonylation reaction of the *p*-toluenesulfonyl radical to yield an aryl radical which reacts with either O_2, to form an arylperoxy radical, or a hydrogen-donor, to form toluene.

A feature of these results which must be addressed is the fact that desulfonylation of the arylsulfonyl radical is able to compete with its reaction with O_2. This seems unlikely given that desulfonylation has an upper limit on its rate constant, as imposed by the lifetime of the arylsulfonyl radical in N_2-saturated acetonitrile, of $5 \times 10^4 s^{-1}$, and the arylsulfonyl radical decays with a rate constant of $1 \times 10^7 s^{-1}$ in O_2-saturated acetonitrile. The former value likely represents a very large overestimation of the rate constant for desulfonylation because the lifetime in N_2-saturated acetonitrile is primarily determined by the dimerization reaction and not desulfonylation. The only explanation for the observed desulfonylation is that the reaction of the arylsulfonyl radical with O_2 is reversible, resulting in a low equilibrium concentration of arylsulfonyl radicals available for desulfonylation.

The reversibility of the addition of O_2 to the arylsulfonyl radical may also have implications on the kinetics of arylperoxy radical formation. The lifetime of an aryl radical (the direct precursor of the arylperoxy radical) in an O_2-saturated solution should be approximately 100 ns.[32] The appearance of the arylperoxy radical occurs about one hundred times slower than the expected rate of decay of the aryl radicals, indicating that its kinetics are a reflection of other distinct processes prior to aryl radical formation. While one of these processes may be a slow or reversible desulfonylation reaction[10,33] the equilibrium between arylsulfonyl radical and peroxysulfonyl radical may also have some influence.

Although mechanistic insight into the photochemistry of PAGs is a valuable piece of information, ultimately it is the quantum yield of acid generation (Φ_{acid}) which is the most relevant to a molecule's usefulness as a PAG. The Φ_{acid} of **4-1** is 0.15 at 266 nm as determined via the LFP technique described in Chapter 2. This value is typical for a PAG, as values ranging from 0.05 up to almost 0.5 have been determined in this lab for a variety of molecules.

In addition to the efficiency of acid production by a PAG, one must also be concerned with the type of acid being produced if it is to be useful in a photolithographic application. In the case of **4-1**, the formation of *p*-toluenesulfonic acid is more desirable than the corresponding sulfinic acid because the latter is considered too weak to effectively catalyze the necessary reactions in a CAR. Product studies in the presence of O_2 reveal the formation of a single photoproduct, *p*-toluenesulfonic acid, even under exhaustive photolysis. Apparently, the reaction between the arylsulfonyl radical and O_2 competes effectively with dimerization to the extent that the expected products of the dimerization (see Scheme 4-1) are not formed in appreciable amounts. It is proposed that *p*-toluenesulfonic acid is the stable decomposition product of a first formed peroxysulfonic acid. The peroxysulfonic acid is formed via the reaction of arylsulfonyl radicals with O_2, followed by hydrogen abstraction (Scheme 4-5). The absence of *p*-toluenesulfinic acid is consistent with the lack of reactivity of the arylsulfonyl radical with hydrogen donors, a process which would presumably yield the sulfinic acid. However, sulfinic acids have been observed by others as products in the photolysis of diaryl-α-disulfones.[1] More extensive studies on acid generation from arylsulfonyl radicals were performed using 1,2-*di*(arylsulfonyl)hydrazines as the arylsulfonyl radical generators (see next section).

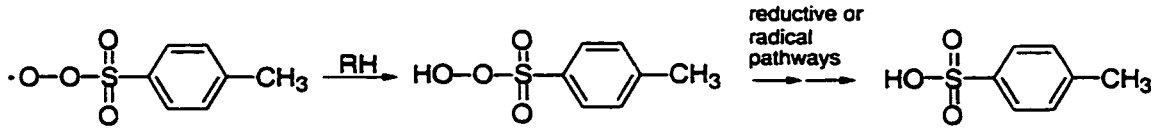

Scheme 4-5. Proposed mechanism for sulfonic acid formation from arylsulfonyl radicals in the presence of O_2.

An interesting aspect of the fact that *p*-toluenesulfonic acid is formed in such a high chemical yield is that it eliminates concerns over both the compatibility of any other photoproducts with the CAR and photoproducts acting to filter light away from

the PAG. The cleanliness of this reaction may be due, at least in part, to the manner in which the arylsulfonyl radicals are generated, i.e., a geminate pair. The dimerization process, which is reported to heavily favour dimerization through S-O bond formation, was postulated from results on homolysis of arylsulfonyliodides, a system in which arylsulfonyl radicals dimerize from encounter pairs, not geminate pairs. Contrarily, in the oxidation of **4-2b**, which generates arylsulfonyl radicals as a geminate pair after the liberation of N_2, high yields of the S-S dimerization product, **4-1**, were found.[20] In the photolysis of **4-1**, it is possible that when dimerization occurs, it does so via a geminate S-S recombination to reform **4-1** as opposed to other combination products resulting from S-O dimerization.

4.2.2 1,2-di(Arylsulfonyl)hydrazines

The ground state absorption spectra of **4-2a - 4-2d** in acetonitrile (Figure 4-6) are very similar with a main peak at < 240 nm ($\varepsilon < 3.1 \times 10^4$ $M^{-1}cm^{-1}$) and another weaker band ($\varepsilon < 1.7 \times 10^3$ $M^{-1}cm^{-1}$) extending from 250 - 280 nm.

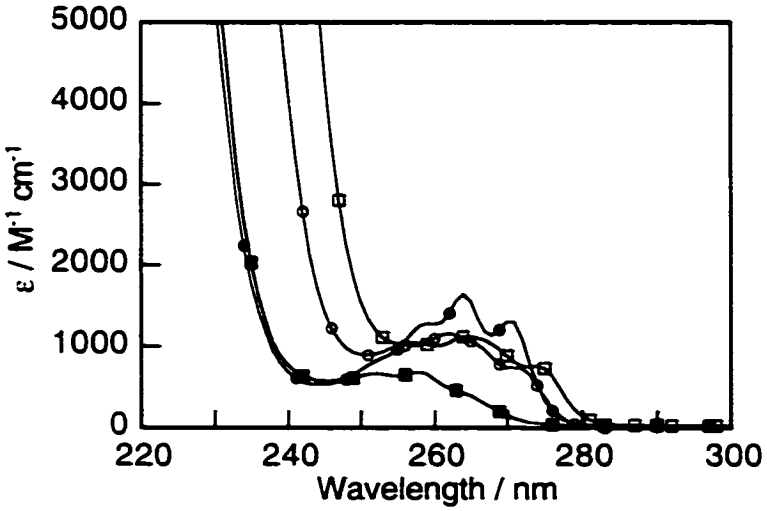

Figure 4-6. Ground state absorption spectra of 4-2a (●), 4-2b (○), 4-2c (■) and 4-2d (□) in acetonitrile solutions.

The transient absorption spectra obtained upon LFP of the PAGs in N_2-saturated acetonitrile also exhibit common features. They all show an intense signal in the UV region, and another weaker band in the visible. The time evolution of the absorption bands in both UV and visible regions reveals the presence of two transients. The transient absorption spectra of **4-2d** appears in Figure 4-7, and serves as a representative example of this behaviour. The longer-lived species decays with first-order kinetics with lifetimes ranging from 130-240 μs (Figure 4-7: inset a), and absorbs primarily in the UV region with a tail extending out to 400 nm. There is also a residual absorption in the UV region of the spectrum, evident in inset a of Figure 4-7, which is presumably due to the formation of photoproducts. The shorter-lived species also decays with first-order kinetics with lifetimes ranging from 6-31 μs and absorbs from 300-600 nm. The kinetics of this species can be monitored at 470 nm without interference from the aforementioned longer-lived species. (Figure 4-7: inset b).

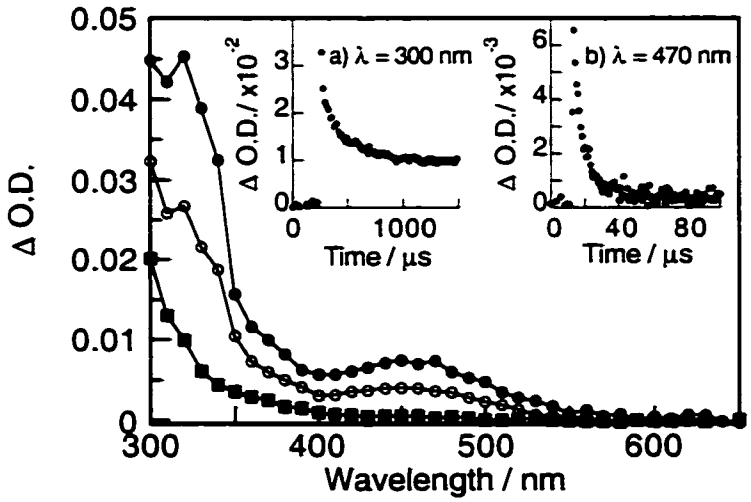

Figure 4-7. Transient absorption spectrum obtained upon LFP of 4-2d at 266 nm in N_2-saturated acetonitrile solutions, recorded 0.8 μs (●), 7.2 μs (○) and 78 μs (■) after the laser pulse. Insets: a) A kinetic decay trace monitored at 300 nm. b) A kinetic decay trace monitored at 470 nm.

The absorption spectra of arylsulfonyl radicals have been previously characterized[5,6] and have been encountered in this lab in the LFP of **4-1** and **4-3a - 4-3d**. In order to determine if these species contribute to the transient absorption spectra obtained in this study, the signal due to the long-lived species and the residual absorption were substracted from the overall spectrum shown in Figure 4-7. The remaining spectrum (Figure 4-8), which has well-defined maxima just above 300 and 450 nm, is consistent with those appearing in the literature for arylsulfonyl radicals, as well as those obtained in this lab, and is tentatively ascribed as such here.

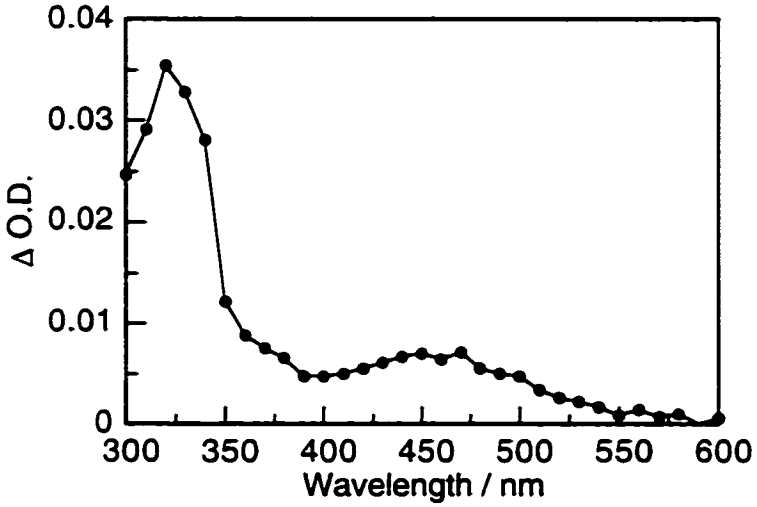

Figure 4-8. Absorption spectrum assigned to the arylsulfonyl radical, obtained from Figure 2 by subtracting the trace obtained at 78 μs after the laser pulse from that obtained at 0.8 μs after the laser pulse.

In order to further aid in the confirmation of the shorter-lived transients as arylsulfonyl radicals, experiments with various quenchers were performed on **4-2a - 4-2d**. These experiments are identical to those described earlier in the LFP of **4-1**. The observed transient reacts with O_2 to give rate constants slightly below diffusion-controlled limits. There was no effect on the lifetime of the transients in the presence of tetrabutylammonium chloride (0.115 M), anthracene (0.07 mM), and 2-

propanol (2.2 M). This indicates that the transient is not a cation, triplet or a reactive radical centered on carbon or oxygen. The rate constants for reaction with copper chloride were also measured. The results of these quenching studies as well as other LFP data are summarized in Table 4-1 and are consistent with the results from the LFP of **4-1** and **4-3a - 4-3d**, thereby suggesting that the shorter-lived transients are arylsulfonyl radicals.

Table 4-1. Kinetic data for the arylsulfonyl radicals generated in the LFP of 4-2a - 4-2d in acetonitrile at 266 nm.

PAG	τ (μs)[a]	k_{oxygen} ($x10^9$ $M^{-1}s^{-1}$)	$k_{cupric\ chloride}$ ($x\ 10^9$ $M^{-1}s^{-1}$)
4-2a	17	0.94	1.59
4-2b	32	1.91	1.31
4-2c	7.6	1.00	1.75
4-2d	5.9	1.14	2.23

[a] N_2-saturated acetonitrile

A result which has become indicative of the presence of arylsulfonyl radicals, is the formation of arylperoxyl radicals in the presence of O_2. This behaviour is also seen in the case of compounds **4-2a - 4-2d** (Figure 4-9) and serves as further evidence for the involvement of arylsulfonyl radicals in their photolyses.

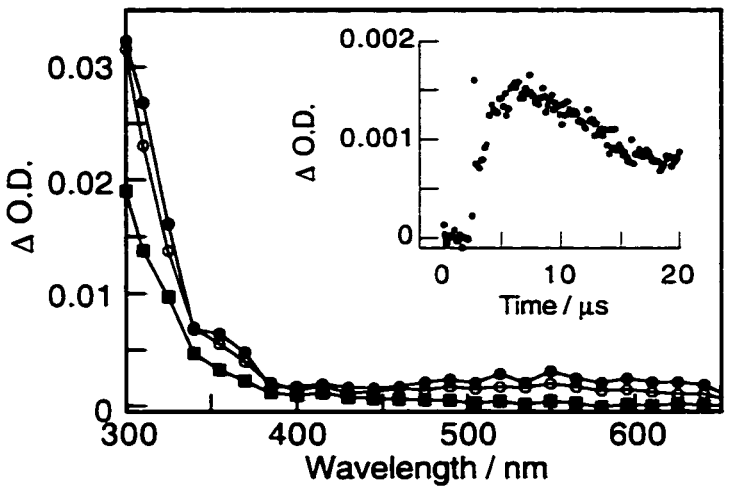

Figure 4-9. Transient absorption spectrum obtained during LFP of 4-2d at 266 nm in O_2-saturated acetonitrile solutions, recorded 1.2 μs (●), 6.8 μs (○) and 78 μs (■) after the laser pulse. Inset: A kinetic trace monitored at 560 nm.

Based on the LFP studies, the primary photochemical step is homolytic cleavage to yield the arylsulfonyl radical and a nitrogen-centered radical (**4-4**), as shown in Scheme 4-6.

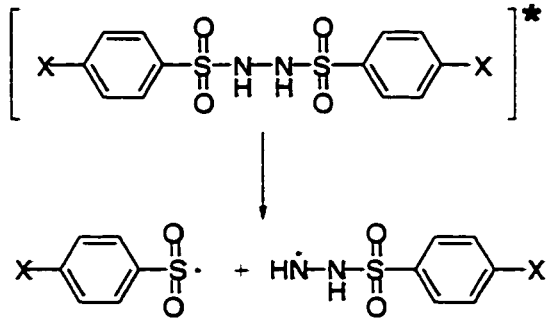

4-4

Scheme 4-6. Homolytic cleavage of the S-N bond from an excited state of 4-2a-d to generate an arylsulfonyl radical and the nitrogen-centered radical, 4-4.

Radical **4-4** is a likely candidate for the heretofore unidentified transient signal observed in the LFP experiments. In order to determine if **4-4** is responsible for this transient signal, quenching experiments were again performed. The

observed transient is not quenched by O_2, anthracene, tetrabutylammonium chloride or 2-propanol. The reactivity of a nitrogen-centered radical derived from an arylsulfonyl substituted hydrazine, i.e., **4-4**, is difficult to predict but the behaviour displayed by this transient is not inconsistent with its assignment as **4-4**. Its lack of reactivity with O_2 and 2-propanol, can be rationalized by the delocalization of the radical center on both nitrogen atoms.

In order to better confirm the nature of this transient, the possibility of generating **4-4** unambiguously via an independent process and comparing the spectral characteristics with those observed in the direct photolysis of **4-2b** is considered. For this purpose, *tert*-butylperoxide was employed as a source of *tert*-butoxy radicals and *p*-toluenesulfonhydrazide as a precursor for **4-4**. The proposed reaction involves hydrogen abstraction by the *tert*-butoxy radical from the hydrazide to form **4-4** exclusively. The transient absorption spectra generated in this reaction and in the direct photolysis of **4-2b** appear in Figure 4-10 and its inset, respectively.

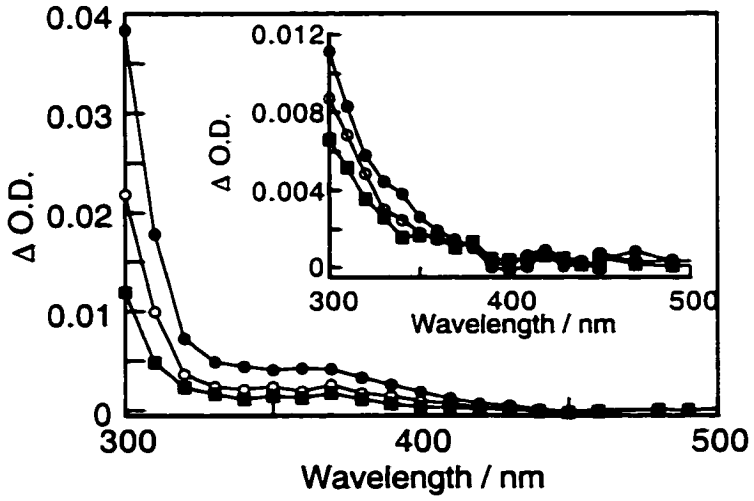

Figure 4-10. Transient absorption spectra obtained upon LFP of *t*-butylperoxide in the presence of *p*-toluenesulfonhydrazide at 308 nm, recorded 84 μs (●), 256 μs (○) and 628 μs (■) after the laser pulse. Inset: Transient absorption spectra resulting from LFP of PAG 4-2b at 266 nm recorded 84 μs (●), 192 μs (○) and 560 μs (■) after the laser pulse.

The rate constant for hydrogen abstraction between the *tert*-butoxy radical and the hydrazide was found to be 6.5 x 10^6 $M^{-1}s^{-1}$. This value is more than an order of magnitude larger than one would expect for the reaction of *tert*-butoxy radicals with the methyl substituent of a derivative of toluene,[34] therefore it is presumably due to reaction with the hydrazine moiety of the hydrazide. It is assumed that the radical is formed β to the sulfonyl group due to the greater number of hydrogens available for abstraction and the increased distance between the electrophilic radical center being formed on nitrogen and the electron withdrawing sulfonyl moiety. A comparison of the two transients reveals that they are sufficiently similar in lifetime (< 100 μs) and appearance to conclude that the transient observed in the LFP of **4-2b** is the same as that formed in the reaction of tert-butoxy radicals with *p*-toluenesulfonhydrazide, and has the structure assigned to **4-4**.

The potential involvement of **4-4** in further acid generation via its sulfonyl moiety is an interesting possibility as it allows for generation of two acid molecules from a single PAG molecule. In order to probe the fate of this fragment, the relative arylsulfonyl radical yields were measured by means of LFP (Table 4-2) and compared to Φ_{acid}. The Φ_{acid} measurements are based on the protonation of Rb by photogenerated acid which is accompanied by a dramatic change in its absorption spectra. Details of the experiment were discussed in Chapter 2 but here it should be noted that the protonation of Rb by photogenerated acid typically occurs over the course of several milliseconds following the laser pulse, and as such, can contain contributions from chemical processes which occur long after the primary photochemical step. In contrast, the relative yields of arylsulfonyl radicals, determined for **4-2b** and **4-2d**, are measured ≤ 100 ns following the laser pulse and hence only contain contributions from species generated in the primary photochemical step, or very quickly thereafter. For purposes of comparison, similar measurements were performed with **4-3b** and **4-3d** and these results also appear in

Table 4-2. Compounds **4-3b** and **4-3d** were used for such a comparison because these molecules have only one sulfonyl moiety, whereas **4-2b** and **4-2d** contain two such moieties. The interesting result, also shown in Table 4-2, is that the ratio of Φ_{acid} to arylsulfonyl radical is about twice as large for **4-2b** and **4-2d** as for **4-3b** and **4-3d**. If one makes the reasonable assumption that arylsulfonyl radicals have the same efficiency for generating acid in both PAG classes, this result indicates that **4-2b** and **4-2d** generate twice the amount of acid for a given primary yield of arylsulfonyl radicals. This result clearly indicates that not only does **4-4** decompose to yield an acid precursor, but the factor of two suggests that **4-4** decomposes very efficiently and yields a second arylsulfonyl radical.[35] This arylsulfonyl radical does not contribute to the measured arylsulfonyl radical yields because it results from the decay of **4-4** at times long after the laser pulse, and hence, long after the arylsulfonyl yields have been determined. Additionally, this extra source of arylsulfonyl radicals does not affect the kinetics observed via LFP because the decay of **4-4**, which generates the arylsulfonyl radical, is slow relative to the decay of the arylsulfonyl radical itself and therefore its steady state concentration is very low.

Table 4-2. Φ_{acid} and arylsulfonyl radical yields obtained upon LFP at 266 nm of 4-2a - 4-2d and 4-3a - 4-3d in N_2-saturated acetonitrile.

PAG	Φ_{acid}[a]	$ArSO_2$[b,c]	$\Phi_{acid}/ArSO_2$	PAG	Φ_{acid}	$ArSO_2$	$\Phi_{acid}/ArSO_2$
4-2a	0.05	---	---	**4-3a**	0.04	---	---
4-2b	0.06	0.7	0.08	**4-3b**	0.04	1.0	0.04
4-2c	0.1	---	---	**4-3c**	0.05	---	---
4-2d	0.1	0.9	0.09	**4-3d**	0.05	1.0	0.05

[a]Random errors are estimated to be less than 10%, although systematic errors may be significant.
[b]arylsulfonyl radical yield
[c]normalized with corresponding PAG: 4-3b or 4-3c

In order to more directly demonstrate the ability of **4-4** to generate acid, its formation was sensitized via reaction of *p*-toluenesulfonhydrazide with triplet xanthone, (^{3}XAN$^\bullet$). The bimolecular rate constant for triplet quenching was determined to be 9 x 10^8 $M^{-1}s^{-1}$, and is too fast to be due to interaction between xanthone and the aryl moiety,[36] or due to direct hydrogen abstraction from the hydrazide moiety,[37] and is therefore probably a result of electron/charge transfer followed by proton transfer. The overall reaction is the transfer of a hydrogen to ^{3}XAN$^\bullet$, (Scheme 4-7) as evidenced by the decay of the characteristic signal of ^{3}XAN$^\bullet$ (λ_{max} = 630 nm) and the appearance of the signal of the xanthone ketyl radical (XAN(H)$^\bullet$, λ_{max} = 480 nm, see Figure 4-11).

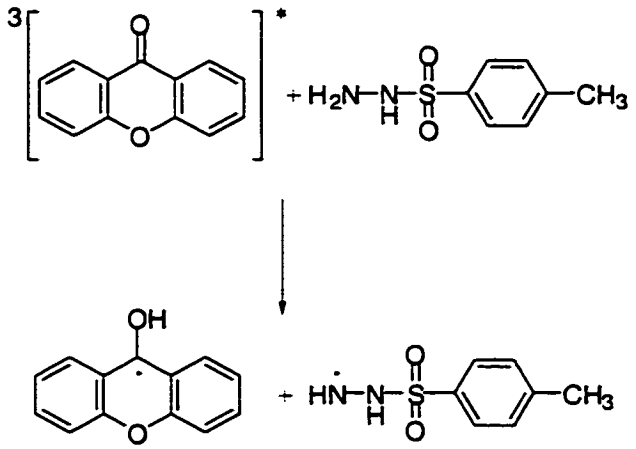

Scheme 4-7. Sensitized formation of radical 4-4 via hydrogen transfer from *p*-toluenesulfonhydrazide to ^{3}XAN$^\bullet$.

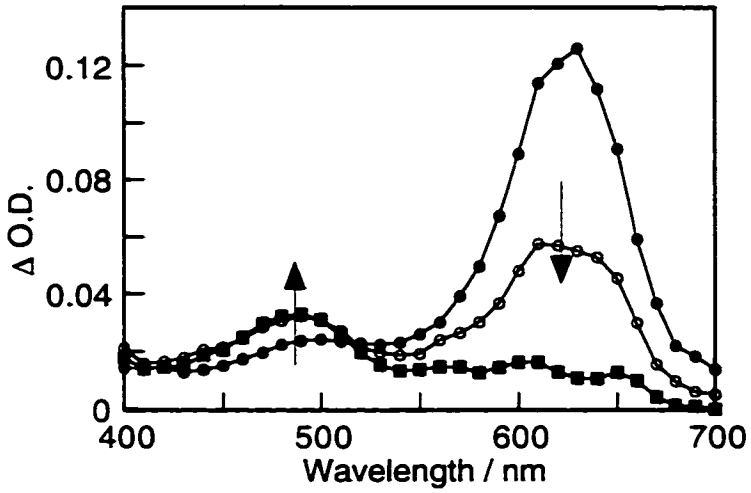

Figure 4-11. Transient absorption spectra obtained upon LFP of XAN in the presence of 36 mM *p*-toluenesulfonhydrazide at 355 nm, recorded 8 ns (●), 40 ns (○) and 472 ns (■) after the laser pulse.

In order to determine if acid is generated after the formation of **4-4**, an irradiation of XAN (absorbance at 350 nm ~0.3) in the presence of *p*-toluenesulfonhydrazide (18 mM) was performed. This concentration is high enough to quench more than 90% of the ^{3}XAN* formed. XAN was used to generate **4-4** in this experiment instead of tert-butoxy radicals because the rate constant for quenching of ^{3}XAN* by *p*-toluenesulfonhydrazide is more than two orders of magnitude larger, thereby allowing for more efficient quenching, and a concomitant increase in the yield of **4-4**. Rb was again used as an acid sensor and a sample of the irradiated solution was added to a stock dye solution. The results of the experiment reveal that sensitized acid formation occurs when XAN is excited in the presence of *p*-toluenesulfonhydrazide (Figure 4-12). This result confirms that radical **4-4** does decompose to yield acid, and thereby makes a significant contribution to overall acid generation in **4-2a - 4-2d**.

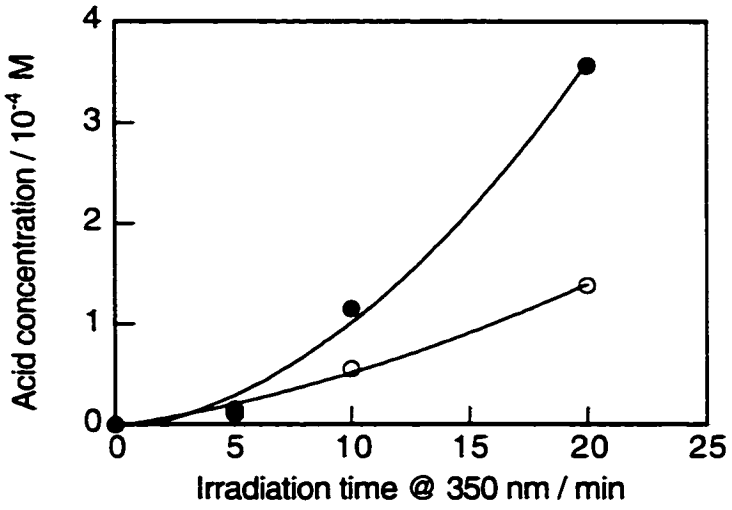

Figure 4-12. Sensitized acid generation by via excitation of XAN in the presence of 21 mM 4-2b (●), and 18 mM *p*-toluenesulfonhydrazide (○) and subsequent detection with Rb.

To this point, details of the mechanism of decomposition of **4-4** have not been discussed apart from the fact that it yields an arylsulfonyl radical. Stoichiometry alone suggests that formation of the arylsulfonyl radical is accompanied by the formation of diimide, N_2H_2. Attempts to detect diimide by exploiting its behaviour as a reducing agent of alkenes[38] were, not entirely surprisingly, unsuccessful given the typical conditions for reactions of this type involve large excesses of diimide. A potential route for decomposition of **4-4** is via a homolytic β-scission reaction (Scheme 4-8). Support for this mechanism comes upon drawing the analogy between **4-4** and *p*-toluenesulfonhydrazide, which decomposes in the presence of bases to yield diimide via a heterolytic β-elimination (Scheme 4-8)[39].

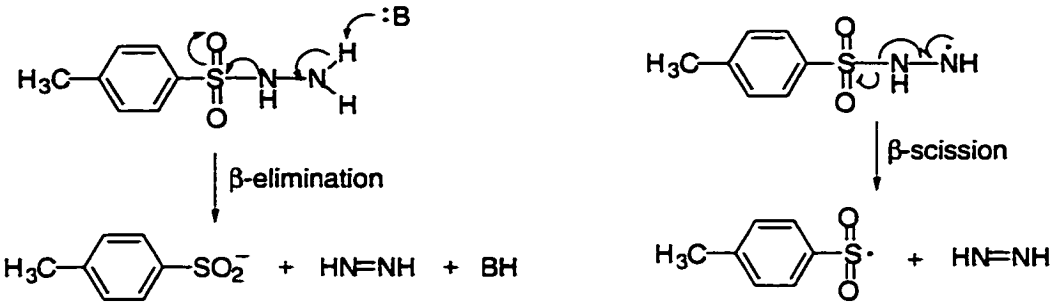

Scheme 4-8. Decomposition of *p*-toluenesulfonhydrazide via β-elimination and the analogous β-scission reaction of the *p*-toluenesulfonhydrazide derived radical, 4-4.

Given the interest in these molecules as PAGs for use in the photolithographic process, both the amount and type of acids produced are of primary concern. The efficiency of acid generation is an important parameter for determining both the amount of PAG and the appropriate exposure dose for catalysis of the required reactions in a CAR. The Φ_{acid} values for **4-2a - 4-2d** and **4-3a - 4-3d** appear in Table 4-2. Additionally, concerns over acid loss and acid diffusion in CAR films prevent the use of PAGs which generate small, volatile acids.[40] It is therefore important to address in what manner the arylsulfonyl radicals and perhaps **4-4** generate acid. Product studies reveal that the main photoproduct from **4-2b** and **4-2d** are the corresponding sulfonic acids. This result is consistent with the fact that **4-3a - 4-3d** also generate sulfonic acids from arylsulfonyl radical intermediates.[7] As was mentioned in the discussion of **4-1**, the sulfonic acid is likely the stable decomposition product of a first formed peroxysulfonic acid. The peroxysulfonic acid is formed via the reaction of arylsulfonyl radicals with O_2, followed by hydrogen abstraction.

While routes to sulfonic acid generation from arylsulfonyl radicals which do not involve O_2 do not explicitly appear in Scheme 4-1, they can be inferred. The formation of the arylsulfonyloxyl radical in the disproportionation of the S-O arylsulfonyl radical dimer should lead to sulfonic acid formation upon hydrogen

abstraction.[27] The anhydride products in Scheme 4-1 are likely hydrolyzed to sulfonic acids, if not by residual water in the solvent during reaction then certainly afterwards upon aqueous work-up of the reaction mixture or exposure to water during chromatography. Finally, although the arylsulfonyl radical has not demonstrated any affinity for hydrogen abstraction on the LFP timescale it has been suggested that the sulfinic acids, which would result from such a reaction disproportionate easily to yield a sulfonic acid and a thiolsulfonate ester.[4,41] Individually, each of these reactions can explain the formation of sulfonic acids but more likely some combination of them is involved. Product studies on other systems in which arylsufonyl radicals are intermediates also show high yields of sulfonic acids under a wide range of conditions.[4,17,20]

The Φ_{acid}, quantum yield of sulfonic acid formation ($\Phi_{sulfonic\ acid}$) and quantum yield of PAG decomposition (Φ_{decomp}) were determined for **4-3b** and **4-2d** under a variety of conditions during steady-state irradiation and appear in Table 4-3. In order to interpret these results, one must appreciate that the Φ_{acid} is determined photometrically, and as such, does not discriminate between different acids, while $\Phi_{sulfonic\ acid}$ is determined via HPLC, and hence is selective for *p*-chlorobenzenesulfonic acid in the case of **4-2d** and *p*-toluenesulfonic acid in the case of **4-3b**. The good agreement between Φ_{acid} and $\Phi_{sulfonic\ acid}$ under all conditions employed indicates that sulfonic acids are the only acids formed in an appreciable amount. This result indicates that, as expected, the SO_2 resulting from desulfonylation reaction, in evidence via the laser experiments, does not generate significant amounts of acid under these conditions. This result also suggests that **4-4** decomposes to give an arylsulfonyl radical which behaves in the same manner as the arylsulfonyl radical generated in the primary photochemical step, i.e., reaction with O_2 as the first step towards yielding a sulfonic acid.

Yet another confirmation of the fact that **4-4** decomposes to yield acid comes from the fact that Φ_{decomp} is smaller than that of Φ_{acid} and $\Phi_{sulfonic\ acid}$. Clearly, this can only be the case if each PAG molecule is capable of decomposing to generate more than one acid molecule. Further, the fact that the Φ_{acid} and $\Phi_{sulfonic\ acid}$ are double that of Φ_{decomp} indicates that, once formed, **4-4** decomposes essentially quantitatively to yield an arylsulfonyl radical.

For **4-3b**, the Φ_{acid} is essentially the same as the $\Phi_{sulfonic\ acid}$, in both O_2 and N_2-saturated solutions, indicating that *p*-toluenesulfonic acid is the only acid formed in significant yields even under conditions in which O_2 concentrations are low. The fact that Φ_{decomp} values are also very similar to $\Phi_{sulfonic\ acid}$ values indicates that for every PAG molecule destroyed by photolysis, a *p*-toluenesulfonic acid molecule is formed. This can only be the case if the desulfonylation reaction, observed in LFP, is either a very minor process or reversible.

Table 4-3. **Φ_{acid}, $\Phi_{sulfonic\ acid}$ and Φ_{decomp} for 4-2d and 4-3b under a variety of conditions with steady-state irradiation at 254 nm.**

PAG	Conditions[a]	Φ_{acid}	$\Phi_{sulfonic\ cid}$	Φ_{decomp}
4-2d	O_2, H-donor	0.43	0.56	0.28
4-2d	O_2, no H-donor	0.64	0.62	0.27
4-3b	N_2, H-donor	0.15	0.20	0.18
4-3b	O_2, H-donor	0.38	0.32	0.32

[a] All reactions were performed in acetonitrile degassed with N_2 or O_2. 2-methoxyethyl ether (0.5 mM) was used as a hydrogen donor.

Given the importance of O_2 in the reaction path it is not surprising that the quantum yields are larger in a solution purged with O_2 than with N_2. In a solution purged with N_2, Φ_{decomp} values are also very similar to $\Phi_{sulfonic\ acid}$ values yet both are lower than the corresponding values in O_2 purged solutions. This indicates the presence of a pathway which competes with trapping of the arylsulfonyl radical by

O_2 but does not result in a decomposed PAG molecule. This pathway may be the recombination of the arylsulfonyl radical and the n-oxysuccinimide radical to generate starting material. This process is expected to be more prevalent in the O_2-depleted environment of a solution purged with N_2 than one purged with O_2 and therefore accounts for the observed reduction in acid production.

It should also be noted from Table 4-3 that the Φ_{acid} determined under steady-state conditions is approximately 4 times larger than the Φ_{acid} determined under LFP. This result was also encountered in the studies with **4-3a - 4-3d** and was attributed to the inherent differences between lamp and laser irradiation.[7] The greater photon fluency present in a laser experiment as compared to a lamp results in a corresponding increase in the concentration of reaction intermediates formed in the light path. The effect of this is that radical-radical recombination pathways e.g., arylsulfonyl radical with **4-4** to regenerate starting material, are able to compete much more effectively with other pathways which generate acid. Similar effects as a result of an enhancement of radical-radical combination pathways under laser irradiation are well established. Although this phenomenon can result in the formation of different products under laser and lamp irradiation, there is no need to consider the possibility of different acids being formed under differing irradiation conditions in the reactions of the PAGs currently under consideration. The competition between the desulfonylation reaction of arylsulfonyl radicals, which can conceivably yield sulfurous acid, and reaction with O_2, which is the first step in the generation of a sulfonic acid, should be unperturbed by the differing concentrations of radical species which result from different light sources. Reactions of the arylsulfonyl radical and previously discussed competive processes appear in Scheme 4-9.

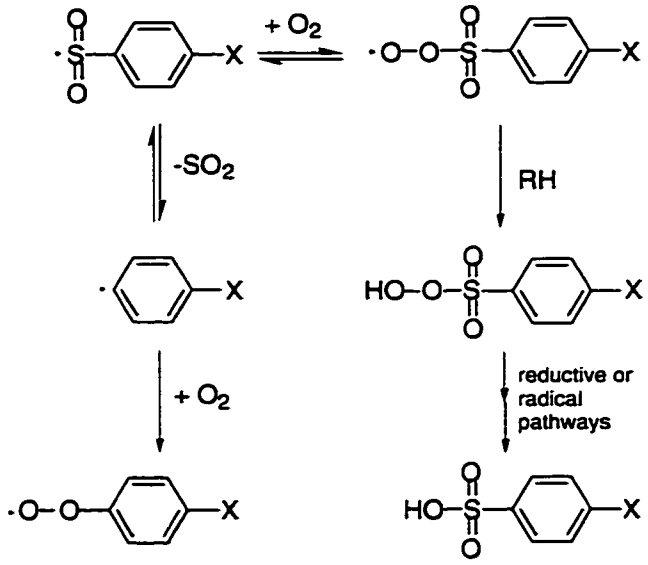

Scheme 4-9. Reactions of the arylsulfonyl radical in the presence of O_2.

Further confirmation of the involvement of O_2 in the acid generation process comes from the fact that the Φ_{acid} for **4-2d** measured via LFP in O_2-saturated solution is 0.17, or almost double the value in solutions degassed with nitrogen[42] (Table 4-2). The presence of residual O_2 in solutions purged with N_2 may be the source of acid in these experiments as evidenced by the fact that a preliminary experiment in which more rigorous degassing with Ar was employed instead of N_2 prior to lamp irradiation reduces the yield of acid by a factor of 3 compared to N_2 and a factor of 9 compared to O_2.[43] These results clearly indicate that any acid generation pathways which do not involve O_2 are minor contributors to overall acid production.

A process which, to this point, has not been discussed is the potential hydrogen abstraction reaction between ground state PAG molecules and oxygen-centered radicals produced in their photodecomposition to generate another nitrogen-centered radical (**4-5**) (reaction i, in Scheme 4-10). As indicated in Scheme 4-9, hydrogen abstraction from some substrate is a likely step in sulfonic acid formation. The behaviour of *p*-toluenesulfonhydrazide as a hydrogen donor has

been established in reactions with tert-butoxy radicals and $^3XAN^{\bullet}$ and it is reasonable to assume that **4-2a - 4-2d** will behave similarly. More interesting than this simple 'induced decomposition' pathway, is the possibility that once **4-5** is formed it will decompose in a manner similar to that observed in the case of the hydrazide and, in this way, generate acid. Therefore, it seems that there is potential for involvement of a radical chain process in the acid generation of **4-2a - 4-2d**, the propagation steps of which appear in Scheme 4-10.

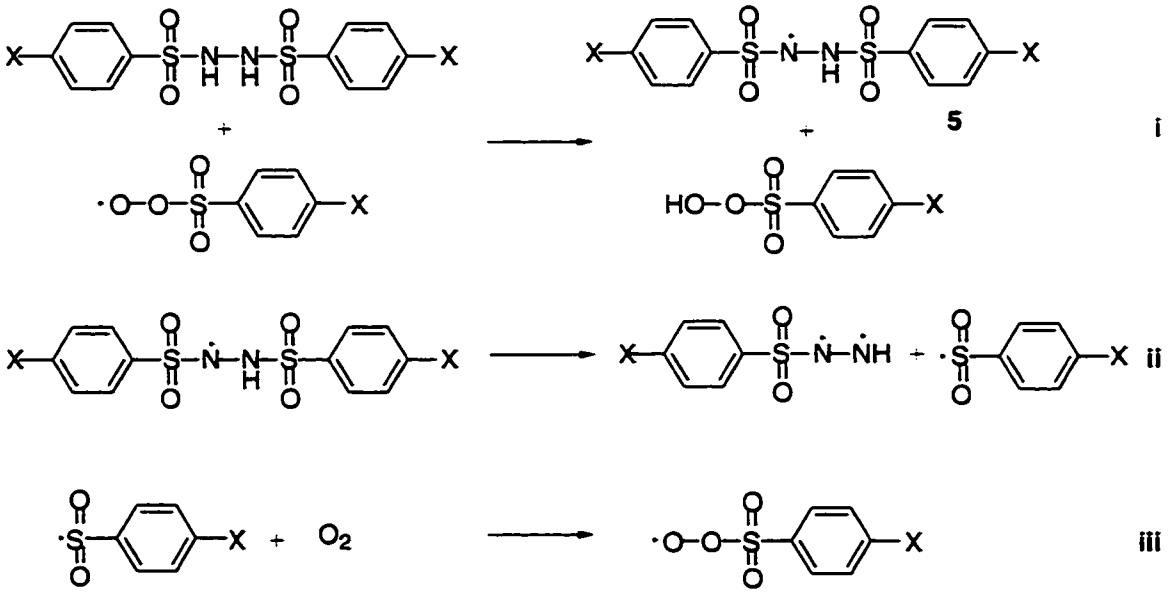

Scheme 4-10. Possible induced decomposition pathway of 4-2a - 4-2d via a radical chain process.

In a manner similar to that used with *p*-toluenesulfonhydrazide, the interaction of **4-2b** with $^3XAN^{\bullet}$ was studied. The hydrogen transfer process was again identified via the detection of the formation of XAN(H)•, and a rate constant of 8×10^8 M^{-1} s^{-1} was determined. In order to determine if acid is generated subsequent to the formation of **4-5**, an irradiation of XAN at 350 nm was performed in the presence of **4-2b** (21 mM) in order to quench more than 90% of the $^3XAN^{\bullet}$ formed. The results of the experiment appear in Figure 4-12 in which it is shown that sensitized acid formation does occur when XAN is excited in the presence of **4-2b**.

This result indicates that **4-5** does decompose to yield acid, presumably in a manner similar to that of **4-4**. Interestingly, the yield of acid is approximately doubled when **4-2b**, which contains two arylsulfonyl moieties, is used as compared to the *p*-toluenesulfonhydrazide, which contains only one. Given that conditions were chosen so that efficiencies of sensitization were the same, this result seems to suggest that **4-5** decomposes quantitatively to generate two fragments containing the sulfonyl moiety. Reaction ii in Scheme 4-10 illustrates a potential first-step in this decomposition process as loss of an arylsulfonyl radical. Although the specifics of this reaction are highly speculative, the generation of acid precursors of some kind from **4-5** is unquestionable.

Based on the 'model system' with XAN and **4-2b**, in which hydrogen abstraction from the PAG was ensured, all of the reactions shown in Scheme 4-10 appear to be viable; their contributions in the direct photolysis of **4-2a - 4-2d**, however, remain to be seen. In order to study this, the Φ_{acid}, Φ_{decomp} and $\Phi_{sulfonic\ acid}$ were again determined under conditions of steady-state irradiation in O_2-saturated solutions in the absence of 2-methoxyethyl ether (0.5 M) as a hydrogen donor; while 2-methoxyethyl ether is only a modest hydrogen donor, this experiment is consistent with earlier work, where chlorine atoms were involved. These results also appear in Table 4-3. In the absence of a hydrogen donor the potential for interaction between species capable of hydrogen abstraction and the ground state PAG should increase, thereby resulting in an increase in Φ_{acid}, Φ_{decomp} and $\Phi_{sulfonic\ acid}$. However, this effect is not observed, which suggests that hydrogen abstraction from the PAG by reaction intermediates is either not involved, or that a competition with 2-methoxyethyl ether is not favorable. The source of hydrogen atoms in solution remains uncertain at this point.

In an attempt to bias the system in favour of interaction between PAG and a species capable of hydrogen abstraction, experiments in thin polymer films in which

the PAG concentration was much higher than in solution (5 wt% of polymer), were performed. Thin films of poly(methyl methacrylate) and either **4-2a** or **4-3a** were optically matched at 254 nm and irradiated. Acid generation was detected by extracting the film in a solution containing Rb as an acid sensor. Compound **4-3a** was used as a model in which there is no possibility of a radical chain mechanism. The results reveal the two PAGs to have essentially the same Φ_{acid}, which is in agreement with the fact that they have very similar Φ_{acid} in solution. One is forced to conclude from this result that the radical chain pathway is again not active under the conditions employed. Apparently, hydrogen abstraction from the polymer matrix is favoured over the PAG. Interestingly, the ratio of Φ_{acid} in solution is retained in polymer films for a given set of PAGs with similar mechanisms for photodecomposition.

4.3 Conclusions

LFP studies indicate that irradiation of *di-p*-toluene-α-disulfone results in the generation of the corresponding arylsulfonyl radicals. The arylsulfonyl radicals react with O_2 to form peroxysulfonyl radicals in competition with both dimerization and desulfonylation. Decomposition of a peroxysulfonic acid is the likely source of the sulfonic acid detected in product studies although sulfonic acids are also formed under conditions in which O_2 concentrations are low. Similarly, irradiation of 1,2-*di*(arylsulfonyl)hydrazines leads to production of an arylsulfonyl radical and a nitrogen-centered radical. Decomposition of the nitrogen-centered radical yields another arylsulfonyl radical which is available for further acid generation.

For a variety of reasons, interest in employing these molecules as PAGs in an actual lithographic application has been muted. Generation of small, volatile molecules such as SO_2 and N_2H_2 in a CAR is undesirable because of their potential to deform the imaged polymer as they desorb from the film. There are also concerns over the shelf-life of the 1,2-*di*(arylsulfonyl)hydrazines in a CAR formulation due to their tendency to behave as electron and hydrogen donors, as demonstrated by their reactivity with photoexcited XAN. The limited solubility of *di-p*-toluene-α-disulfone in typical resist formulations has prevented it from being evaluated in these environments. Perhaps most importantly, the key role of O_2 in the photoacid generation process, brings into question the usefulness of these PAGs for 193 and 157 nm lithography. Lithography at these wavelengths requires the exculsion of O_2 from the exposure tool because O_2 absorbs both 193 and 157 nm light.

4.4 Experimental

4.4.1 Materials

Compounds **4-1**, **4-2a - 4-2d** and **4-3a - 4-3d** were prepared by St. Jean Photochemical Co. and used as received.[7,44] Anthracene (zone-refined, 99+%), *p*-toluenesulfonic acid monohydrate (98.5%) and poly(methyl methacrylate) were obtained from Aldrich and used as received. Tetrabutylammonium chloride was obtained from Fluka (>99%) and used without further purification. *p*-Chlorobenzenesulfonic acid (ClSOH, 90%) obtained from Aldrich and recrystallized from ethanol/water. MTT was purchased from Panchim and purified by recrystallization from methanol (2 times) and subsequent sublimation. Rb was obtained from Aldrich and purified by column chromatography on silica gel (230-400 mesh) using acetone as eluent. Acetonitrile, tetrahydrofuran, 2-methoxyethyl ether were all OmniSolv grade solvents from VWR and used as received. 2-propanol, HPLC grade from Sigma-Aldrich, was used as received.

4.4.2 General Techniques

Details of the LFP system and techniques to measure Φ_{acid} using various chemical actinometers and light sources were described in Chapter 2.

Quantum yield determinations and product studies involving steady-state irradiations were performed on a HPLC (Varian 9010 pump with Model 9065 autosampler, and a Model 9090 diode array detector interfaced to a 386 computer equipped with Star Workstation software) employing a 25-cm Zorbax C-18 column with a 25:75 water-methanol mobile phase. Product yields were determined by comparison with standard calibration curves. Some products were further characterized by LC/MS analysis in a Millennium system using a reverse phase column and a combination of UV diode array and mass spectroscopic detection.

For these experiments the PAG concentration was ~4 mM as compared to the LFP experiments in which it was ~0.4 mM.

The relative yields of arylsulfonyl radical formation were determined via LFP by measuring the absorbance change (ΔO.D.) at 470 nm, where only the arylsulfonyl radical absorbance contributes to the observed signal. This measurement was taken ≤ 100 ns following the laser pulse, before significant decay of the signal occurred, for **4-2b** and **4-2d** at various laser powers. For purposes of comparison, similar measurements were performed with **4-3b** and **4-3d**. The slopes of the linear plots obtained between PAGs which generate the same arylsulfonyl radical i.e., **4-2b** with **4-3b** and **4-2d** with **4-3d**, give a relative yield of the amount of arylsulfonyl radical generated within the laser pulse. The yields can only be stated relative to another molecule which yields the same arylsulfonyl radical because the molar absorptivities of these species are not known.

4.5 References

(1) Aoai, T.; Aotani, Y.; Umehara, A.; Kokubo, T. *J. Photopolym. Sci. Technol.* **1990**, *3*, 389.

(2) Shirai, M.; Tsunooka, M. *Bull. Chem. Soc. Jpn.* **1998**, *71*, 2483.

(3) Kawamura, K.; Sasaki, F. *J. Photopolym. Sci. Technol.* **2001**, *2*, 265.

(4) Kobayashi, M.; Tanaka, K.; Minato, H. *Bull. Chem. Soc. Jpn.* **1972**, *45*, 2906.

(5) Chatgilialoglu, C.; Griller, D.; Guerra, M. *J. Phys. Chem.* **1987**, *91*, 3747.

(6) Thoi, H. H.; Ito, O.; Iino, M.; Matsuda, M. *J. Phys. Chem.* **1978**, *82*, 314.

(7) Ortica, F.; Coenjarts, C.; Scaiano, J. C.; Liu, H.; Pohlers, G.; Cameron, J. F. *Chem. Mater.* **2001**, *13*, 2297.

(8) Rajasekharan Pillai, V. N. *Photochemical Methods for Protection and Deprotection of Sulfur-Containing Compounds*; CRC Press: New York, 1995.

(9) Pincock, J. A. *The Photochemistry of Sulfonamides and Sulfenamides*; CRC Press: New York, 1995.

(10) Squire, J. M.; Wates, W. A. *J. Chem. Soc.* **1962**, 2068.

(11) da Silva Correa, C. M. M.; Lindsay, A. S.; Waters, W. A. *J. Chem. Soc. (C)* **1968**, 1872.

(12) da Silva Correa, C. M. M.; Waters, W. A. *J. Chem. Soc. (C)* **1968**, 1874.

(13) Chatgilialoglu, C.; Gilbert, B. C.; Norman, R. O. C. *J. Chem. Soc., Perkin Trans. 2* **1979**, 770.

(14) Benett, J. E.; Brunton, G.; Gilbert, B. C.; Whittall, P. E. *J. Chem. Soc., Perkin Trans. 2* **1988**, 1359.

(15) Overberger, C. G.; Rosenthal, A. J. *J. Am. Chem. Soc.* **1960**, *82*, 117.

(16) Kobayashi, M.; Minao, H.; Kojima, M.; Kamigata, N. *Bull. Chem. Soc. Jpn.* **1971**, *44*, 2501.

(17) Kobayashi, M.; Fujii, S.; Minato, H. *Bull. Chem. Soc. Jpn.* **1972**, *45*, 2039.

(18) Kharasch, N.; Khodair, A. I. A. *Chem. Commun.* **1967**, 98-100.

(19) McMillan, M.; Waters, W. A. *J. Chem. Soc. (B)* **1966**, 422.

(20) Kohara, Y.; Kobayashi, M.; Minato, H. *Bull. Chem. Soc. Jpn.* **1970**, *43*, 2933.

(21) Mochizuki, T.; Hayakawa, S.; Narasaka, K. *Bull. Chem. Soc. Jpn.* **1996**, *69*, 2317.

(22) Percec, V.; Barboiu, B.; Kim, H. J. *J. Am. Chem. Soc.* **1998**, *120*, 305 and references therein.

(23) The experiments involving **4-1** were performed with the aid of Priscilla Brastianos, an undergraduate student from the University of Victoria, while she worked in our labs for 4 months as part of the Reactive Intermediates Student Exchange (RISE) program.

(24) Chatgilialoglu, C.; Lunazzi, L.; Ingold, K. U. *J. Org. Chem.* **1983**, *48*, 3588.

(25) Chatgilialoglu, C. *J. Org. Chem.* **1986**, *51*, 2871.

(26) Gould, I. R.; Tung, C.-H.; Turro, N. J.; Givens, R. S.; Matuszewski, B. *J. Am. Chem. Soc.* **1984**, *106*, 1789.

(27) Mellier, D.; Pete, J. P.; Portella, C. *Tetrahedron Lett.* **1971**, *47*, 4559.

(28) Alfassi, A. B.; Marguet, S.; Neta, P. *J. Phys. Chem.* **1994**, *98*, 8019.

(29) Khaikin, G. I.; Alfassi, Z. B.; Neta, P. *J. Phys. Chem.* **1995**, *99*, 11447.

(30) Alfassi, Z. B.; Khaikin, G. I.; Neta, P. *J. Phys. Chem.* **1995**, *99*, 265.

(31) Hancock-Chen, T.; Scaiano, J. C. *Photochem. Photobiol.* **1998**, *67*, 174.

(32) Sommeling, P. M.; Mulder, P.; Louw, R.; Avila, D. V.; Lusztyk, J.; Ingold, K. U. *J. Phys. Chem.* **1993**, *979*, 8361.

(33) Fossey, J.; Lefort, D.; Sorba, J. *Free Radicals in Organic Chemistry*; John Wiley & Sons: Paris, 1995.

(34) Paul, H.; Small, R. D. J.; Scaiano, J. C. *J. Am. Chem. Soc.* **1978**, *100*, 4520.

(35) An acid precursor other than the arylsulfonyl radical may have a different efficiency for generation of acid than the arylsulfonyl radical and would therefore not result in a factor of 2 in the values.

(36) Coenjarts, C.; Scaiano, J. C. *J. Am. Chem. Soc.* **2000**, *122*, 3635.

(37) The hydrogen abstraction ability of xanthone in acetonitrile is similar to that of the *tert*-butoxy radical. See reference 28 and references therein.

(38) Back, R. A. *Rev. Chem. Intermed.* **1984**, *5*, 293 and references therein.

(39) Gavina, F.; Luis, S. V.; Costero, A. M. *React. Polym.* **1987**, *6*, 291.

(40) Coenjarts, C.; Cameron, J. F.; Pohlers, G.; Scaiano, J. C.; Zampini, A. *J. Appl. Polym. Sci.* **2000**, *78*, 1897.

(41) Kice, J. L.; Bowers, K. W. *J. Am. Chem. Soc.* **1962**, *84*, 605.

(42) The difference in acid generation efficiency is not a result of a difference in the yield of arylsulfonyl radicals, which is essentially the same in both solutions.

(43) This acid yield experiment was performed in a 7x7 mm quartz cell containing 2 ml of solvent as compared to the acid yield experiments performed on the laser system in which as much as 500 mL in a flow system are used. Clearly, the potential for residual O_2 in the solution after degassing as well as introduction of O_2 during the experiment is much greater under the conditions in which laser excitation is employed.

(44) Coenjarts, C.; Ortica, F.; Cameron, J.; Pohlers, G.; Zampini, A.; Desilets, D.; Liu, H.; Scaiano, J. C. *Chem. Mater.* **2001**, *13*, 2305.

5. Photoacid Generation by N–Heteroaromatic Salts

5.1 Introduction

All of the photoacid generators (PAGs) mentioned in previous chapters are similar in that, upon photoexcitation, they undergo a bond cleavage reaction as the first chemical step towards acid generation. As part of our general efforts to study PAG photochemistry we are interested in designing new PAGs with varying mechanisms for photoacid generation. It is for this purpose that we consider molecules which participate in electron transfer (ET) as the initial photochemical step.

Photoinduced electron transfer (PET) involves ET between a photochemically excited molecule and a ground state molecule (Scheme 5-1a). The other type of ET process of concern here is indirect photoinduced electron transfer (IPET), which involves ET between a photochemically generated reaction intermediate and a ground state species (Scheme 5-1b). If the participating molecules are neutral, closed-shell species then the products are radical cations and radical anions, as depicted in Scheme 5-1. However, ET between a variety of charged and/or open-shelled species is also possible and, as expected, yields a variety of different products. Although these intermediates can have a variety of fates, cations and radical cations often undergo reactions which involve release of a proton.

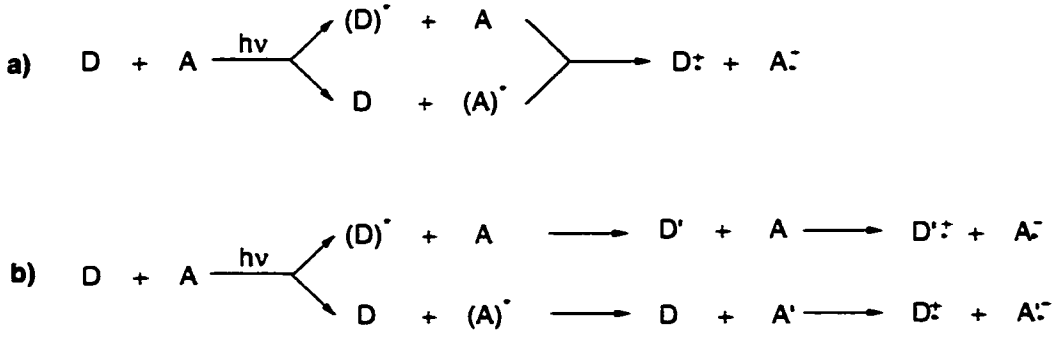

Scheme 5-1. Photoinduced electron transfer (a) and indirect photoinduced electron transfer (b).

The diphenyl sulfide radical cation is an intermediate in the photochemistry of sulfonium salts which is proposed to generate acid upon hydrogen abstraction from the solvent (Scheme 5-2).[1]

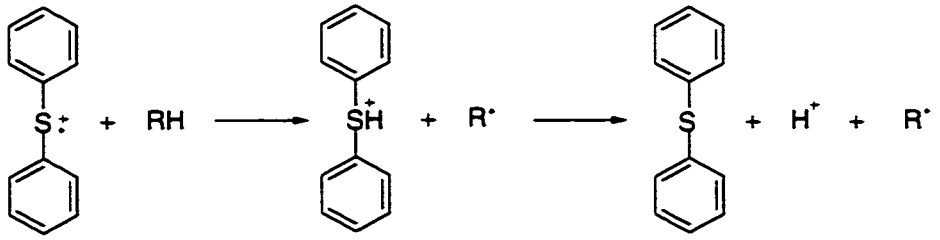

Scheme 5-2. The diphenyl sulfide radical cation generates acid via hydrogen abstraction.

Aromatic radical cations containing β-hydrogens often decompose to yield benzylic radicals upon proton release (Scheme 5-3).[2]

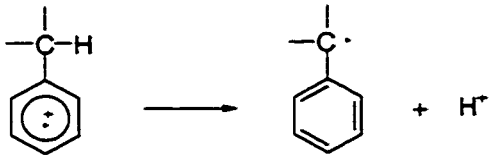

Scheme 5-3. β-cleavage of an aromatic radical cation to yield acid.

Although interesting examples of PET abound in the literature, the focus is primarily mechanistic in nature and is rarely concerned with acid generating efficiency.[3] As such, many of the systems explored in this chapter are inspired by reactions whose mechanisms are already well understood.

Exploiting ET reactions to generate acid is not without precedent. An intramolecular PET is the key step to very efficient photoacid generation in an interesting class of sulfonium salts (Scheme 5-4).[4] The analogous intermolecular reaction proceeds in much the same manner to yield acid.[5,6] A PET process is believed to be involved in some chemically amplified resists (CARs) in which a phenolic polymer is photochemically excited and is oxidized by an onium salt.[7] An

IPET process is involved in the oxidation of photochemically generated ketyl radicals to ketones by iodonium salts (*vide infra*).[8]

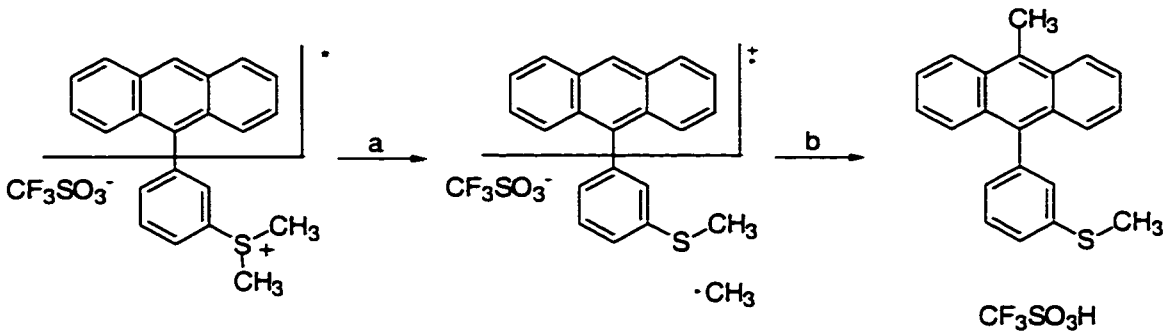

Scheme 5-4. Photoacid generation by an anthracenyl sulfonium salt via a) PET and bond cleavage and b) radical/radical cation coupling and proton release.

All of the aforementioned examples of ET processes are governed by the energetics of said process as described by the Rehm-Weller equation:[9]

$$\Delta G_{et} = E^{\circ}_{ox}(D) - E^{\circ}_{red}(A) - E^{*} + C \qquad \textbf{(Equation 5-1)}$$

E°_{ox} is the oxidation potential of the donor, D, E°_{red} is the reduction potential of the acceptor, A, E^{*} is the energy of the excited state participating in the reaction, and C is the Coulomb energy of the ion-pair formed after electron transfer. In order to ensure an efficient PET reaction, a system must be designed with these features in mind.

The focus of the work in this chapter is quite different from that for the PAGs discussed in Chapter 4. For those molecules there was interest in both the mechanism for photoacid generation and in evaluating their effectiveness as PAGs. The N-heteroaromatic salts presented here are discussed primarily in terms of the latter because their photochemical behaviour has already been described in the literature. By avoiding detailed mechanistic studies, evaluating many different PAG systems and discarding less-promising molecules before investing much time and effort in studying them is possible.

5.2 Pyridinium Salts

5.2.1 Introduction

The PET reactions of N-heteroaromatic salts containing the pyridinium moiety and iminium salts have been studied extensively both from a mechanistic and synthetic standpoint, with much of the ground-breaking work being done by Mariano et al.[10-13] In general, the system involves an electron-deficient pyridinium or iminium group tethered to an electron-rich donor, which participate in PET. One can imagine a variety of fates for the species generated by the PET step, the most obvious of which appear in Scheme 5-5: reactions (a)-(d) for the system in which the donor is a polyalkylbenzene. These reactions are as follows: (a) back electron transfer to regenerate starting materials, (b) deprotonation of the benzylic group, (c) fragmentation and (d) radical coupling.[14]

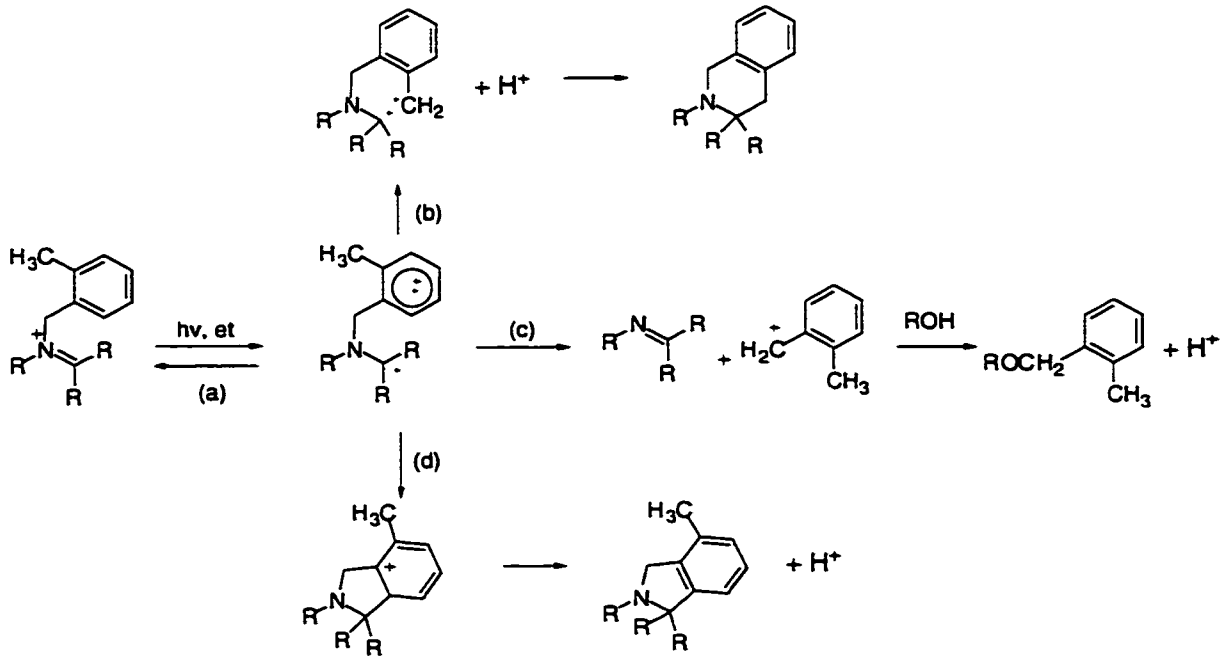

Scheme 5-5. Expected reaction pathways for the intermediate formed from an intramolecular PET from a polyalkylbenzene donor to an iminium or pyridinium acceptor.

Apart from reaction (a), a proton is produced in all of the pathways available to the first-formed radical cation/radical species. Although these molecules seem to behave as PAGs, their potential for actual use in this regard is difficult to predict. The difficulty arises from the fact that in addition to generating a proton, all of the reactions also generate an amine, which may limit the amount of acid free to react with other substrates. Although these reactions proceed with a high chemical yield for cyclization, there is little data concerning the quantum yields for reaction and none specifically dealing with quantum yield of acid generation (Φ_{acid}). Quantum yields for the formation of cyclized products range from ~0.01-0.05 (Scheme 5-6a,b).[12,14] If these values also correspond to the Φ_{acid} then they are probably too low for serious consideration as PAGs. It is hoped that these values can be improved upon by designing a molecule specifically with acid generation in mind.

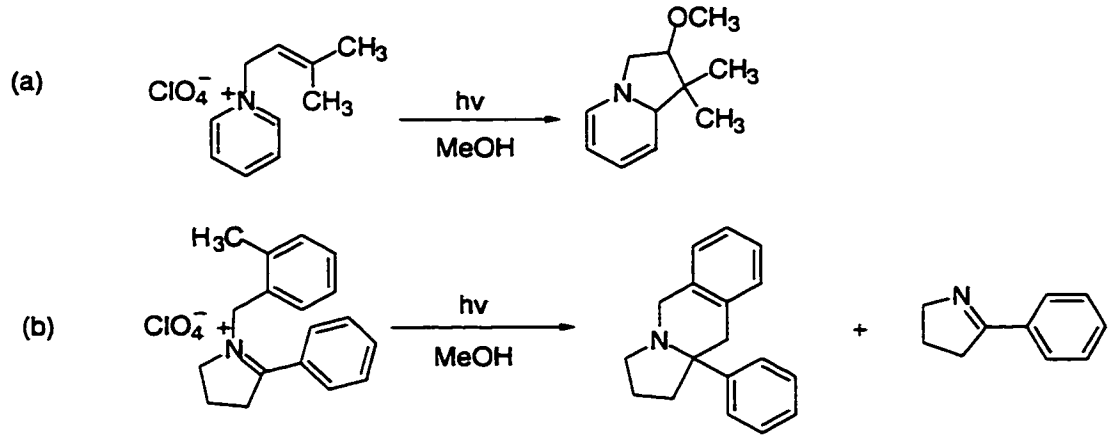

Scheme 5-6. PET reactions of some representative iminium and pyridinium salts.

For the studies performed here, the pyridinium moiety was chosen as an acceptor because its excited state energy ($\Delta E_{0,0}$ = 99 kcal/mol)[10] and reduction potential ($-E_{red}$ = 1.3 V vs. SCE)[10] act to make it the most easily reduced among typical iminium and N-heteroaromatic salts. Polyalkylbenzenes were chosen as the donors due to their enhanced oxidizability relative to the alcohols, ethers and alkenes, which are typically employed in these types of systems.[10]

5.2.2 Results and Discussion[15]

PAGs **5-1a** - **5-1c** were easily prepared via reaction of the appropriate pyridines and benzylic halides followed by anion exchange to yield the trifluoromethanesulfonate salt. In this way, the donor and acceptor properties were altered independently of one another in order to determine their effect on acid generating efficiency. The use of the trifluoromethanesulfonate salt is required so that the photogenerated acid is trifluoromethanesulfonic acid, which is much more relevant to current photolithographic processes than perchloric or halo acids.

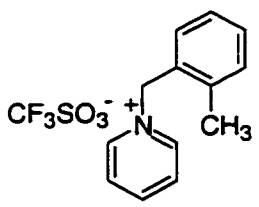

5-1a

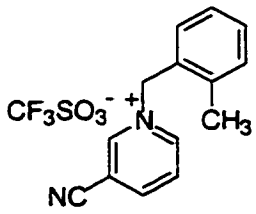

5-1b

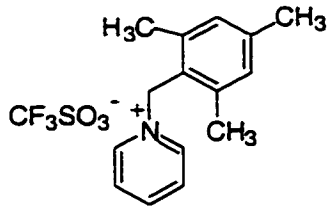

5-1c

Figure 5-1. PAGs 5-1a - 5-1c which contain an electron-deficient pyridinium moiety tethered to an electron rich aromatic group.

The relative Φ_{acid} for **5-1a** - **5-1c** in acetonitrile were measured under conditions of steady-state irradiation at 254 nm while employing triphenylsulfonium (TPS) triflate as a standard. The Φ_{acid} values were 8.0, 0.6 and 0.4% of that for TPS triflate, respectively. It is unclear why the compounds in which electron transfer is more energetically favourable, **5-1b** and **5-1c**, give much lower acid yields than **5-1a**. Perhaps the groups designed to facilitate electron transfer, i.e., the cyano substituent in **5-1b** and the trimethylated benzene in **5-1c**, also stabilize the radical cation and radical intermediates thereby allowing back electron transfer (reaction (a), Scheme 5-5) to increase in importance. Apart from this speculation, little effort was exerted to resolve this question as this class of compounds showed little potential for attaining appreciable Φ_{acid}.

5.3 1,4-Bipyridinium Salts

5.3.1 Introduction

The PET reactions of N-heteroaromatic salts containing a 1,4-bipyridinium moiety have been studied extensively, with much of the initial mechanistic insight being provided by the work of Ledwith et al. in the 1970's.[11,16,17] These molecules are referred to here as 1,4-bipyridinium salts for clarity, although the names paraquat and viologen also appear in the literature. Whereas initial interest in 1,4-bypridinium salts arose from their herbicidal activity, the prolonged attention paid to these molecules is due to their ease of both reduction ($-E_{red}$ ~ 0.6-0.7 V vs. SCE)[18] and spectroscopic detection of the reduction product. The single-electron reduction product of a 1,4-bipyridinium salt is a radical cation which is very persistent and has an intense blue colour.[19-21] Both properties combine to allow this radical cation to be detected and quantified without the benefit of time-resolved techniques.

The PET reaction of interest here is the photo-oxidation of alcohols containing an α-hydrogen to ketyl radicals by 1,4-bipyridinium salts (Scheme 5-7).[22-25] Although these reactions have not been studied in terms of photoacid generation, acid is a necessary product in the reaction.

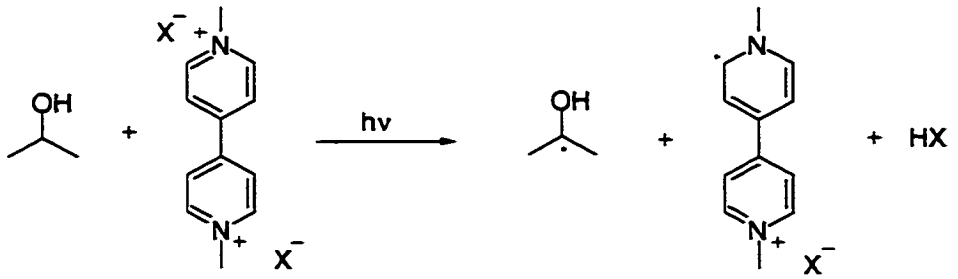

Scheme 5-7. Oxidation of 2-propanol to its ketyl radical by a 1,4-bipyridinium salt, which is reduced to its radical cation.

The oxidation of ketyl radicals to carbonyl compounds is also a well-established reaction in the chemistry of 1,4-bipyridinium salts.[23,24,26] Ketyl radicals, in addition to being formed in the oxidation of alcohols (Scheme 5-7), are generated in the photoreduction of aromatic ketones by a variety of hydrogen and electron donors as well as by photoinduced bond-cleavage of a variety of appropriately substituted molecules (*vide infra*). A process which begins with photogeneration of a ketyl radical in one of the three aforementioned ways, followed by its oxidation to the corresponding ketone by a 1,4-bipyridinium salt, may be another viable route to photogenerated acid (Scheme 5-8). The oxidation of aromatic ketyl radicals, as opposed to aliphatic ones, is studied here both because it should occur more efficiently due to their increased electron donor capacity and because these radicals can be easily detected spectroscopically.

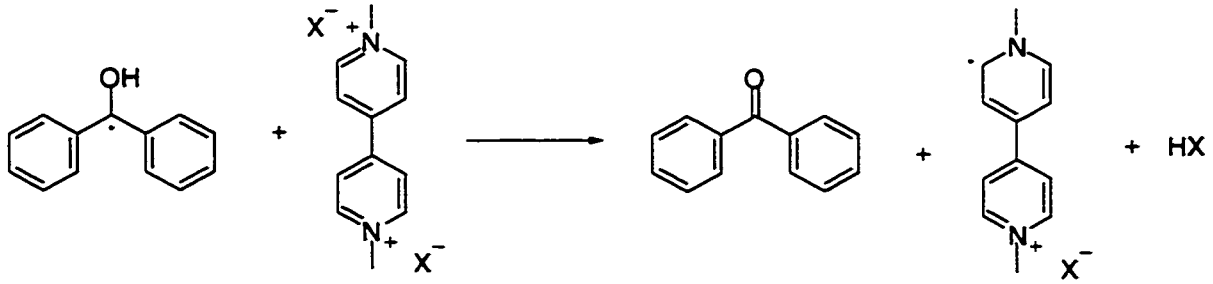

Scheme 5-8. Oxidation of the diphenyl ketyl radical to benzophenone by a 1,4-bypridinium salt.

To the best of our knowledge, neither of the reactions in Scheme 5-7 and 5-8 have been exploited as a means to photogenerate acid despite the fact that a proton is necessarily a product and high yields of the 1,4-bipyridinium radical cation under a variety of conditions are attainable.[25] As was the case for the pyridinium salts, **5-1a - 5-1c**, one must be cautious about gauging the usefulness of 1,4-bipyridinium salts as PAGs due to the coinciding photogeneration of a base via further reduction of the 1,4-bipyridinium derived radical cation.

5.3.2 Results and Discussion[15]

5.3.2.1 PET with Alcohols as Reducing Agents

PAGs **5-2a** and **5-2b** (Figure 5-2) were easily prepared via reaction of 4,4'-dipyridyl and the appropriate alkyl halide followed by anion exchange to yield the trifluoromethanesulfonate salt.

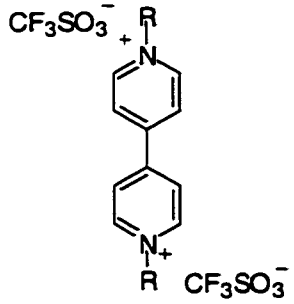

5-2a: R = CH_3
5-2b: R = n-propanol

Figure 5-2. PAGs 5-2a and 5-2b are electron deficient 1,4-bipyridinium salts.

Irradiation of **5-2a** in water/acetonitrile (1:99, v/v) with 2-propanol (1 M) under steady-state conditions at 254 nm and under laser irradiation at 266 nm caused a persistent blue colour in the solution. This solvent system was used in all subsequent experiments which involve 1,4-bipyridinium salts. The water is required to aid in the solubilization of the salt. The blue colour was attributed to the radical cation of 5-2a (**5-2a**$^{\bullet+}$), based on the characteristic absorption spectrum of 1,4-bipyridinium radical cations (Figure 5-3).[19-21] The same absorption spectrum was obtained under laser flash photolysis (LFP) of the same sample (Figure 5-3 inset.).

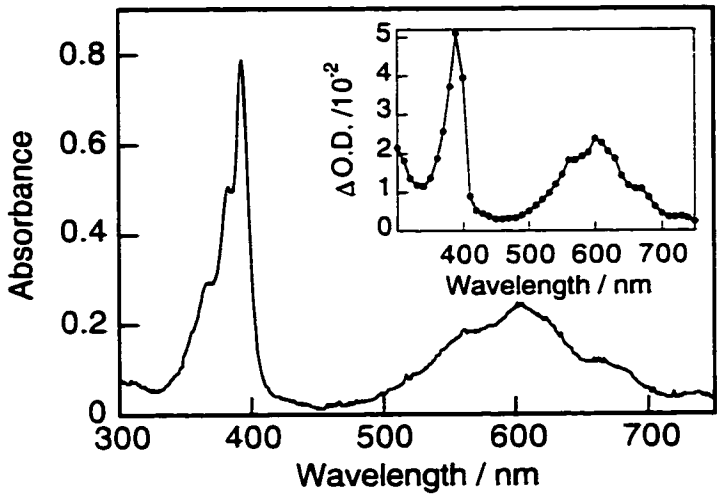

Figure 5-3. Absorption spectrum of 5-2a with 2-propanol (1 M) in water/acetonitrile after steady-state irradiation at 254 nm. Inset: Transient absorption spectrum of the same sample obtained 9.6 μs after a 266 nm laser pulse.

The relative Φ_{acid} of **5-2a** in N_2-saturated water/acetonitrile with either 2-propanol or ethanol, at a variety of both alcohol and **5-2a** concentrations, was measured under steady-state conditions at 254 nm with TPS triflate as a standard. The Φ_{acid} did not exceed 10 % of that for TPS triflate under any conditions. Initially, the possibility that **5-2a**$^{\bullet+}$ was absorbing the incident light, thereby lowering the amount of light available for absorption by **5-2a**, was considered. However, irradiations in air-equilibrated solutions, which do not develop a persistent blue colour because **5-2a**$^{\bullet+}$ is efficiently oxidized back to **5-2a** by O_2,[20] did not result in an enhancement in acid generation.

PAG **5-2b** was designed to give similar chemistry to that observed for **5-2a** in the presence of alcohols but via an intramolecular pathway. As far as usefulness as a PAG is concerned, this is a far superior system since a volatile additive in a CAR mixture such as 2-propanol would evaporate from the CAR during processing steps which occur prior to irradiation. Once again, LFP at 266 nm gave a signal consistent with a 1,4-bipyridinium derived radical cation although it was not as

persistent as found for **5-2a**. The decrease in lifetime may be due an intramolecular recombination reaction between the ketyl radical and the 1,4-bipyridinium radical cation which destroys the characteristic chromophore, although this reaction was not further investigated. The Φ_{acid} of **5-2b** in air and N_2-saturated water/acetonitrile was measured using 254 nm lamps and with TPS triflate as a standard at a variety of **5-2b** concentrations. The Φ_{acid} values were improved over **5-2a** but still remained below 25 % of that for TPS triflate.

It is suspected that the low yields of the 1,4-bipyridinium radical cation and consequently acid, may be due to the involvement of a back ET reaction following initial PET. In order to circumvent this problem an IPET process in which a reactive intermediate is the species to be oxidized, is considered. In this way, back ET does not yield unreactive starting materials which require another photon in order to participate in ET, but the reactive intermediate and a 1,4-bipyridinium salt which are immediately available to undergo ET once again.

5.3.2.2 ET with Ketyl Radicals as the Reducing Agents

The species investigated for use in IPET reactions with 1,4-bipyridiniums are aromatic ketyl radicals. Employing an IPET process instead of a PET process adds a further complication to achieving efficient acid generation. That being, one must find a means to photogenerate the ketyl radical with a high quantum yield. This is extremely important because the quantum yield of ketyl radical formation (Φ_{ketyl}) represents an upper limit for the Φ_{acid}. This strategy is different from that employed in the preceding section in which excess energy is introduced to the system by absorption of a photon by the 1,4-bipyridinium salt. Here, the photon is used to generate the ketyl radical, which must then be oxidized by a 1,4-bipyridinium salt in its ground state. Once again, **5-2a** was employed as the 1,4-bipyridinium salt

oxidizing agent. As a means to generate ketyl radicals, a variety of intermolecular and intramolecular reactions were investigated

5.3.2.2.1 Generation of Ketyl Radicals: Intermolecular Processes

The reduction of photoexcited ketones by a variety of hydrogen and electron donors is probably the most obvious way to form ketyl radicals with a high quantum yield. Employing this strategy, the series of reactions which must occur in order to generate acid are outlined in Scheme 5-9. In order to efficiently generate acid, each of the processes which precede acid generation must occur efficiently. As a first step towards gauging the viability of this IPET system as a PAG, the photoreduction of aromatic ketones by polyalkylbenzene (ArH) donors to generate ketyl radicals which are then available for oxidization by **5-2a**, was studied.

$$\text{ketone} \xrightarrow{h\nu,\ isc} {}^3(\text{ketone})^* \xrightarrow{k_{red}[RH]} \text{ketone(H)}\bullet \xrightarrow{k_{ox}[5\text{-}2a]} \text{ketone} + H^+ + 5\text{-}2a^{\bullet}$$

Scheme 5-9. Photoreduction of triplet-excited ketones by hydrogen donors (RH) and subsequent oxidation of the ketyl radicals by 5-2a.

The rate constants for electron transfer from aromatic ketyl radicals to molecules similar to **5-2a** (differing only in the anion) are ~10^9 $M^{-1}s^{-1}$.[26] The large rate constant is encouraging because it suggests that perhaps conditions can be chosen such that, once formed, the ketyl radicals can be quantitatively oxidized. ArHs were chosen as the reducing agents for the photoexcited ketones because of their wide range of rates of reaction with aromatic ketone triplets, (10^5-10^9 $M^{-1}s^{-1}$)[27] and the fact that the more highly substituted ones are solids and could conceivably be employed in a CAR. A pair of related aromatic ketones, xanthone (XAN) and 1-azaxanthone (AZAX) (Figure 5-4), were chosen because their transient photochemistry is well described, primarily due to the fact that XAN has proven to be useful as a probe for polarity[28-30] and AZAX as a potential probe for studying radical pair dynamics in heterogeneous systems.[31-33].

XAN AZAX

Figure 5-4. Aromatic ketones XAN and AZAX.

As is obvious from Section 5.2.2 and 5.3.2.1, the PAG evaluation strategy in use here typically involves a quick screening of acid generating ability to avoid expending effort on systems which show little promise. However, in the current case, detailed mechanistic studies are required in order to determine the efficiency and mechanism of ketyl radical production. This indulgence is justified because of the substantial literature precedence, in the form of the aforementioned rate constants for the various reactions, which suggest that this type of system can be employed to generate **5-2a**$^{\bullet+}$ in high yield. The leap of faith at this point is that acid yields will be high as well.

In polar solvents, there is an appreciable difference in reactivity between the xanthone triplet (^{3}XAN$^\bullet$), which is predominantly π,π^* in character,[34,35] and the 1-azaxanthone triplet (^{3}AZAX$^\bullet$), which is predominantly n,π^* in character,[31] with various hydrogen and electron donating substrates. The specific origin of the differences in reactivity cannot be immediately attributed to either the increased reactivity of n,π^* triplets towards hydrogen abstraction or electron acceptor properties of the triplets. The uncertainty arises from the fact that the formation of ketyl radicals, XAN(H)$^\bullet$ and AZAX(H)$^\bullet$, as products in these reactions can be visualized as occurring in one-step via hydrogen abstraction (H) from the donor, or in multiple-steps via ET followed by proton transfer (PT) or by formation of a charge transfer (CT) type encounter complex[36] prior to hydrogen atom transfer (HT). The involvement of each of these processes in the reduction of aromatic ketones is well established.[37,38] The potential competition between these pathways in the reactions of photoexcited

aromatic ketones with ArH donors appears in Scheme 5-2 with XAN used as an example.

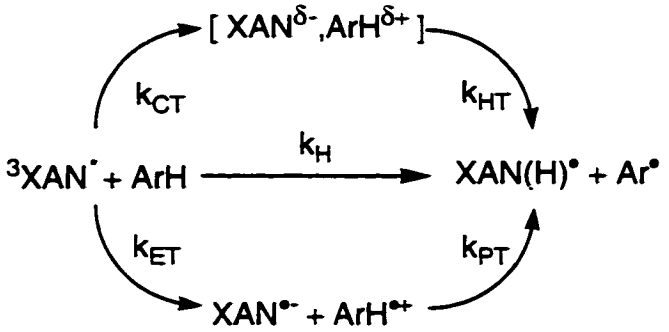

Scheme 5-10. Possible reactions involved in the photoreduction of an aromatic ketone by a polyalkylbenzene (refer to text for definitions of abbreviations).

Systems involving ArH donors in which CT pathways are active are believed to proceed through formation of an encounter complex between excited acceptor and ground state donor.[27,39-43] With this species as a reaction intermediate one is forced to consider both the kinetics for encounter complex formation as well as its subsequent reactivity. It has been established that the structures of encounter complexes differ for n,π^* and π,π^* triplets and that stereoelectronic effects are important to their formation and reactivity.[40] It has also been shown that the reaction between photoexcited quinones and ArH donors with bulky alkyl groups is slowed down relative to their methylated counterparts.[41,42] This result was rationalized on the basis of a difficulty in forming CT type encounter complexes between photoexcited quinones and sterically encumbered aromatics.

In order to gain further insight into the competition between the various reaction pathways and the potential involvement of encounter complexes of different structures in the reaction between ^{3}XAN* and ^{3}AZAX* with ArH donors, the bimolecular rate constants, k_{obs}, isotope effects and product yields for several combinations of donor and acceptor pairs were determined. Additionally,

experiments on sterically encumbered ArH donors are expected to aid in the investigation of the nature of the encounter complexes involved in these reactions. Clearly, an involved mechanistic study such as this is more than a little removed from the issue of photoacid generation. Once again, this diversion is justified because mechanistic insights, although valuable in their own right, are also useful for evaluating the feasibility of the reactions in an actual CAR.

5.3.2.2.1.1 Results and Discussion

LFP of solutions of XAN and AZAX in acetonitrile at 337 nm generates their triplet states, ^{3}XAN* and ^{3}AZAX*, as judged by their characteristic absorption spectra,[31,34,35] with lifetimes of ≤ 3 μs.[44] In the presence of benzene and ArH donors (Figure 5-5) these lifetimes are shortened significantly. In the case of benzene and an ArH donor without benzylic hydrogens, such as DTB, the triplets decay to their spectral baseline (Figure 5-6a,b). In contrast, in the presence of ArH donors with benzylic hydrogens, the spectra of the triplets is replaced by that of their ketyl radicals, XAN(H)$^\bullet$ and AZAX(H)$^\bullet$ (Figure 5-6a,b).[31] The benzylic radicals of the ArH donors, which are also generated, are not observed because they are masked by overlap with the absorptions due to XAN(H)$^\bullet$ or AZAX(H)$^\bullet$.[45,46] Interestingly, there is no evidence for the formation of the expected products from electron transfer, i.e., radical anions, XAN$^{\bullet-}$ and AZAX$^{\bullet-}$,[31] and radical cations of the ArH donors[47,48] (*vide infra*). Whatever the specific nature of the reactions responsible for the reaction, the k_{obs} values were determined for the quenching of ^{3}XAN* and ^{3}AZAX* by various ArH donors and appear in Table 5-1.

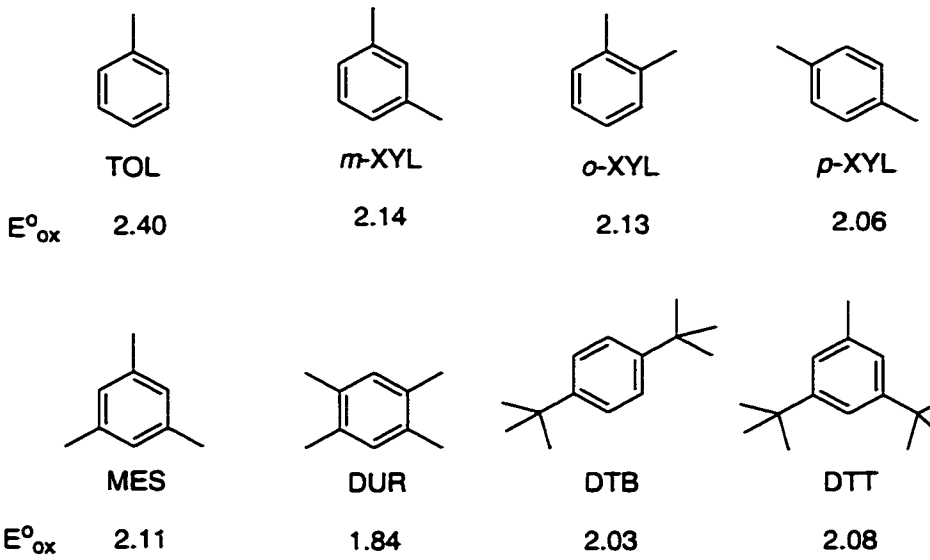

Figure 5-5. Polyalkylbenzenes and their oxidation potentials.

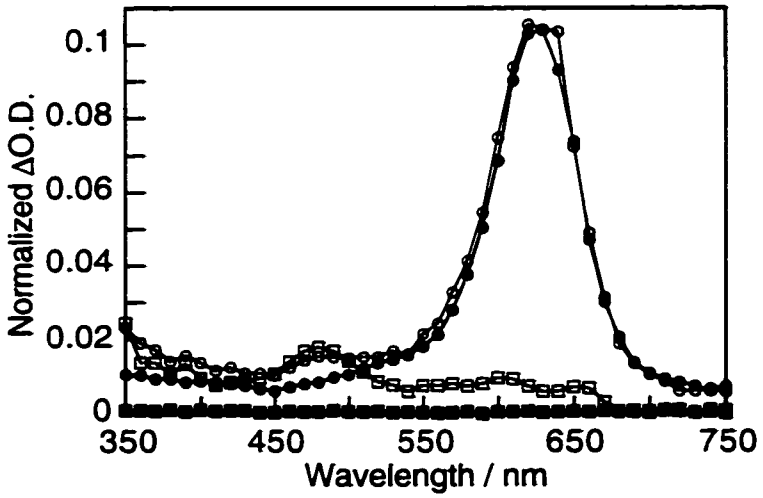

Figure 5-6a. Transient absorption spectra obtained upon LFP of XAN at 337 nm in N_2-saturated acetonitrile solutions with 7.3 mM DUR, recorded 0.056 μs (○) and 1.1 μs (□) after the laser pulse and 150 mM DTB, recorded 0.2 μs (●) and 5.5 μs (■) after the laser pulse.

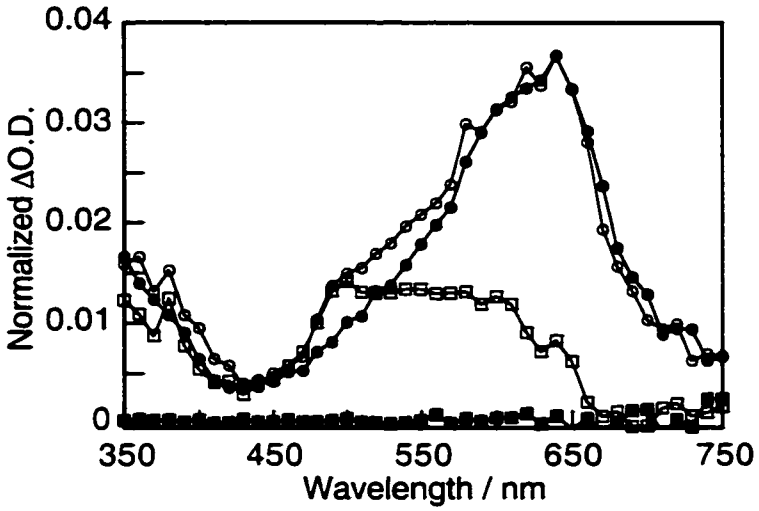

Figure 5-6b. Transient absorption spectra obtained upon LFP of AZAX at 337 nm in N_2-saturated acetonitrile solutions with 1.0 mM DUR, recorded 0.024 μs (○) and 1.1 μs (□) after the laser pulse, and 605 mM benzene, recorded 0.024 μs (●) and 1.1 μs (■) after the laser pulse.

Table 5-1. Kinetic and quantum yield data for the quenching of XAN and AZAX by alkylbenzenes in acetonitrile.

	XAN			AZAX		
Quencher	ΔG_{et} (eV)[a]	k_{obs} ($M^{-1}s^{-1}$)	ϕ_{ketyl}	ΔG_{et} (eV)	k_{obs} ($M^{-1}s^{-1}$)	ϕ_{ketyl}
TOL	1.00	5.8×10^6	0.53	0.66	1.6×10^8	0.38
***o*-XYL**	0.73	3.1×10^7	0.43	0.39	1.2×10^9	0.31
***m*-XYL**	0.74	4.6×10^7	0.49	0.40	1.1×10^9	0.36
***p*-XYL**	0.66	5.9×10^7	0.74	0.32	1.7×10^9	0.58
MES	0.71	2.2×10^8	0.45	0.37	3.1×10^9	0.46
DUR	0. 44	1.1×10^9	1.0	0.10	1.1×10^{10}	0.70
DTB	0.63	7.9×10^6	0	0.29	2.0×10^8	0
DTT	0.68	2.7×10^7	0.55	0.34	5.2×10^8	0.52

[a]The energetics for electron-transfer as determined by the Rehm-Weller equation (*vide supra*). The C term was neglected in view of the solvent used being acetonitrile. E^o_{red} values for XAN and AZAX were determined by cyclic voltammetry to be -1.76 V and -1.48 V vs. SCE, respectively. The triplet energies of XAN and AZAX were taken to be 74.1 kcal/mol[49], and 72.7 kcal/mol[31] respectively.

From Table 5-1 it can be seen that the k_{obs} for $^3AZAX^{\bullet}$ with any given ArH donor is ~10x larger than that determined for $^3XAN^{\bullet}$. This difference in reactivity can be rationalized in terms of both potential deactivation pathways.

Firstly, the relative reactivities of $^3XAN^{\bullet}$ and $^3AZAX^{\bullet}$ towards electron transfer reactions can be inferred by comparing their k_{obs} values obtained in the reaction with benzene.[50] Based on these values, it can be assumed that, in general, the rate of quenching of $^3AZAX^{\bullet}$ strictly by CT processes is ~10x faster than the same reaction with $^3XAN^{\bullet}$.[51] The increased reactivity towards CT processes by $^3AZAX^{\bullet}$ relative to $^3XAN^{\bullet}$ is expected given the lower E°_{red} of AZAX which makes the reaction more energetically favourable.

In a similar manner, the relative reactivities of $^3XAN^{\bullet}$ and $^3AZAX^{\bullet}$ towards hydrogen abstraction can be inferred by comparing their k_{obs} for quenching by cyclohexane, which were determined to be $8.8 \times 10^5\ M^{-1}s^{-1}$ and $7.5 \times 10^6\ M^{-1}s^{-1}$, respectively. Based on these values, it can be assumed that, in general, the rate of quenching of $^3AZAX^{\bullet}$ strictly by hydrogen abstraction is ~10x faster than the same reaction with $^3XAN^{\bullet}$. Although the lowest triplet of XAN in acetonitrile is $\pi,\pi^{\bullet}$ in nature, a low-lying $n,\pi^{\bullet}$ triplet which is thermally accessible is probably responsible for much of the hydrogen abstraction behaviour.[52-54] The increased reactivity towards hydrogen abstraction by $^3AZAX^{\bullet}$ relative to $^3XAN^{\bullet}$ is expected owing to its $n,\pi^{\bullet}$ nature.

In order to gain some insight into the reactivities of the ArH donors to a strictly hydrogen abstraction pathway, one can consider their reactivities towards *tert*-butoxy radicals. Given that it is well established that $n,\pi^{\bullet}$ ketone triplets show parallel and comparable reactivity towards hydrogen abstraction reactions as alkoxy radicals,[55] any triplet ketone that reacts with ArH donors only by hydrogen abstraction should display the same ratio of rate constants as their reaction with *tert*-

butoxy radicals.[55-59] The ratio of the rate constants for hydrogen abstraction, k_H, from TOL, *m*-XYL, *p*-XYL, MES and cyclohexane by *tert*-butoxy radicals is 1.0 : 2.3 : 3.0 : 4.0 : 6.0.[60] Based on the k_{obs} values obtained for cyclohexane with XAN and AZAX, the contribution of k_H to the k_{obs} for the reactions of ArH donors with $^3XAN^{\bullet}$ and $^3AZAX^{\bullet}$ can be estimated. The results from this analysis appear in Table 5-2. The important idea to extract from this data is that while the expected k_H values are all within a factor of 5 of one another, the k_{obs} values span 2 orders of magnitude. Typically, $^3XAN^{\bullet}$ and $^3AZAX^{\bullet}$ react ~100x faster with the various ArH donors than one would expect for a simple hydrogen abstraction. On the basis of these simple arguments, > 99% of the reaction with ArH donors can be attributed to some form of CT interaction.

Table 5-2. Calculated contribution of k_H to k_{obs}.

	XAN		AZAX	
Quencher	**k_H[a] ($M^{-1}s^{-1}$)**	**k_H/k_{obs} (x100)**	**k_H ($M^{-1}s^{-1}$)**	**k_H/k_{obs} (x100)**
TOL	1.5×10^5	2.6	1.2×10^6	0.75
***m*-XYL**	3.4×10^5	0.74	2.9×10^6	0.26
***p*-XYL**	4.4×10^5	0.74	3.7×10^6	0.22
MES	5.9×10^5	0.27	5.0×10^6	0.16

[a]See text for method of determination of rate constants.

While results based on this type of indirect analysis should be interpreted cautiously, they do suggest rather clearly that the greater reactivity of $^3AZAX^{\bullet}$ towards hydrogen abstraction is balanced by its increased reactivity towards electron transfer. The somewhat serendipitous implication of this is that the competition between hydrogen abstraction and CT pathways is similar for $^3XAN^{\bullet}$ and $^3AZAX^{\bullet}$.

A confirmation of the lack of a direct hydrogen abstraction pathway is the absence of any significant isotope effects in the reactions with ArH donors, as shown in Table 5-3. Experiments were performed using benzene and cyclohexane as model compounds for which quenching should occur entirely via CT and direct hydrogen abstraction, respectively; the values obtained were 1.0-1.3 and 2.9-3.9, respectively. The kinetic isotope effect observed for TOL and *o*-XYL, compounds for which both electron transfer and hydrogen abstraction can occur are intermediate to those observed for the isolated processes, and range from 1.1 to 1.6. Given the absence of any discernible trend in these isotope effects, either in acceptor or donor properties, one can conclude that they are small enough to be consistent with a mechanism based entirely on CT interactions. Given the apparent lack of involvement of direct hydrogen abstraction in these reactions, the specific nature of the CT pathway, i.e., direct electron transfer or partial electron transfer within an encounter complex, can be addressed.

Table 5-3. Kinetic isotope effects observed in selected systems.[a]

	XAN			AZAX		
Quencher	k_{obs} ($M^{-1}s^{-1}$)	k_H/k_D[b]	ϕ_{ketyl}	k_{obs} ($M^{-1}s^{-1}$)	k_H/k_D	ϕ_{ketyl}
cyclohexane-d_{12}	2.2×10^5	3.9	1.0	2.6×10^6	2.9	1.0
benzene-d_6	5.0×10^5	1.3	0.0	9.3×10^6	1.0	0.0
TOL-d_8	3.8×10^6	1.5	0.20	1.0×10^8	1.4	0.16
***o*-XYL-d_{10}**	2.7×10^7	1.1	0.16	7.6×10^8	1.6	0.14

[a]Same conditions as in Table 1. [b]Errors estimated at ± 10%.

In light of the assessment that direct hydrogen abstraction is an unimportant pathway, the fact that efficient quenching is observed even though electron transfer is an endergonic process for all of the XAN and AZAX/ArH pairs (as shown in Table 5-1) suggests that quenching does not involve full electron transfer. It is more likely

due to CT within an encounter complex between excited ketone and ArH donor and is followed by facile hydrogen transfer to yield ketyl and benzylic radicals. Such CT complexes have been detected in the interaction of quinones with ArH donors.[41] Further to this point, a pathway involving direct electron transfer, which would yield a solvent separated radical ion pair, is not considered to be reasonable, since products from electron transfer are not observed under these experimental conditions. In a polar solvent, such as acetonitrile, one would not expect proton transfer or back electron transfer between a solvent separated radical ion pair to completely overwhelm ion separation.

Full electron transfer after the formation of the encounter complex is also deemed to be an unimportant pathway since it should yield a contact radical ion pair which typically dissociate or recombine in polar solvents with rate constants much larger than those expected for proton transfer.[61-64] The inability to detect ionic products, coupled with large yields of radical products, is inconsistent with a pathway involving full electron transfer at any point along the reaction path. Although a contact-pair that undergoes no escape cannot be ruled out, it seems rather unlikely for a triplet-derived pair in a low viscosity solvent. This result is consistent with the low ion yields and large radical yields reported for the reactions of benzophenone with ArH donors in acetonitrile, a system in which encounter complex intermediates are proposed to be important.[27]

The involvement of an encounter complex is more directly indicated by the difference in k_{obs} obtained for ArH donors with similar E^{o}_{ox} but very different steric characteristics. As previously mentioned, sterically encumbered ArH donors have been shown to have reduced reactivity towards formation of CT encounter complexes relative to their unencumbered analogs. Here, DTB and DTT are employed as sterically encumbered donors which have similar E^{o}_{ox} to *p*-XYL and MES, respectively. In the reactions with both $^{3}XAN^{\bullet}$ and $^{3}AZAX^{\bullet}$ the k_{obs} obtained

are reduced by ~6-8x relative to their unencumbered analogs. The reduction in reactivity in these systems is reasonably attributed to a difficulty in forming encounter complexes and assume that the involvement of this reaction intermediate can be extended to all of the donor/acceptor pairs currently under consideration.

The reversibility of the formation of a CT encounter complex in these types of reactions is a matter of the competition between decay of the encounter complex to regenerate excited state species with other decay processes to yield ground state species. Since complete electron transfer has been ruled out as a likely pathway, these deactivation processes include only hydrogen atom transfer and non-radiative decay. In order to determine the extent of reversibility of the complexes formed in the systems currently under consideration one must examine the kinetic isotope effects obtained.

The presence of a sizeable isotope effect is expected if the reaction involves either direct hydrogen atom abstraction or hydrogen atom transfer following reversible complexation. Hydrogen atom transfer following irreversible complexation will not affect the observed kinetics because there is no means by which a decrease in the rate of the hydrogen transfer can feed back on the initial complexation dynamics. The magnitude of the isotope effects expected for a hydrogen abstraction reaction have already been discussed, and an isotope effect for the proton transfer following electron transfer of 2.4-5.6 have been reported for similar systems.[46] The negligibly small values obtained in this work are much more consistent with those expected to occur in a situation in which complex formation is rate-determining and irreversible. Additional evidence for this kinetic scheme is that while there is no appreciable isotope effect on the kinetics there is an isotope effect of > 2.5 on the efficiency of ketyl radical formation (ϕ_{ketyl}) (Table 5-1). This clearly indicates that the hydrogen atom transfer occurs after the rate determining step, i.e.,

complexation. The relevant processes involved in these reactions are shown in Scheme 5-11.

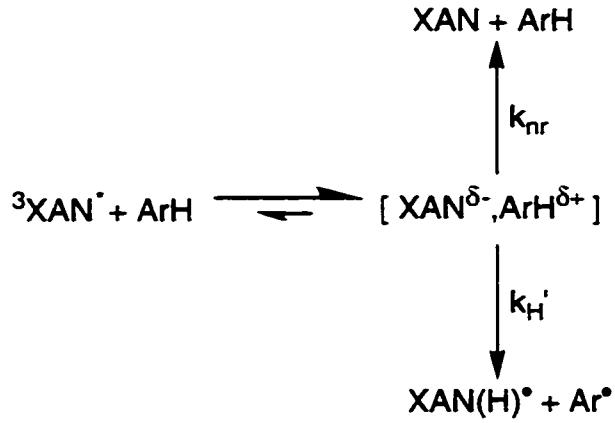

Scheme 5-11. Irreversible complex formation between $^3XAN^{\bullet}$ and ArH followed by decay to ground state or hydrogen atom transfer.

Given that the rate-determining step appears to be charge transfer with the formation of encounter complexes, it is not surprising that the kinetics correlate well with the energetics of electron transfer as shown in Figure 5-7. Interestingly, XAN and AZAX not only respond to changes in the energetics in the same manner but reactions with similar ΔG's give almost the same k_{obs}. However, it should be acknowledged that a larger group of donors and acceptors which span a greater ΔG may reveal a trend indicating different reactivities. For the purposes of interest here, it is satisfactory to state that for the systems studied here the quenching is entirely controlled by redox properties of the pairs forming the encounter complex and the electronic configuration of the triplet is important only inasmuch as it affects the reduction potential of the ketone.

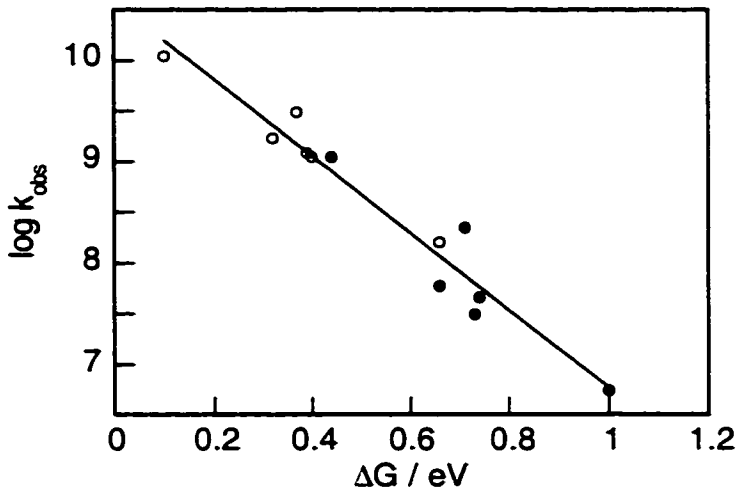

Figure 5-7. Correlation between the logarithm of the rate constant, log(k_{obs}), for reaction of ^{3}XAN* (●) and ^{3}AZAX* (○) and the driving force for an electron transfer reaction, ΔG.

In order to determine which factors control the reactivity of the encounter complex once formed, the competition between the possible deactivation pathways: hydrogen atom transfer within the encounter complex and non-radiative decay of the encounter complex as gauged by the ϕ_{ketyl}, were considered.

The ϕ_{ketyl} from ^{3}XAN$^{\cdot}$ and ^{3}AZAX$^{\cdot}$ in the presence of ArH donors were determined using cyclohexane as a standard for which it is assumed that $\phi_{ketyl} = 1$. These values also appear in Table 5-1. The ϕ_{ketyl} values are related to the Φ_{ketyl} by the expression:

$$\Phi_{ketyl} = \Phi_{isc} \times \phi_{ketyl} \times f \qquad \textbf{(Equation 5-2)}$$

Where Φ_{isc} is the quantum yield of intersystem crossing of the photoexcited keotne to the triplet state and *f* is the fraction of triplets which react with ArH donors. The ϕ_{ketyl} values are a measure of the tendency to form ketyl radicals from the CT encounter complex, and as such are mechanistically interesting. The Φ_{ketyl} values are concerned with the efficiency of the conversion of photons to ketyl radicals and

will be the more important piece of information in terms of acid generating applications.

Although ϕ_{ketyl} values are governed by the relative rates of both deactivation pathways, the results are rationalized based entirely on the expected effects on the rate of hydrogen transfer because it is easier to conceptualize factors which affect this well-defined process as compared to the more general process of non-radiative decay. With the exception of TOL, the ϕ_{ketyl} values for XAN and AZAX correlate well with the energetics for an electron transfer reaction, decreasing with increasing endergonicity as shown in Figure 5-7. The observed trend can be rationalized based on the presumed degree of CT within the encounter complexes. The observation of a kinetic acidity affect on the product ratios in the quenching of *p*-cymene with aromatic ketones by Wagner et al., suggest that the more energetically favorable electron transfer is for a given donor/acceptor pair, the greater the amount of charge separation within an encounter complex between them.[39] This conclusion is further supported by an observed red-shift in the near-IR bands assigned to the encounter complex between photoexcited quinones and ArH donors as the driving force for electron transfer increases.[40] The greater the charge separation in an encounter complex the lower the activation energy for hydrogen atom transfer;[39] which should allow hydrogen atom transfer to compete more favourably with other deactivation pathways and result in a higher ϕ_{ketyl}.

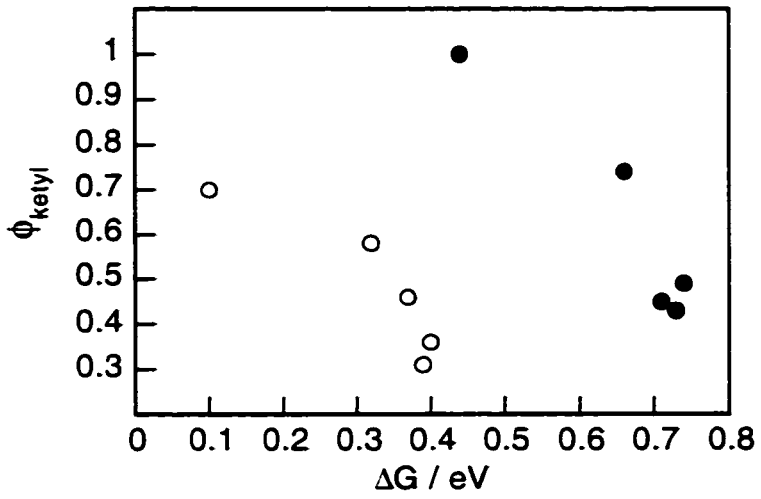

Figure 5-8. Effect of changes in the driving force for electron transfer, ΔG, on the quantum yield for ketyl radical formation, ϕ_{ketyl}, for XAN (●) and AZAX (○) in the reaction with ArH donors.

Though the ϕ_{ketyl} for XAN and AZAX follow the same trend, those for AZAX are lower than XAN despite the much increased exergonicity. Based on the previous argument these systems should have greater CT within the encounter complex than the XAN systems, thereby facilitating hydrogen atom transfer. In order to rationalize this result, the structure of the encounter complexes must be considered. It is generally accepted that encounter complexes of this kind involve overlap between donor HOMO and a half-filled orbital of the excited state acceptor.[40,65,66] Therefore, for ^{3}XAN$^\bullet$, an encounter complex is expected to form between overlap of an ArH π orbital and the benzoyl π orbital, but for ^{3}AZAX$^\bullet$, the involvement of the carbonyl n orbital is expected (Figure 5-8). The different geometries of the encounter complexes formed have been used to rationalize stereoelectronic effects observed due to tighter π,π$^\bullet$ encounter complexes and more loose n,π$^\bullet$ encounter complexes.[40]

As can be seen in Figure 5-8, in the case of π,π$^\bullet$ encounter complexes there is the potential for formation of structures in which the carbonyl oxygen is located in

close proximity to a benzylic hydrogen. As charge separation occurs the donor begins to develop a positive charge and the methyl group bears some of this charge. The carbonyl oxygen of the π,π^* triplet is initially nucleophilic and becomes even more so as charge separation increases and it develops a negative charge. A structure in which these groups are close to one another obviously facilitates hydrogen atom transfer and should be favoured over other structures due to electrostatic interactions.

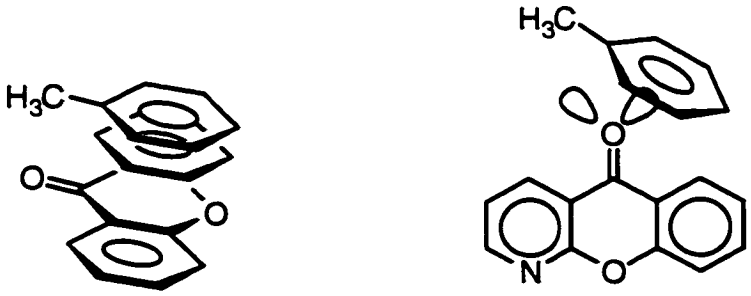

Figure 5-9. Suggested excited-state interactions, see text.

In contrast, for n,π^* encounter complexes the n orbital is buried in the π system, much less closely associated with the benzylic hydrogens than in the case of the π,π^* encounter complexes. Given the n,π^* nature of the triplet the carbonyl oxygen is actually electrophilic, so the electrostatic preference displayed in the case of π,π^* triplets is less important. As such, one would expect slower rates of hydrogen atom transfer which leads to lower ϕ_{ketyl}.

Toluene breaks the trend described above by giving larger ϕ_{ketyl} than expected based on the energetics of the reaction as compared to other ArH donors. TOL is unique among the donors in that it contains only one methyl group to stabilize the positive charge which develops in the aromatic ring of the donor as the encounter complex forms. As such, that methyl should bear a greater charge than in a donor with multiple substituents, in which the positive charge is shared more evenly throughout the molecule. Consequently, the encounter complex geometry in

which this group and the carbonyl oxygen are closely associated should be even more favoured than for other ArH donors. Additionally, given that CT within the encounter complex activates the benzylic C-H bond, when there is only one such group this so-called activation is entirely focused on that group and a larger ϕ_{ketyl} results.

5.3.2.2.1.2 Mechanistic Summary

The reactions of the photoexcited aromatic ketones, XAN and AZAX with ArH donors has been studied by LFP. The main reaction pathway is the irreversible formation of CT encounter complexes followed by hydrogen atom transfer in competition with nonradiative decay via reverse CT. There was no need to invoke direct hydrogen abstraction or complete electron transfer as being at all competitive in these reactions. The reactivities of the XAN π,π^* triplet and AZAX n,π^* triplet towards these donors is governed by their reduction potentials, with their electronic configuration being unimportant to the kinetics of encounter complex formation with sterically unencumbered donors.

The extent of CT within the encounter complexes increases as the energetics for electron transfer become more favorable as judged by an increase in ϕ_{ketyl} with decreasing endergonicity. This effect arises from the fact that CT facilitates hydrogen atom transfer. The aforementioned different structures of the encounter complexes creates a difference in response to this stereoelectronic effect as the n,π^* encounter complexes have structures in which hydrogen transfer is less facile due to the lack of proximity between the benzylic groups.

5.3.2.2.1.3 Photoacid Generation

The first step in exploiting this newly acquired mechanistic insight into ketyl radical formation by these systems, is to decide which pairing of ketones and ArH donors will give the largest Φ_{ketyl} values. As demonstrated by Equation 5-2, Φ_{ketyl} is a

product of *f*, ϕ_{ketyl} and Φ_{isc}. The value of *f* depends on the concentration of ArH and the k_{obs} for the reaction. Among the ArH's employed, DUR reacts with $^3XAN^{\bullet}$ and $^3AZAX^{\bullet}$ the fastest and 10x faster with $^3AZAX^{\bullet}$ than $^3XAN^{\bullet}$. Additionally, the highest ϕ_{ketyl} values are obtained with DUR as a donor. The AZAX/DUR system is preferred for exploring the acid generation pathway over the XAN/DUR system despite a slightly lower ϕ_{ketyl} ,0.7 as compared to 1.0, because of the larger k_{obs}. The increased rate constant is particularly important in light of the fact that these reactions must work in a polymer film in which diffusion of reagents is slowed relative to solution. Employing Equation 5-2 in which the relevant values are: Φ_{isc} = 0.82,[32] ϕ_{ketyl} = 0.7 and *f* = 0.95 (for 1 mM DUR), gives a value of Φ_{ketyl} = 0.55, which is also the upper limit for the quantum yield of **5-2a**$^{\bullet+}$ ($\Phi_{5\text{-}2a^{\bullet+}}$) and Φ_{acid}. Preliminary experiments using 355 nm excitation, in N_2-saturated acetonitrile with DUR (1 mM) , **5-2a** (0.2 mM) and enough AZAX to give an absorbance of ~0.3, gave a $\Phi_{5\text{-}2a^{\bullet+}}$ of 0.4, based on benzophenone actinometry. The discrepancy between this value and the calculated value of 0.55 is likely a result of inefficient reaction between the AZAX(H)$^{\bullet}$ and **5-2a** at the concentration employed.

As depicted in Scheme 5-9, the reaction of AZAX(H)$^{\bullet}$ with **5-2a** is the final step in acid generation which begins with the reaction of $^3(AZAX)^{\bullet}$ and DUR to yield AZAX(H)$^{\bullet}$. The efficiency of the entire process requires that none of the components participate in reactions other than the ones intended. However, an undesired side reaction, which does not appear in Scheme 5-9, is the oxidation of $^3(AZAX)^{\bullet}$ by **5-2a**, which occurs with rate constants similar to the desired reaction with AZAX(H)$^{\bullet}$, to yield intermediates which may or may not yield acid themselves.[26] In order to reduce contributions from this pathway, the concentrations of DUR and **5-2a** must be chosen carefully so that **5-2a** cannot effectively compete for reaction with the $^3(AZAX)^{\bullet}$. Solutions of DUR (5 mM) and **5-2a** (5 mM) were used with these concerns in mind. The Φ_{acid} at 355 nm in N_2-saturated solution was determined to

be 0.16, based on benzophenone actinometry. It is unclear why this value is substantially lower than expected based on the $\Phi_{5\text{-}2a^{\bullet+}}$.

Although this particular system is limited by the inefficiencies in Φ_{acid} inherent to the process, as well as by inefficiencies introduced by side reacions, this result does succeed in demonstrating that the concept of acid generation via oxidation of ketyl radicals by **5-2a** is viable. The success of this system in this regard prompted the search for a more efficient means to photochemically generate ketyl radicals.

Along these lines, the use of benzhydrol as a hydrogen donor in place of DUR was considered. The use of benzhydrol as a hydrogen donor for aromatic ketones is intriguing because upon oxidation, benzhydrol yields the diphenyl ketyl radical. Thus, reaction between an aromatic ketone and benzhydrol yields two ketyl radicals, one derived from each species. Unfortunately, this approach is limited by the relatively slow rate constants for reaction between aromatic ketones and benzhydrol (8.8×10^6 $M^{-1}s^{-1}$ for benzophenone and 2.5×10^8 $M^{-1}s^{-1}$ for AZAX) which requires prohibitively high concentrations of benzhydrol to achieve efficient formation of ketyl radicals.

The generation of ketyl radicals by intermolecular processes for the purposes of acid generation was abandoned in favour of intramolecular processes so as to avoid complications associated with the aforementioned side-reaction as well as the involvement of multiple bimolecular reactions.

5.3.2.2.2 *Generation of Ketyl Radicals: Intramolecular Processes*

The generation of ketyl radicals via unimolecular processes can be accomplished by the photodecomposition of appropriately substituted alcohols. Acid generation following ketyl radical formation can be accomplished in the exact same way as discussed in the previous section, i.e., oxidation of ketyl radicals by **5-2a** to the corresponding ketone with release of a proton. An important feature of

this approach is that the Φ_{ketyl} is an intrinsic property of the molecule. This is unlike in the previous section in which the Φ_{ketyl} could be altered by changing the identity or the concentration of the donor molecule employed. The two molecules chosen as sources of ketyl radicals were α-phenylbenzoin and benzopinacole.

α-Phenyl benzoin was prepared via reaction of phenylmagnesium bromide with benzil.[67] This molecule has been studied by others as a source of diphenyl ketyl radicals upon homolytic α-cleavage of the triplet excited state (Scheme 5-12).[67,68] The signal observed upon LFP of α-phenyl benzoin at 355 nm was assigned to the diphenyl ketyl radical, based on its characteristic absorption spectrum.[69] The benzoyl radical which is also generated, may contribute to some of the signal observed around 300 nm. The Φ_{ketyl} at 355 nm in N_2-saturated solution was determined to be 0.46, based on benzophenone actinometry. The Φ_{acid} in the presence of **5-2a** (0.2 mM) under the same conditions was determined to be 0.36, based on benzophenone actinometry. This value is in fairly good agreement with the Φ_{ketyl}, the discrepancy may be due to a small amount of quenching of the α-phenyl benzoin triplet excited state by **5-2a**.

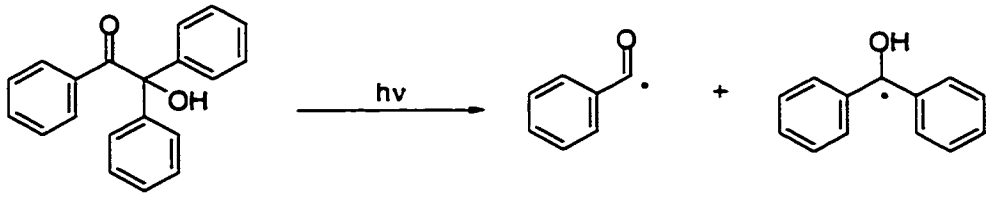

Scheme 5-12. Photochemical generation of the diphenyl ketyl radical from α-phenyl benzoin.

Benzopinacole was easily prepared via photolysis of benzophenone in isopropanol.[70] The ground state absorption of benzopinacole does not extend above 300 nm, thus, 266 nm excitation was employed in photochemical studies. Upon laser excitation at 266 nm, the only transient observed is the diphenyl ketyl radical as determined by its characteristic absorption spectrum, (Figure 1-9). Since

the diphenyl ketyl radicals are the only products from photolysis of benzopinacole, Figure 1-9 is unperturbed by other absorbing species and serves as a very good example of the diphenyl ketyl radical absorption spectrum. The diphenyl ketyl radical is presumably formed via simple homolytic bond cleavage from the singlet excited state of benzopinacole (Scheme 5-13). The Φ_{ketyl} at 266 nm in N_2-saturated acetonitrile was determined to be 0.65, based on benzophenone actinometry. Therefore, the photodecomposition of benzopinacole occurs with a quantum yield of half this value, i.e., 0.32.

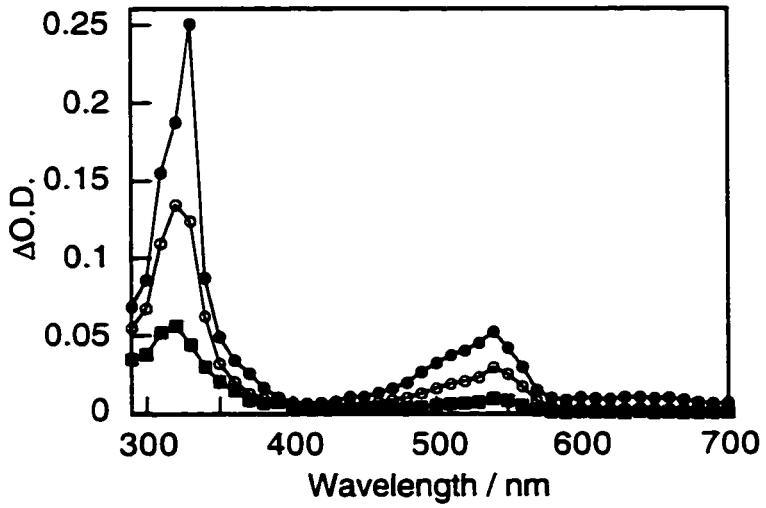

Figure 5-10. Transient absorption spectrum of the diphenyl ketyl radical obtained upon LFP of benzopinacole at 266 nm in N_2-saturated acetonitrile solution, recorded 8 μs (●), 68 μs (○) and 790 μs (■) after the laser pulse.

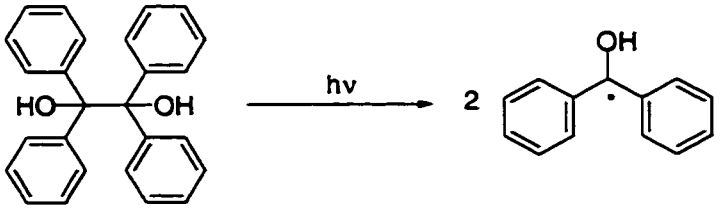

Scheme 5-13. Photochemical generation of the diphenyl ketyl radical from benzopinacole.

Attempts to measure the Φ_{acid} in this system were thwarted by the absorption of **5-2a** at 266 nm, which, at concentrations sufficiently high to give an efficient reaction with diphenyl ketyl radicals, prevents light from being absorbed by benzopinacole. This reveals a problem with the use of **5-2a** as the oxidant, that being, at wavelengths below 300 nm it filters light away from the ketyl radical source, thereby lowering the yield of ketyl radicals. Such behaviour is in direct conflict with the primary goal of much PAG research, i.e., the discovery of PAGs with high Φ_{acid} which allow for the preparation of more photosensitive CARs. This fact tends to eliminate **5-2a** as a potential component in any PAG system except for those which involve wavelengths in excess of 300 nm.

In order to salvage this approach to photoacid generation, a more transparent oxidizing agent must be employed. Unfortunately, the prospect of finding such a molecule is complicated by the fact that good electron acceptors tend to contain highly conjugated systems which have unacceptably high molar absorptivities. Alternatively, one might consider using a typical PAG molecule as an oxidizing agent. In this way, as the PAG filters light away from the ketyl radical source acid is still generated via the conventional PAG route. A system which uses an IPET process in competition with normal PAG photochemistry only poses an advantage if the IPET route gives a larger Φ_{acid}. In fact, PET and IPET processes involving PAGs have been employed for the purposes of acid generation for many years.[5,71] As mentioned in Section 5.1, the PET reactions typically employ sulfonium or iodonium salt PAGs as the oxidizing agents with the photosensitizer/reducing agent typically being an electron rich aromatic molecule. The IPET approach as described in this work is much less common but has also been studied using onium salts as oxidizing agents with benzophenone/isopropanol[8] and 2,2-dimethoxy-2-phenylacetophenone[72] as photochemical sources of diphenyl ketyl radicals and dimethoxybenzylic radicals, respectively.

5.4 Conclusions

The use of pyridinium salts and 1,4-bipyridinium salts as PAGs has been explored under a variety of different conditions. Intramolecular PET of pyridinium salts tethered to polyalkylbenzenes and 1,4-bipyridiniums salts tethered to alcohols proved too inefficient to be practical as PAGs. IPET via oxidation of ketyl radicals by 1,4-bipyridinium salts was investigated for its usefulness in photoacid generation. A variety of different strategies for photogenerating ketyl radicals were explored and the mechanism for formation of ketyl radicals from some aromatic ketones and polyalkylbenzenes was elucidated. The absorption due to 1,4-bipyridiniums tends to interfere with photogeneration of ketyl radicals at short wavelengths although encouraging results were obtained at longer wavelengths.

The evolution of the systems considered in this chapter began with the novel use of pyridinium salts as PAGs and eventually became more sophisticated with the use of 1,4-bipyridiniums and even more so with the use of systems for generating ketyl radicals. Unfortunately, the next logical step in this evolution led to the consideration of systems involving PAGs as oxidizers for electron rich radicals, which have already been studied in similar contexts.

5.5 Experimental

5.5.1 Materials

XAN (Aldrich) and AZAX (Lancaster) were recrystallized twice from ethanol. Acetonitrile, cyclohexane, benzene and toluene (BDH) were Omnisolv grade and were used as received. With the exception of DTT which was recrystallized twice from ethanol and heptane, the ArH donors were obtained from Aldrich and used as received. The deuterated compounds used for determing kinetic isotope effects were obtained from Cambridge Isotope Laboratories and used as received.

5.5.2 General Techniques

Details of the LFP system and techniques to measure Φ_{acid} using various chemical actinometers and light sources were described in Chapter 2.

Bimolecular rate constants for quenching were obtained using static cells while ketyl radical yields were determined using a flow system to avoid build-up of photoproducts. The ϕ_{ketyl} were determined by using cyclohexane as a standard for which we assume $\phi_{ketyl} = 1$. The ratio of the transient change in absorbance (ΔO.D.) due to the ketyl radical and the initial ΔO.D. due to the triplets upon quenching with cyclohexane was measured in order to determine the ratio of their molar absorptivities, ε. At 410 nm: $\varepsilon_{XAN(H)^{\bullet}} / \varepsilon_{^3XAN^{\bullet}} = 0.5 \pm 0.1$ and at 500 nm: $\varepsilon_{AZAX(H)^{\bullet}} / \varepsilon_{^3AZAX^{\bullet}} = 1.0 \pm 0.1$. Upon quenching with ArH donors with 95% efficiency the ratio of the initial ΔO.D., due to the triplet, and the final ΔO.D., due to the ketyl radical, were corrected based on ratio of the ε values and used to determine $\phi_{ketyl^{\bullet}}$.[73]

Reduction potentials of XAN and AZAX were measured using a cyclic voltammeter (50 mV- 200 mV/s) with platinum, glassy carbon and Ag/AgCl used as the counter, working and reference electrodes, respectively. Tetrabutylammonium

tetrafluoroborate was employed as the electrolyte for ~1 x 10^{-4} M solutions of XAN and AZAX in acetonitrile. Ferrocence was employed as an internal standard ($E_{1/2}$ = 0.51 vs. SCE).

5.5.3 Synthesis

The procedures used to prepare compounds **5-1a - 5-1c** and **5-2b** were adapted from those used by Mariano et al. in the preparation of similar compounds.[12-14] The halide salts obtained from these reactions were converted to the corresponding trifluoromethanesulfonate salts by dissolving in refluxing acetonitrile/methanol with an equimolar amount of silver trifluoromethanesulfonate. A grey precipitate of silver bromide formed immediately and the solutions were allowed to stir for an additional 30 minutes. The precipitate was removed by filtration and the filtrate was evaporated under reduced pressure. The solid obtained was recrystallized to give the products as white crystals. These reactions were performed only once and no attempts were made to optimize reaction conditions.

5-1a: A solution of pyridine (0.6 mL, 7.5 mmol) and 2-methylbenzyl bromide (1.0 mL, 7.5 mmol) in dry ether (40 mL) was refluxed for 24 hours. The bromide of **5-1a** precipitated out as a white solid and was collected by filtration (0.46 g, 28%). After anion exchange, recrystallization from ethyl acetate/hexanes gave the product as white crystals in an overall yield of 25%. ^{1}H NMR (200 MHz, $CDCl_3$) δ 2.23 (s, 3H), 5.90 (s, 2H), 7.20-7.40 (m, 4H), 7.99 (t, 2H) 8.44 (t, 1H), 8.84 (d, 2H). MS (ESI) m/z (%) 1182.9 (0.15, 4m-149), 849.9 (0.54, 3m-149), 517.0 (3.9, 2m-149), 183.9 (70, m-149), 104.8 (100).

5-1b: A solution of α-chloroisodurene (1.05g, 6.24 mmol) in pyridine (5 mL) was refluxed for 1 hour. The bromide of **5-1b** precipitated out as a white solid and was collected by filtration (0.97 g, 63%). After anion exchange, recrystallization from

ethyl acetate/hexanes gave the product as white crystals in an overall yield of 35%. ^{1}H NMR (200 MHz, $CDCl_3$) δ 2.22 (s, 6H), 2.30 (s, 3H), 5.93 (s, 2H), 6.97 (s, 2H) 8.02 (t, 2H), 8.48 (t, 1H), 8.71 (d, 2H). MS (ESI) m/z (%) 573.0 (0.11, 2m-149), 211.9 (5.0, m-149), 132.8 (100).

5-1c: A solution of 3-cyanopyridine (1.55 g, 14.9 mmol) and 2-methylbenzyl bromide (2.0 mL, 14.9 mmol) in acetonitrile (50 mL) was refluxed for 5 hours. The bromide of **5-1c** precipitated out as a white solid and was collected by filtration (2.41 g, 56%). After anion exchange, recrystallization from ethyl acetate/methanol gave the product as white crystals in an overall yield of 37%. ^{1}H NMR (200 MHz, DMSO-d_6) δ 2.31 (s, 3H), 5.90 (s, 2H), 7.20-7.40 (m, 4H), 8.31-8.38 (m, 2H) 9.11-9-21 (m, 2H), 9.79 (s, 1H). MS (ESI) m/z (%) 1282.8 (0.11, 4m-149), 924.9 (0.56, 3m-149), 567.0 (1.7, 2m-149), 208.8 (14, m-149), 104.8 (100).

5-2a: Anion exchange of 1,1'-dimethyl-4,4'-bipyridinium dichloride in the manner previously described yields the product as white crystals after recrystallization from methanol (90%). ^{1}H NMR (200 MHz, DMSO-d_6) δ 4.43 (s, 6H), 8.74 (d, 4H), 9.26 (d, 4H). MS (ESI) m/z (%) 818.8 (36, 2m-149), 334.9 (58, m-149), 184.7 (100).

5-2b: A solution of 4,4'-dipyridyl (1.53 g, 9.8 mmol) and 3-bromo-1-propanol (1.95 mL, 21 mmol) in dimethyl sulfoxide (25 mL) was heated at 80°C for 20 hours. The resulting orange solution was added to ether (250 mL) and vigorously stirred until a yellow solid separated. ^{1}H NMR revealed a 2:1 mixture of the disubstituted product and the monosubstituted product. Multiple recrystallizations from methanol/isopropanol isolated the disubstituted product as yellow crystals (0.86 g, 20%). After anion exchange, recrystallization from ethyl acetate/methanol gave the product as white crystals in an overall yield of 14%. ^{1}H NMR (200 MHz, DMSO-d_6) δ 2.15 (p, 4H), 3.49 (t, 4H), 4.40 (br, 2H), 4.80 (t, 4H), 8.84 (d, 4H), 9.45 (d, 4H). MS (ESI) m/z (%) 995.0 (2.0, 2m-149), 423.1 (3.6, m-149), 273.1 (76), 215.0 (100).

5.6 References

(1) Dektar, J. L.; Hacker, N. P. *J. Am. Chem. Soc.* **1990**, *112*, 6004.

(2) Baciocchi, E.; Bietti, M.; Lanzalunga, O. *Acc. Chem. Res.* **2000**, *33*, 243.

(3) Kavarnos, G. J. *Fundamentals of Photoinduced Electron Transfer*, VCH: New York, 1993, and references therein.

(4) Saeva, F. D. *J. Photochem. Photobiol. A: Chem.* **1995**, *86*, 149.

(5) Welsh, K. M.; Dektar, J. L.; Garcia-Garibaya, M. A.; Hacker, N. P.; Turro, N. J. *J. Org. Chem.* **1992**, *57*, 4179.

(6) Eckert, G.; Goez, M. *J. Am. Chem. Soc.* **1999**, *121*, 2274.

(7) Hacker, N. P. *ACS Symp. Ser.* **1994**, *579*, 93, and references therein.

(8) Gatechair, L. R.; Pappas, S. P. "Initiation of Polymerization," Bailey, J., F. E., Ed. ACS Symp. Ser. 212, Amer, Chem. Soc., Washington, DC, 1983, 173.

(9) Rehm, D.; Weller, A. *Isr. J. Chem.* **1970**, *8*, 259.

(10) Mariano, P. S. *Acc. Chem. Res.* **1983**, *16*, 130.

(11) Mariano, P. S. *Tetrahedron* **1983**, *39*, 3845 and references therein.

(12) Yoon, U. C.; Quillen, S. L.; Mariano, P., S.; Swanson, R.; Stavinoha, J. L.; Bay, E. *J. Am. Chem. Soc.* **1983**, *105*, 1204.

(13) Borg, R. M.; Heuckeroth, R. O.; Lan, A. J. Y.; L., Q. S.; Mariano, P. S. *J. Am. Chem. Soc.* **1987**, *109*, 2728.

(14) Lan, A. J. Y.; Heuckeroth, R. O.; Mariano, P. S. *J. Am. Chem. Soc.* **1987**, *109*, 2738.

(15) Some of these experiments were performed with the aid of Larisa Mickelsons, an undergraduate student at the University of Waterloo, while she worked in our labs for 8 months as part of her CO-OP program.

(16) Ledwith, A. *Acc. Chem. Res.* **1972**, *5*, 133 and references therein.

(17) Ledwith, A., *Electron Transfer Reactions of Paraquat* in *Biochemical Mechanisms of Paraquat Toxicity* ; Academic Press, Inc.: New York, 1977, pp 21-37.

(18) Bird, C. L.; Kuhn, A. T. *Chem. Soc. Rev.* **1981**, *10*, 49.

(19) Kosower, E. M.; Cotter, J. L. *J. Am. Chem. Soc.* **1964**, *86*, 5524.

(20) Farrington, J. A.; Ebert, M.; Land, E. J.; Fletcher, K. *Biochem. Biophys. Acta* **1973**, *314*, 372.

(21) Farrington, J. A.; Ebert, M.; Land, E. J. **1977**, 665.

(22) Hopkins, A. S.; Ledwith, A.; Stam, M. F. *Chem. Comm.* **1970**, 494.

(23) Ledwith, A.; Russell, P. J.; Sutcliffe, L. H. *Proc. R. Soc. Lond. A.* **1973**, *332*, 151.

(24) Hyde, P.; Ledwith, A. *J. Chem. Soc., Perkin Trans. 2* **1974**, 1768.

(25) Brown, N. M. D.; Cowley, D. J.; Hashmi, M. *J. Chem. Soc., Perkin Trans. 2* **1979**, 462.

(26) Baral-Tosh, S.; Chattopadhyay, S. K.; Das, P. K. *J. Phys. Chem.* **1984**, *88*, 1404.

(27) Jacques, P.; Allonas, X.; Von Raumer, M.; Suppan, P.; Haselbach, E. *J. Photochem. Photobiol. A: Chem* **1997**, *111*, 41.

(28) Scaiano, J. C.; Selwyn, J. C. *Can. J. Chem.* **1981**, *59*, 2368.

(29) Barra, M.; Bohne, C.; Scaiano, J. C. *J. Am. Chem. Soc.* **1990**, *112*, 8075.

(30) Evans, C. H.; Prud'homme, N.; King, M.; Scaiano, J. C. *J. Photochem. Photobiol., A* **1999**, *121*, 105.

(31) Scaiano, J. C.; Weldon, D.; Pliva, C. N.; Martinez, L. J. *J. Phys. Chem.* **1998**, *102*, 6898.

(32) Martinez, L. J.; Scaiano, J. C. *J. Phys. Chem. A.* **1999**, *103*, 203.

(33) Corrent, S.; Martinez, L. J.; Scaiano, J. C.; Garcia, H.; Fornes, V. *J. Phys. Chem. B* **1999**, *103*, 8097.

(34) Garner, A.; Wilkinson, F. *J. Chem. Soc., Faraday Trans. 2* **1976**, *72*, 1010.

(35) Scaiano, J. C. *J. Am. Chem. Soc.* **1980**, *102*, 7747.

(36) We use the term 'encounter complex' in place of 'exciplex' to avoid confusion generated by the fact that 'exciplex' often refers to an emissive species and is sometimes used to indicate which may be better deemed 'contact-ion pairs'.

(37) Cohen, S. G.; Parola, A.; Parsons, G. H. *Chem. Rev.* **1973**, *73*, 141.

(38) Wagner, P. J. *Top. Curr. Chem.* **1976**, *66*, 1.

(39) Wagner, P. J.; Leavitt, R. A. *J. Am. Chem. Soc.* **1973**, *95*, 3669.

(40) Wagner, P. J.; Truman, R. J.; Puchalski, A. E.; Wake, R. *J. Am. Chem. Soc.* **1986**, *108*, 7727.

(41) Rathore, R.; Hubig, S. M.; Kochi, J. K. *J. Am. Chem. Soc.* **1997**, *119*, 11468.

(42) Hubig, S. M.; Rathore, R.; Kochi, J. K. *J. Am. Chem. Soc.* **1999**, *121*, 617.

(43) Hubig, S. M.; Kochi, J. K. *J. Am. Chem. Soc.* **1999**, *121*, 1688.

(44) These are clearly not "intrinsic" lifetimes and may be partially determined by trace impurities in the solvent (including some residual oxygen), and to a lesser degree by some triplet-triplet annihilation. These effects do not interfere with the determination of accurate quenching rate constants based on the decay dependence with the quencher concentration.

(45) Christensen, H. C.; Sehested, K.; Hart, E. J. *J. Phys. Chem.* **1973**, *77*, 983.

(46) Bockman, T. M.; Hubig, S. M.; Kochi, J. K. *J. Am. Chem. Soc.* **1998**, *120*, 2826.

(47) Bockman, T. M.; Karpinski, Z. J.; Sankararaman, S.; Kochi, J. K. *J. Am. Chem. Soc.* **1992**, *114*, 1970.

(48) Sehested, K.; Holcman, J.; Hart, E. J. *J. Phys. Chem.* **1977**, *81*, 1363.

(49) Herkstroeter, W. K.; Lamola, A. A.; Hammond, G. S. *J. Am. Chem. Soc.* **1964**, *86*, 4537.

(50) The k_{obs} values for XAN with benzene and pyridine are 6.3 x 10^5 $M^{-1}s^{-1}$ and 7.23 x 10^5 $M^{-1}s^{-1}$, respectively. These values for AZAX are 9.3 x 10^6 $M^{-1}s^{-1}$ an 7.75 x 10^7 $M^{-1}s^{-1}$, respectively. For the oxidation potentials for benzene and pyridine see: Miller, L.L, Nordblom. G.D., Mayeda, E. A. *J. Org. Chem.* **1971**, 37, 916.

(51) Although some moderation of the selectivity could be expected for the higher reactivities, a rather common observation.

(52) Wagner, P. J.; Kemppainen, A. E.; Schott, H. N. *J. Am. Chem. Soc.* **1973**, *95*, 5604.

(53) Berger, M.; McAlpine, E.; Steel, C. *J. Am. Chem. Soc.* **1978**, *100*, 5147.

(54) Wagner, P. J.; Siebert, E. J. *J. Am. Chem. Soc* **1981**, *103*, 7329.

(55) Scaiano, J. C. *J. Photochem.* **1973/74**, *2*, 81.

(56) Wagner, P. J. *Acc. Chem. Res.* **1971**, *4*, 168.

(57) Wagner, P. J.; Kemppainen, A. E. *J. Am. Chem. Soc.* **1972**, *94*, 7495.

(58) Walling, C.; Gibian, M. A. *J. Am. Chem. Soc.* **1965**, *87*, 3361.

(59) Paul, H.; Small, R. D. J.; Scaiano, J. C. *J. Am. Chem. Soc.* **1978**, *100*, 4520.

(60) Walling, C.; Jacknow, B. B. *J. Am. Chem. Soc.* **1960**, *82*, 6108.

(61) Hubig, S. M. *J. Phys. Chem.* **1992**, *96*, 2903.

(62) Mattes, S. L.; Farid, S. *J. Am. Chem. Soc.* **1983**, *105*, 1387.

(63) Schlesener, C. J.; Amatore, C.; Kochi, J. K. *J. Am. Chem. Soc.* **1984**, *106*, 7472.

(64) Masnovi, J. M.; Sankararaman, S.; Kochi, J. K. *J. Am. Chem. Soc.* **1989**, *111*, 2263.

(65) Turro, N. J.; Dalton, J. C.; Farrington, G.; Niemczyk, M.; Pond, D. M. *J. Am. Chem. Soc.* **1970**, *92*, 6978.

(66) Wolf, W. M.; Brown, R. E.; Singer, L. A. *J. Am. Chem. Soc.* **1977**, *99*, 526.

(67) Baumann, H.; Schumacher, K. P.; Timpe, H.-J.; Rehavk, V. *Chem. Phys. Letters* **1982**, *89*, 315.

(68) Baumann, H.; Merckel, C.; Timpe, H.-J.; Graness, A.; Kleinschmidt, J.; Gould, I. R.; Turro, N. J. *Chem. Phys. Letters* **1984**, *103*, 497.

(69) Bensasson, R. V.; Gramain, J. C. *J. C. S. Faraday I* **1980**, *76*, 1801.

(70) Durst, T. "CHM 3126: Laboratory Manual," The University of Ottawa, 2001.

(71) Pappas, S. P. *J. Imaging Technology* **1985**, *11*, 146 and references therein.

(72) Ledwith, A. *Macromol. Chem., Suppl.* **1979**, *3*, 348.

(73) The systematic errors in the molar absorptivities cannot influence the order within a homologous series.

6. Intramolecular Triplet Energy Transfer in Sulfonium Salt Photochemistry

6.1 Introduction

The photochemical studies of new photoacid generators (PAGs) described in Chapters 4 and 5, while informative and valuable from an academic perspective, have not yielded a PAG which shows potential for industrial use in chemically amplified resists (CARs). In order to garner such attention, a PAG must give some indication that its use would represent an improvement over existing PAGs, i.e., increased photosensitivity and better image quality of the CAR, as controlled by the quantum yield of acid generation (Φ_{acid}), absorbance characteristics and thermal stability of the PAG. As judged by their extensive employment in industry, sulfonium salts have singled themselves out as very effective photoinitiators for cationic polymerization and as PAGs.[1-4] In an effort to direct our research towards targets with the potential to have more impact on the microelectronics industry, we focused our attention on sulfonium salt photochemistry.

Driven by their effectiveness as PAGs, the photodecomposition of sulfonium salts and in particular triphenylsulfonium (TPS) triflate has been the subject of many mechanistic studies.[5-12] As such, the mechanisms for direct and sensitized photoreactions of TPS triflate are well-established, having received wide acceptance. As a researcher, it is difficult to navigate through this large body of work and identify an area which would benefit from additional studies. Furthermore, investigations on triarylsulfonium (TAS) salts reveal that most structural modifications to the TPS framework act to reduce the Φ_{acid}.[9] Those non-TPS sulfonium salts which do generate acid with equal or greater efficiency than TPS triflate tend to underperform relative to TPS triflate in an actual CAR.[13] All of these factors contributed to our perception that, as a PAG, TPS triflate could not be improved upon, and conspired to keep us from studying sulfonium salts for many years.

6.1.1 Triphenylsulfonium Salt Photochemistry

It was only upon close consideration of the mechanism for photodecomposition of TPS salts, including some very specific results found in the literature, (*vide infra*) that we became interested in working with these PAGs. The main features of the photoacid generation process by a TPS salt appear in Scheme 6-1.[12] Briefly, upon absorption of a photon, a TPS salt reaches its singlet excited state which decomposes homolytically or heterolytically via sulfur-carbon bond cleavage. Homolytic cleavage yields phenyl radical ($Ph^{\bullet}$) and diphenylsulfide radical cation ($Ph_2S^{\bullet+}$), while heterolytic cleavage yields phenyl cation (Ph^{+}) and diphenylsulfide (Ph_2S). Reactions of these species within the solvent cage yield either (phenylthio)biphenyls and acid or the original TPS salt. If the species escape the solvent cage, they are free to react with available nucleophiles or hydrogen donors, and give various benzenes and Ph_2S in addition to acid as products. An interesting feature of this mechanism is that there are a variety of different reactions, both uni- and bimolecular which yield acid, a property which may contribute to the success of sulfonium salts as PAGs under a variety of conditions. Values for the Φ_{acid} of TPS triflate in acetonitrile are in the range of 0.5-0.7.[12,14]

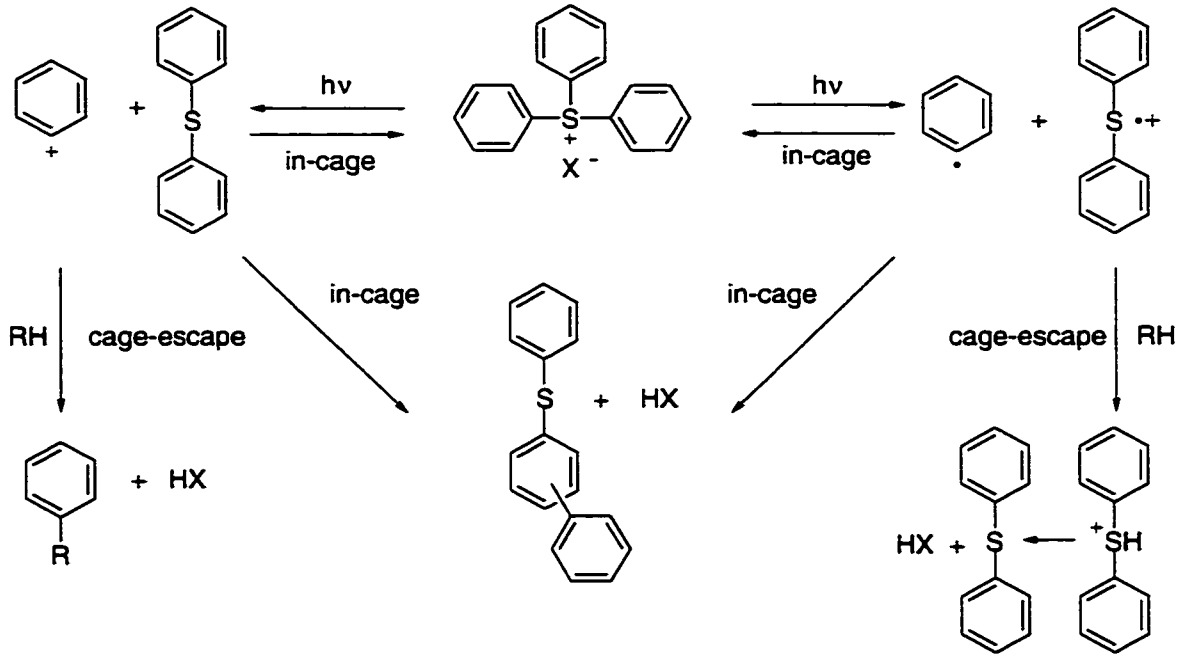

Scheme 6-1. Mechanism for photoacid generation by a TPS salt.

From Scheme 6-1, the only reaction which does not yield acid once the sulfur-carbon bond has been cleaved is an in-cage recombination reaction to regenerate starting materials. The relative importance of this pathway can be inferred from work by Dektar and Hacker in which the photodecomposition of TPS triflate was studied in solvents of differing viscosities (Table 6-1).[9] In general, an increase in the viscosity of a solvent acts to increase the contribution from in-cage reactions due to reduced rates of cage-escape.[15,16] This effect is apparent in the reactions of TPS triflate as demonstrated by a dramatic reduction in the quantum yield of decomposition of PAG (Φ_{decomp}) and an increase in the ratio of in-cage to cage-escape products on changing the solvent from methanol to glycerol. The same effect of viscosity on product distribution has been observed in the photolysis of TPS triflate in polymer films as compared to non-viscous solvents.[17] The implication of these results is that in the solid matrix of a CAR, in-cage reactions dramatically reduce the ability of TPS salts to generate acid.

Table 6-1. Viscosity dependance on product formation in the photochemistry of TPS triflate.

solvent	viscosity (cP)	relative Φ_{decomp}	in-cage: cage-escape[a]
methanol	0.55	1.0	1.28
1,2-ethandiol	18.0	0.35	2.07
glycerol	1500	0.12	5.63

[a]Ratio of products resulting from in-cage reactions to cage-escape reactions.

A second set of results from the same lab indicates that sensitized photodecomposition of TPS salts via triplet energy tranfer (TET) from ketones in a non-viscous solvent results in a dramatic increase in the quantum yield of diphenyl sulfide formation (Φ_{Ph2S}), a product of cage-escape reactions, relative to direct excitation of TPS (Table 6-2).[18] The triplet excited state of TPS triflate, generated in this way, decomposes homolytically to give Ph$^{\bullet}$ and $Ph_2S^{\bullet+}$ as a triplet geminate pair, i.e., having parallel electron spins, within the solvent cage.[10,11,18] Recombination of this triplet radical/radical cation pair would give a triplet product, as demanded by conservation of spin angular momentum, a process which is generally endothermic and unable to compete with cage-escape.[19,20] This is markedly different from the direct excitation of TPS salts in which a singlet geminate pair is formed which can recombine very quickly to give singlet ground state products. By preventing the recombination reaction in this way, accessing the triplet manifold allows Ph$^{\bullet}$ and $Ph_2S^{\bullet+}$ to escape the solvent cage and eventually give benzene and Ph_2S as products. The effectiveness of different ketones in inducing triplet reactivity in TPS triflate suggests that the triplet energy (E_T) of TPS triflate is 75 kcal/mol, which is in agreement with phosphorescence results.[21]

Table 6-2. Effect of sensitizer triplet energy on the yield of Ph_2S in the sensitized photodecomposition of TPS triflate.

sensitizer	relative Φ_{Ph2S}	E_T (kcal/mol)
none	1.0	---
acetone	81	79-82
1-indanone	10.1	75.8
acetophenone	7.5	74.1

The results in Tables 6-1 and 6-2 indicate that the triplet excited state of TPS salts decompose in a manner that increases cage-escape reactions relative to the singlet excited state, and that in-cage reactions act to reduce the Φ_{decomp} and thereby the Φ_{acid} in viscous media. Together, these results suggest that a sulfonium salt with triplet reactivity could be an extremely effective PAG. To the best of our knowledge, these two ideas have never been deliberately incorporated into a single strategy in PAG design.

6.1.2 The Triplet Excited States of Sulfonium Salts

6.1.2.1 Forming theTriplet Excited States of Sulfonium Salts

Theoretically, the triplet excited state of a TPS salt can be formed either by photochemically exciting the TPS salt to its singlet excited state which can intersystem crossing (ISC) to the triplet excited state, or by TET from a photochemically excited sensitizer, as described earlier with ketones as the sensitizers.

TPS salts do not ISC efficiently and hence do not reach their triplet excited states upon direct excitation. In general, ISC is accomplished via spin-orbit coupling (SOC); a process whereby the magnetic moment of an electron, i.e., its spin,

interacts with its orbital angular momentum and causes a simultaneous spin flip and switching of orbital occupancy.[22] This process tends to be important for molecules with a small singlet-triplet energy gap, such as ketones, and those containing 'heavy atoms' whose large nuclear charge increases the strength of the coupling.[22,23] TPS derivatives containing halogen or benzoyl substituents on the phenyl rings have been studied for the purpose of inducing ISC in sulfonium salts, but give no indication of having triplet reactivity and have lower Φ_{acid} than TPS triflate.[9] The drop in acid generating ability is likely due to the extended conjugation in these molecules relative to TPS salts which lowers the energy of the excited states, making the necessary bond-cleavage reactions less favourable. Interestingly, a thiophenol substituted TPS salt shows triplet reactivity and is the only reported TPS derivative with a higher Φ_{acid} than TPS triflate in solution;[9,24] although it underperforms relative to TPS triflate in a CAR.[13]

TET from a sensitizer is a means to access the excited triplet state of a TPS salt without perturbing the TPS salt via introduction of new substituents. In general, TET occurs via an electron exchange mechanism which was originally proposed by Dexter and is shown schematically in Figure 6-1.[25]

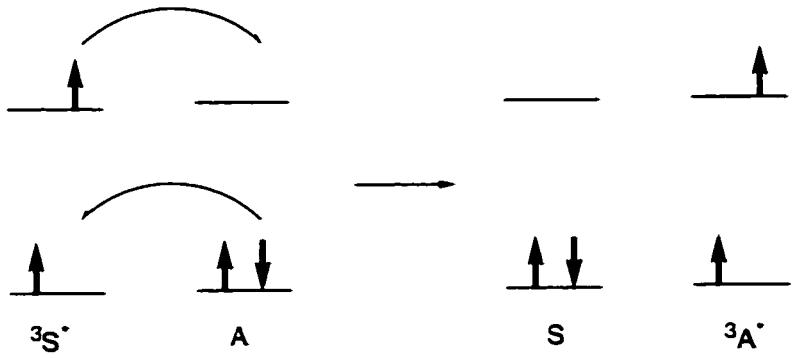

Figure 6-1. Schematic representation of the electron exchange mechanism for triplet energy transfer between a sensitizer (S) and an acceptor molecule (A).

As described earlier, intermolecular TET between the triplet excited states of various ketones and TPS triflate yields the triplet excited state of TPS triflate.[18] The difficulty in using this approach to design an actual PAG system is in being able to selectively excite the ketone preferentially over TPS triflate while still having a sufficiently high concentration of TPS triflate to react with most of the ketone triplet excited states. This task becomes particularly difficult in the solid matrix of a CAR in which diffusional processes, such as TET, are slowed. At long wavelengths (> 300 nm) at which TPS salts do not absorb light, this type of process may be possible, but these wavelengths are largely irrelevant to current lithographic research which is exploring 193 and 157 nm lithography. Essentially the same hurdle was encountered in the previous chapter in which 1,4-bipyridinium salts were employed to oxidize photochemically generated ketyl radicals. In order to avoid this problem in the current system we reject an intermolecular TET reaction in favour of an intramolecular TET reaction. The advantage being that in the intramolecular case the TET between sensitizer and acceptor does not require diffusion of the species together because they are part of the same molecule.

The TPS salt used in the intermolecular TET reaction is now replaced by a TAS salt, no longer TPS because at least one of the phenyl groups must be substituted with the sensitizer moiety. Molecules which contain two distinct chromophores, one the sensitizer and the other the acceptor can participate in an intramolecular TET reaction which is exactly analogous to the intermolecular case. Intramolecular TET reactions have been the topic of many mechanistic studies concerning the nature of the spacer between the chromophores in order to probe whether the process occurs through-space or through-bond.[26] As the primary concern here is with photoacid generation and not fundamental mechanistic issues, the finer points of these studies are ignored, noting only that the rate constants and efficiencies of TET are larger for systems in which the two moieties are either held

close to one another or are allowed to closely approach one another. Perhaps it is worth mentioning here that the reaction of interest, i.e., sensitization of a TAS triplet excited state with ketones, does occur intermolecularly (as previously discussed) and no reason to question its viability in an intramolecular sense is immediately obvious.

6.1.2.2 Triplet Radical/Radical Cation Pairs

Once formed, the triplet excited state of a TAS is expected to cleave homolytically to give an aryl radical ($Ar^{\bullet}$) and a diarylsulfide ($Ar_2S^{\bullet+}$) as a triplet geminate pair within the solvent cage, in the same manner as in the intermolecular case. This triplet radical/radical cation pair can react in one of two ways: separate and escape the solvent cage or ISC to a singlet pair and recombine within the solvent cage.

The tendency for a geminate pair to escape the solvent cage is a function of the competition between diffusing apart, as controlled by solvent viscosity, and the rate of the recombination reaction. The lifetimes of a solvent cage can range from ~100 ps in non-viscous solvents (η < 10 cP)[15] to longer than 1 μs in a viscous solvent (η > 1000 cP).[27] The singlet geminate $Ph^{\bullet}/Ph_2S^{\bullet+}$ pair, obtained from direct excitation of TPS triflate, recombine within the solvent cage in < 25 ps with only ~20% of the pairs escaping the cage in acetonitrile.[12] As mentioned earlier, the same triplet geminate pair would be unable to recombine so rapidly. One should be reminded here that heterolysis of the singlet excited state of TPS also occurs and that no information about the cage processes of the singlet geminate Ph^{+}/Ph_2S pair can be inferred from these results.

For radical pairs, SOC is replaced as the primary mechanism for ISC by hyperfine coupling between the magnetic moment of the unpaired electron and the magnetic moment of a nearby nucleus. This interaction can cause concomitant

electron and nuclear spin flips, thereby transforming a triplet radical pair into a singlet pair.[19] Typically, the amount of time required for triplet-singlet ISC in radical pairs is ~10-100 ns,[15,28] although lifetimes as short as 120 ps have been seen for some sulfur centered triplet radical pairs, due to rapid ISC aided by the fact that sulfur is a 'heavy atom'.[28]

Although in non-viscous media, the geminate triplet $Ph^{\bullet}/Ph_2S^{\bullet+}$ pair are able to escape the solvent cage efficiently, as judged by product studies[18] and transient detection,[10,11] it remains to be seen if this is also the case in viscous media. Based on some of the aforementioned literature results it is quite possible, even probable, that ISC of a triplet geminate $Ar^{\bullet}/Ar_2S^{\bullet+}$ pair to the singlet pair will occur more quickly than cage-escape, thereby negating the perceived advantage of accessing triplet pathways in sulfonium salt chemistry. An additional concern is that although the involvement of a triplet pathway decreases the yield of in-cage reactions, it is unclear if this will result in an improvement in the Φ_{acid}.[29]

6.2 Results and Discussion[30]

6.2.1 Photoacid Generator Design

As a means to reach the triplet excited state of TAS salts, a system in which a ketone is tethered to the TPS framework is investigated. In this way, the molecule consists of two distinct chromophores; absorption of a photon by either chromophore is possible. Figure 6-2 shows the molar absorptivities of TPS triflate and a variety of ketones. A 1:1 mixture of TPS triflate and a ketone serves as an adequate model for the target PAG. Figure 6-2 indicates that there should be a competition for photons between the chromophores at any given wavelength; except for an aliphatic ketone which cannot compete effectively with TPS.

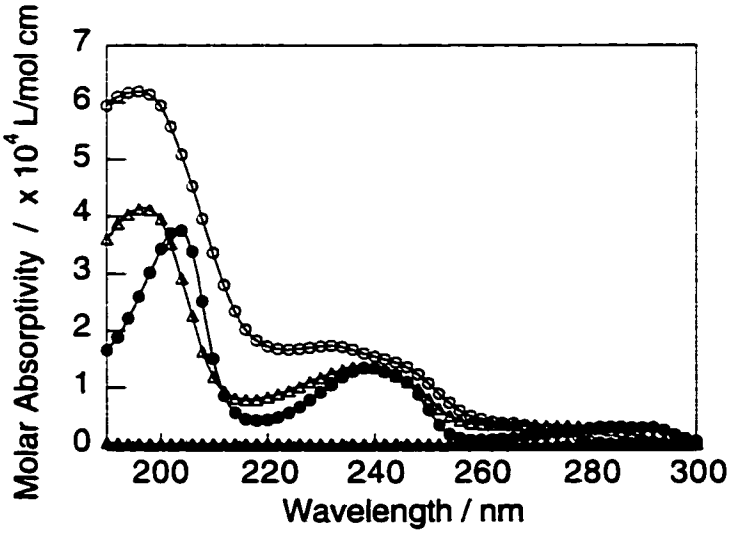

Figure 6-2. Molar absorptivities of TPS triflate (○), acetophenone (△), 1-indanone (●) and 2-butanone (▲) in acetonitrile.

Some of the potential photochemical pathways available to such a bichromophoric molecule are shown in Scheme 6-2. If the TPS chromophore absorbs the photon, typical sulfonium chemistry results, i.e., singlet-derived products are formed. Alternatively, the ketone absorbs the photon and forms its

triplet excited state after ISC, which transfers its energy to the TPS moiety. The triplet excited state of the sulfonium salt then decomposes to yield triplet-derived products. It should be noted that TET in this system does not necessarily occur with 100% efficiency; other relaxation pathways of the triplet excited ketone may also be important. A third pathway which is also thermodynamically feasible is that before decomposing, the singlet excited state of the sulfonium salt transfers its energy to the ketone. The singlet energy of a TPS salt is 92 kcal/mol[8] making singlet energy transfer exothermic to both aliphatic and aromatic ketones (< 82 kcal/mol[22]). The singlet excited ketone, obtained in this way, is able to proceed along the same reaction path had it been formed directly by absorption of a photon. This type of process is commonly referred to as assisted ISC. Although this process cannot be discounted outright, it will likely be unimportant in this system given that the decay of the singlet excited state of TPS triflate occurs in < 1 ps,[12] making it a difficult process to compete with. However, if assisted ISC does occur, it too results in formation of the triplet excited states of sulfoniums salts, as desired.

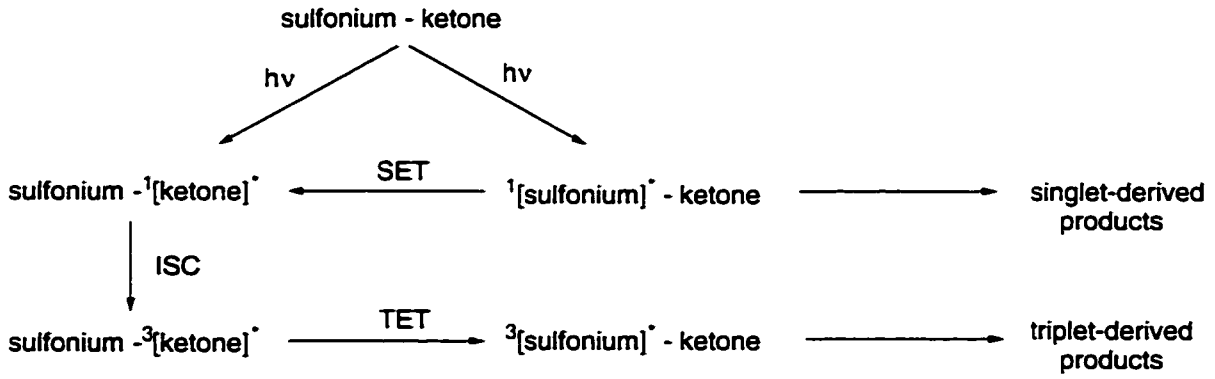

Scheme 6-2. Potential reaction pathways for a bichromophoric molecule containing ketone and sulfonium moieties.

The PAGs **6-1** and **6-2** (Figure 6-3), were prepared in order to investigate the aforementioned TET process; each are TAS triflates with 1-indanone and 5-methylhexanone tethers respectively. They were prepared via Friedel-Crafts

alkylation of diphenyl sulfide with the appropriate halide. A *tert*-butylphenyl group was transferred onto the resulting sulfide from *tert*-butylphenyliodonium triflate using standard techniques.[31] The regiochemistry of the aromatic groups was determined by analysis of the ^{13}C NMR spectra. The *tert*-butyl group in each molecule is for synthetic convenience and is not expected to alter any of the proposed reaction pathways.

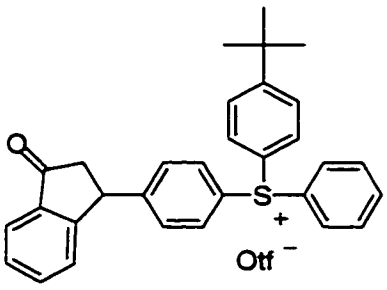

6-1

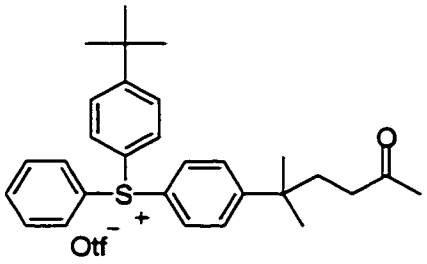

6-2

Figure 6-3. Triarylsulfonium salts designed to participate in intramolecular TET.

The main concern in designing **6-1** and **6-2** was how to attach the ketone sensitizer to the sulfonium acceptor without perturbing the reaction pathways that allowed the intermolecular sensitization to work so effectively. Ideally, the connection or tether between the two moieties should not affect the E_T of either species, so as to make TET less exothermic, and it must also not introduce new reaction pathways which compete with TET.

In order to maintain favourable energetics for TET, the E_T of the sensitizer component must remain high and that of the acceptor stay low. The E_T of aromatic ketones are slightly affected by the choice of substituents on the aromatic ring.[32] In order to avoid causing a decrease in the E_T one must not perturb the π system of the ketone. Additionally, it is undesirable to lower the E_T of the acceptor, despite the fact that this would favour TET, because it may also give a sulfonium salt with an E_T

that it is no longer sufficiently high to efficiently cleave the sulfur-carbon bond. So as not to perturb the E_T of the sulfonium component one must attach the tether with relatively innocuous groups which have a minimal interaction with the π-system. PAG **6-1** is formed via attachment of the aromatic ketone to the sulfonium framework via a benzylic carbon in order to minimize perturbations of the excited state energies of both chromophores. Likewise, PAG **6-2** was formed by attaching a ketone to the sulfonium to form a tertiary carbon far removed from the carbonyl moiety.

In order to maximize the efficiency of TET, the availability of other deactivation pathways to the triplet excited state of the sensitizer must be minimized. A common reaction of excited state ketones is photoreduction by a variety of hydrogen and electron donors.[22] Unfortunately, the presence of certain species in CARs capable of behaving in this manner is necessary for CAR functioning, however most intermolecular reactions should not be able to compete with favourable intramolecular processes. α-Cleavage reactions are also very prominent reactions of ketones but can be minimized by choosing a molecule which does not yield a stable radical.[22] Intramolecular H-abstraction reactions of ketones are also very common but are unimportant in molecules without γ-hydrogens.[22] The structures of **6-1** and **6-2** were chosen to minimize all of the aforementioned pathways.

As mentioned earlier, TET processes can occur both through bonds and through space. In an attempt to ensure the viability of TET in the systems of interest here, whichever the pathway, the sensitizer and acceptor components are kept relatively close together in **6-1** by the molecular framework and are able to adopt a conformation which brings them close to one another in **6-2**.

6.2.2 Triplet Reactivity

In order to investigate whether **6-1** and **6-2** succeed in accessing the triplet excited state of the sulfonium salt upon photoexcitation, laser flash photolysis (LFP) studies were conducted in order to investigate the transients involved in their photodecomposition. For purposes of comparison, experiments were also conducted on TPS triflate under conditions in which intermolecular TET from a ketone was important.

Triplet sensitization of TPS triflate (10 mM) by acetone (240 mM) via LFP at 308 nm gives a signal identified as $Ph_2S^{\bullet+}$ by its characteristic absorption spectrum (Figure 6-4). This signal is not observed in the LFP of TPS triflate upon direct excitation. This result is consistent with that observed by others and is attributed to the fact that in the triplet sensitized photolysis, $Ph_2S^{\bullet+}$ escapes the solvent cage and lives long enough to be detected in the μs time domain.[10,11] Alternatively, in the case of singlet reactivity resulting from direct photolysis, $Ph_2S^{\bullet+}$ is not detected on this timescale because it recombines efficiently within the solvent cage. However, as noted earlier, $Ph_2S^{\bullet+}$ has been observed by others under conditions of direct excitation of TPS triflate, 80% of which decayed in < 25 ps, via in-cage reactions and the remainder lived beyond the timescale of their instrument.[12] This fraction which escape the solvent cage is either not sufficiently plentiful or long-lived for detection on the μs timescale. The detection of $Ph_2S^{\bullet+}$ under these experimental conditions serves as an indicator of the involvement of triplet pathways in the sensitized photodecomposition of TPS triflate. A similar signal, due to $Ar_2S^{\bullet+}$, should be observed following direct excitation of **6-1** and **6-2**, if triplet pathways are involved in their photodecomposition.

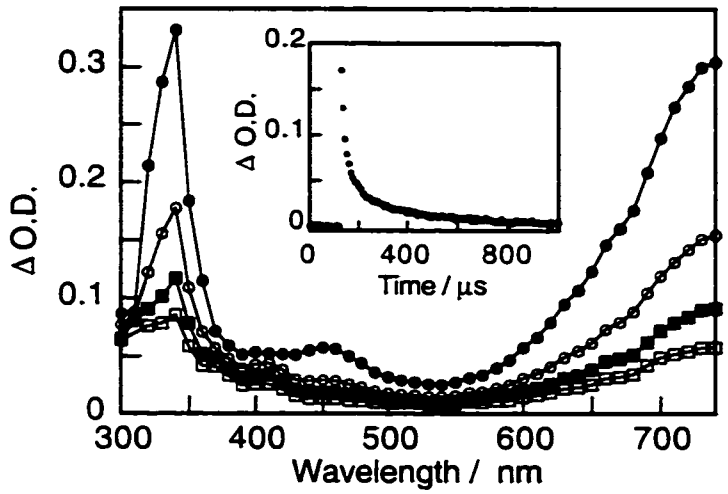

Figure 6-4. Transient absorption spectrum of $Ph_2S^{\bullet+}$ obtained upon LFP of 10 mM TPS in N_2-saturated acetonitrile solution with 240 mM acetone at 308 nm, recorded 0.8 μs (●), 8.8 μs (○), 30 μs (■) and 78 μs (□) following laser excitation. Inset: kinetic decay obtained at 750 nm.

The LFP of **6-1** and **6-2** at 266 nm resulted in signals very similar in lifetime and appearance to those assigned to $Ph_2S^{\bullet+}$, and appear together in Figure 6-5 with that of $Ph_2S^{\bullet+}$ for ease of comparison. The important features of these spectra are that in all cases an intense band at 340 nm and another above 740 nm are observed. The small differences in the appearance of the spectra are likely due to the fact that **6-1** and **6-2** can each form three different $Ar_2S^{\bullet+}$, depending on which sulfur-carbon bond is broken, whereas for TPS triflate the only radical cation possible is that of Ph_2S. Based on the similarities of the spectra, they are attributed to $Ar_2S^{\bullet+}$, resulting from cage-escape reactions of a geminate $Ar^{\bullet}/Ar_2S^{\bullet+}$ pair. While the detection of these cage-escape species does not explicitly confirm that they resulted from a triplet pathway, it strongly suggests as much.

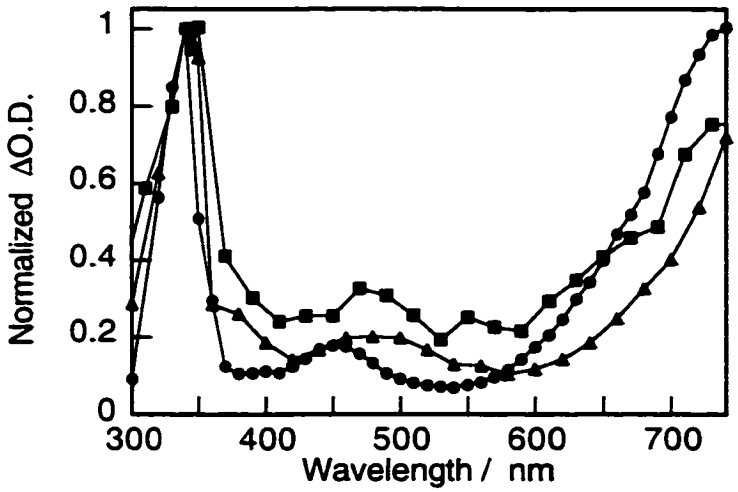

Figure 6-5. Normalized transient absorption spectra obtained upon LFP of 10 mM TPS in N_2-saturated acetonitrile solution with 240 mM acetone at 308 nm (●), and of 6-1 (▲) and 6-2 (■) in N_2-saturated acetonitrile solution at 266 nm.

It should be noted that although there is evidence for triplet reactivity in the photochemistry of **6-1** and **6-2**, this is not intended to suggest that these molecules decompose entirely from triplet excited states. Decomposition of **6-1** and **6-2** from the singlet excited state formed upon photon absorption by the sulfonium chromophore is also likely occurring. Nevertheless, confirmation of enhanced cage-escape reactions from **6-1** and **6-2**, which is heretofore attributed to triplet reactivity, are very encouraging. However, the implications of this reactivity, on acid generation are yet to be addressed.

6.2.3 Acid Generation

The relative Φ_{acid} for **6-1** and **6-2** in air-equilibrated acetonitrile was measured under conditions of steady-state irradiation at 254 nm while employing TPS triflate as a standard. The Φ_{acid} values were both 60% of that for TPS. Purging solutions with N_2 or O_2 did not significantly alter these values. The lower value could be due to a variety of factors including: a lower quantum yield of sulfur-carbon bond cleavage from the triplet state as compared to the singlet excited state and/or

inefficient TET. Apparently, in a low viscosity solvent such as acetonitrile, the formation of triplet geminate $Ar^{\bullet}/Ar_2S^{\bullet+}$ pairs from **6-1** and **6-2** does not pose a significant advantage over the singlet pairs formed from TPS triflate because cage-escape of singlet pairs is an important pathway under these conditions. A more telling result comes from experiments in a more viscous solvent such as 1,2-ethanediol in which in-cage reactions begin to dominate over cage-escape for singlet-derived pairs.[9] The relative Φ_{acid} for **6-1** and **6-2** in air-equilibrated 1,2-ethanediol was measured under conditions of steady-state irradiation at 254 nm while employing TPS triflate as a standard. The Φ_{acid} values were both < 5% of that for TPS triflate, respectively. This result is quite surprising as it indicates that **6-1** and **6-2** are essentially inoperative as PAGs in viscous solvents, the very conditions in which they were designed to excel. Another experiment using **6-1** in PMMA films confirmed this finding as it yielded essentially the same result, i.e., a Φ_{acid} value < 5% of that for TPS triflate.

In order to account for the dramatic reduction in the Φ_{acid} by **6-1** and **6-2** relative to TPS triflate on changing from a non-viscous to viscous media one must reconsider their photodecomposition reactions. The triplet excited state of a TAS salt decomposes homolytically to give $Ar^{\bullet}$ and $Ar_2S^{\bullet+}$ as a triplet geminate pair preferentially over Ar^{+} and Ar_2S which would presumably require an excited state of Ar_2S in order to satisfy spin multiplicity requirements. Alternatively, the singlet excited state of TPS triflate decomposes both homolytically and heterolytically, with the latter pathway dominating, according to product studies.[9,12] Therefore, the difference in Φ_{acid} between **6-1** and **6-2** relative to TPS triflate can be discussed in terms of the behaviour of a triplet geminate $Ar^{\bullet}/Ar_2S^{\bullet+}$ pair versus the singlet geminate Ph^{+}/Ph_2S pair.

The lack of an enhancement in Φ_{acid} by **6-1** and **6-2** relative to TPS triflate in a viscous environment suggests that the triplet $Ar^{\bullet}/Ar_2S^{\bullet+}$ pair are unable to escape the solvent cage before ISC to a singlet pair occurs, thereby allowing in-cage reactions to dominate. This however, cannot account for the suppression of Φ_{acid} by **6-1** and **6-2** relative to TPS triflate because the singlet pairs formed in the photodecomposition of TPS triflate are also expected to undergo significant amounts of in-cage reactions. In order to explain this one needs to recognize that all possible reactions following cage-escape of the intermediates formed either homolytically or heterolytically, yield acid while one of the two possible in-cage reactions yields starting materials and no acid (Scheme 6-1). The low Φ_{acid} found for **6-1** and **6-2** in viscous media suggest that $Ar^{\bullet}$ and $Ar_2S^{\bullet+}$ undergo in-cage recombination to preferentially yield starting materials instead of (phenylthio)biphenyls and acid (Scheme 6-6) whereas $Ph^{\bullet}$ and Ph_2S recombine to preferentially give acid and (phenylthio)biphenyl.

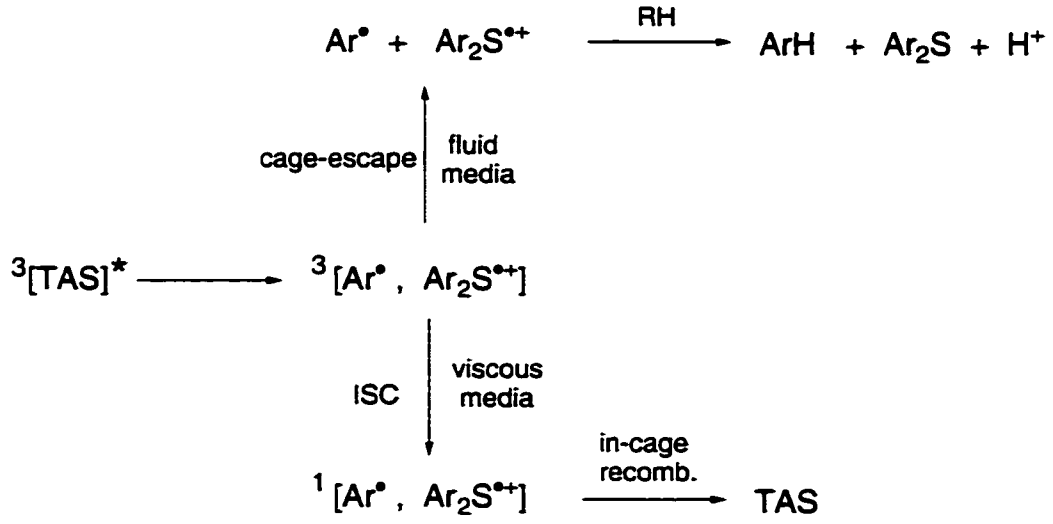

Figure 6-6. Proposed mechanism for decay of a triplet excited TAS salt.

6.3 Conclusions

Sulfonium salts which participate in intramolecular triplet energy transfer processes, as measured by increased yields of transients from out-of-cage reactions, have been prepared. Unfortunately, these compounds were not effective as PAGs due to the dominance of recombination pathways which do not yield acid. This study reveals the importance of heterolysis in the photodecomposition of sulfonium salts. It should be noted that although triplet chemistry proved unsuccessful in improving acid yields, the strategy of minimizing in-cage reactivity by sulfonium salts in order to achieve high Φ_{acid} has not been shown to be unsound.

6.4 Experimental

6.4.1 Materials

All chemicals were obtained from Aldrich except for: TPS triflate and di-*tert*-butylphenyl iodonium triflate which were obtained from Shipley Co. and copper(II) benzoate which was obtained from Pfaltz & Bauer. Acetonitrile was an Omnisolv grade solvent obtained from VWR. All materials were used as received.

6.4.2 General Techniques

Details of the LFP system and techniques to measure Φ_{acid} using various chemical actinometers and light sources were described in Chapter 2.

6.4.3 Synthesis

6-1: 3-bromoindan-1-one was prepared in 68% yield from indan-1-one according to a literature procedure for benzylic brominations[33] and its spectroscopic properties were consistent with those appearing in the literature.[34] 4-(3-indan-1-one)-diphenyl sulfide was prepared via a procedure adapted from one for a similar compound.[35] To a solution of 3-bromoindan-1-one (0.61 g, 2.8 mmol) and diphenyl sulfide (0.48 mL, 2.8 mmol) in anhydrous methylene chloride (20 ml) was added iron(III) chloride (0.50 g, 3.1 mmol) in two portions. The red solution was stirred at 50 °C for 24 hours and washed twice with 30 mL portions of 10% HCl, twice with 30 mL portions of water, twice with 30 mL portions of 5% NaOH, twice with 30 mL portions of water, and finally with 30 mL of brine. Drying over $MgSO_4$ and removal of solvent yielded a red oil which was purified by flash column chromatography (hexanes/ether, 80:20) to yield the product sulfide as a yellow oil (0.2 g, 22%). ^1H NMR (200 MHz, $CDCl_3$) δ 2.64 (dd, 1H), 3.21 (dd, 1H), 4.56 (dd, 1H), 7.01-7.81 (m, 13H). MS (EI) m/z (%) 316.1 (100), 207.1 (71), 178.1 (47), 131.0 (4, m-149), 103.1

(6), 77.0 (8). **6-1** was obtained in 72% yield by the copper-catalyzed reaction of di-*tert*-butylphenyl iodonium triflate with 4-(3-indan-1-one)-diphenyl sulfide.[9,31] ^{1}H NMR (200 MHz, DMSO-d_6) δ 1.31 (s, 9H), 2.67 (dd, 1H), 3.25 (dd, 1H), 4.85 (dd, 1H), 7.25-7.90 (m, 17H). ^{13}C NMR (300 MHz, DEPT, DMSO-d_6) δ 31.0 (CH_3), 43.7 (CH), 45.9 (CH_2), 123.5, 127.3, 128.8, 128.9, 131.1, 131.5, 131.6, 131.8, 132.2, 134.7, 135.8 (CH). MS (ESI) m/z (%) 1047.1 (0.1, 2m-149), 449.2 (100, m-149), 319.2 (30). IR (neat) 1711 cm^{-1} (C=O).

6-2: The sulfide precursor to **6-2** was prepared via a procedure adapted from one for a similar compound.[36] To a solution of diphenyl sulfide (3.85 mL, 23 mmol) and aluminum chloride (4.92 g, 37 mmol) in 50 mL of hexane was added 5-methyl-5-hexen-2-one (0.6 mL, 4.6 mmol) slowly over 5 minutes. The resulting brown mixture was stirred at room temperature for 18 hours then cooled in an ice-bath and decomposed with water (50 mL). The organic layer was separated, washed with water (3 x 50 mL), dried and the solvent removed. The resulting oil was purified by flash column chromatography (hexanes/ether, 80:20) to yield the product as a colourless oil (0.45 g, 33%). ^{1}H NMR (200 MHz, $CDCl_3$) δ 1.28 (s, 6H), 1.87 (m, 2H), 2.03 (s, 3H), 2.16 (m, 2H), 7.18-7.34 (m, 9H). MS (EI) m/z (%) 298 (30), 227 (100), 186 (11), 117 (9). **6-2** was obtained in 14% yield by the copper-catalyzed reaction of di-*tert*-butylphenyl iodonium triflate with the aforementioned sulfide.[9,31] ^{1}H NMR (200 MHz, DMSO-d_6) δ 1.28 (s, 6H), 1.31 (s, 9H), 1.83 (m, 2H), 2.00 (s, 3H), 2.19 (m, 2H), 7.70-7.85 (m, 13H). ^{13}C NMR (300 MHz, DEPT, DMSO-d_6) δ 28.5, 30.2, 31.1 (CH_3), 37.1, 39.0 (CH_2), 128.9, 129.4, 131.4, 131.5, 131.6, 131.8, 134.6 (CH). MS (ESI) m/z (%) 993.4 (0.4), 695.0 (0.8), 431.2 (100, m-149), 114.9 (68.0). IR (neat) 1712 cm^{-1} (C=O).

6.5 References

(1) Crivello, J. V., *UV Curing: Science and Technology* in ; Pappas, S. P., Ed.; Technology Marketing Corporation: Stanford, 1978, 23.

(2) Pappas, S. P. *Radiat. Curing* **1981**, *8*, 28.

(3) Ito, H.; Willson, C. G. *Polym. Eng. Sci.* **1983**, *23*, 1012.

(4) Ito, H.; Willson, C. G., *Polymers in Electronics* in *ACS Symposium Series 242 American Chemical Society* ; Davidson, T., Ed.: Washington, DC, 1984, pp 11-23.

(5) Knapczyk, J. W.; McEwen, W. E. *J. Am. Chem. Soc.* **1969**, *91*, 145.

(6) Knapczyk, J. W.; McEwen, W. E. *J. Org. Chem.* **1970**, *35*, 2539.

(7) Pappas, S. P.; Gatechair, L. R.; Pappas, B. C. *J. Photochem.* **1981**, *17*, 120.

(8) Pappas, S. P. *J. Imaging Technology* **1985**, *11*, 146-157 and references therein.

(9) Dektar, J. L.; Hacker, N. P. *J. Am. Chem. Soc.* **1990**, *112*, 6004.

(10) Welsh, K. M.; Dektar, J. L.; Garcia-Garibaya, M. A.; Hacker, N. P.; Turro, N. J. *J. Org. Chem.* **1992**, *57*, 4179.

(11) Iu, K.-K.; Kuczynski, J.; Fuerniss, S. J.; Thomas, J. K. *J. Am. Chem. Soc.* **1992**, *114*, 4871.

(12) Tagawa, S.; Nagahara, S.; Iwamoto, T.; Wakita, M.; Kozawa, T.; Yamammoto, Y.; Werst, D.; Trifunac, A. D. *Proc. SPIE* **2000**, *3999*, 204.

(13) G. Pohlers: Personal communication.

(14) Pappas, S. P.; Pappas, B. C.; Gatechair, L. R.; Schnabel, W. *J. Polym. Sci., Polym. Chem. Ed.* **1984**, *22*, 69.

(15) Turro, N. J.; Weed, G. C. *J. Am.Chem. Soc.* **1983**, *105*, 1861, and references therein.

(16) Pryor, W. A.; Smith, K. *J. Am. Chem. Soc.* **1970**, *92*, 5403.

(17) Hacker, N. P. *ACS Symp. Ser.* **1994**, *579*, 93, and references therein.

(18) Dektar, J. L.; Hacker, N. P. *J. Org. Chem.* **1988**, *53*, 1833.

(19) Turro, N. J. *Pure & Appl. Chem.* **1981**, *53*, 259.

(20) Ferris, K. F.; Franz, J. A.; Sosa, C. P. *Chem. Phys. Lett.* **1991**, *185*, 251.

(21) Pappas, S.; Jilek, J. H. *Photogr. Sci. Eng.* **1979**, *23*, 140.

(22) Turro, N. J. *Modern Molecular Photochemistry*; University Science Books: Mill Valley, 1991.

(23) Gilbert, A.; Baggott, J. *Essentials of Molecular Photochemistry*; CRC Press, Inc,: Boca Raton, 1991.

(24) Pappas, S. P.; Pappas, B. C.; Gatechair, L. R.; Jilek, J. H.; Schnabel, W. *Polym. Photochem.* **1984**, *5*, 1.

(25) Dexter, D. L. *J. Chem. Phys.* **1953**, *21*, 836.

(26) Wagner, P. J.; Klan, P. *J. Am. Chem. Soc.* **1999**, *121*, 9626, and references therein.

(27) Levin, P. P.; Khudyakov, I. V.; Kuzmin, V. A. *J. Phys. Chem.* **1989**, *93*, 208.

(28) Autrey, T.; Devadoss, C.; Sauerwein, B.; Franz, J. A.; Schuster, G. B. *J. Phys. Chem.* **1995**, *99*, 869.

(29) A preliminary experiment was performed in order to ensure that acid is generated from the triplet sensitized pathway. An acetonitrile solution of 1-indanone (abs > 1.5) and TPS triflate (0.01 M) was irradiated at 300 nm, a wavelength at which TPS triflate does not absorb. Acid generation was observed although no comment could be made about efficiency.

(30) Some of these experiments were performed with the aid of Anne-Marie Boulanger, an undergraduate student at the University of Ottawa, while she worked in our labs for 4 months.

(31) Crivello, J. V.; Lam, J. H. W. *J. Org. Chem.* **1977**, *43*, 3055.

(32) Murov, S. L. *Handbook of Photochemistry*; Marcel Dekker, Inc.: New York, 1977.

(33) Dubey, S. K.; Kumar, S. *J. Org. Chem.* **1986**, *51*, 3407.

(34) Brown, R. F. C. *Aust. J. Chem.* **1987**, *40*, 1687.

(35) Carpino, L. A.; Gao, H.-S.; Ti, G.-S.; Segev, D. *J. Org. Chem.* **1989**, *54*, 5887.

(36) Kretchmer, R. A.; McCloskey, M. B. *J. Org. Chem.* **1972**, *37*, 1989.

7. Claims to Original Research & Future Directions

7.1 Claims to Original Research

7.1.1 The Use of Dyes as Acid Sensors

Acid sensitive dyes were used extensively over the course of this work for the purposes of studying acid mobility in polymer films and acid generating efficiencies of PAGs.

i) The fluorescent properties of the dye Coumarin 1 were shown to be ideal for studying the diffusion of photogenerated acid in imaged polymer films.

ii) Conditions for determining the relative Φ_{acid} for PAGs upon both laser and lamp irradiation were developed and used extensively.

iii) An *in situ* technique for measuring acid desorption from thin polymer films was developed. This technique allowed for determination of half-lives for a variety of acids in polymer films as well as identification of the main factors which control acid desorption from these films.

7.1.2 Photoacid Generation

Many different PAGs were studied for the purpose of evaluating their potential for use in actual photolithographic applications. This work involved elucidating the mechanism for photoacid generation of a variety of molecules as well as developing novel molecules as PAG candidates.

iv) Photoacid generation by di-*p*-toluene-α-disulfone and 1,2-*di*(arylsulfonyl)hydrazines was found to occur primarily via reaction of arylsulfonyl radicals with oxygen.

v) The electron transfer reactions of N-heteroaromatic salts were exploited for the purposes of acid generation.

vi) The intermediacy of encounter complexes and the charge-transfer nature of the reaction between photoexcited aromatic ketones, xanthone and 1-azaxanthone, with polyalkylbenzenes were established.

vii) The efficiencies of ketyl radical formation from a variety of photochemically induced uni- and bimolecular reactions were determined.

viii) The photochemical generation of ketyl radicals and subsequent oxidation by 1,4-bipyridiniums was used as a photoacid generating system.

ix) Triarylsulfonium salts which participate in intramolecular triplet energy transfer upon photoexcitation were designed, prepared and evaluated as PAGs.

x) It was established that inducing triplet reactivity in triarylsulfonium salt photochemistry is not an effective means to increase cage-escape reactions in viscous media.

7.2 Future Directions

7.2.1 Photoacid Generator Photochemistry below 200 nm

In order to remain relevant, the direction of this project must follow that of the microelectronics industry, i.e., to shorter wavelengths. With a recently acquired excimer laser, capable of emitting 193 and 157 nm light, this lab is poised to explore PAG photochemistry at these wavelengths. This will entail some general shifts in the way experiments can be conducted because no solvent is sufficiently transparent to 157 nm light to allow its use in photochemical studies. In order to work at 157 nm, experiments must be conducted in thin polymer films whose short pathlength will allow for excitation of the PAG. Quantifiying acid generating efficiencies under these conditions will involve extracting the films after irradiation with a dye containing solution. The performance of transient studies via LFP in thin films has not been done extensively in our labs but will be required for detailed mechanistic PAG studies at 157 nm. Although photochemical experiments at 193 and 157 nm pose practical challenges they also present the opportunity to study new PAGs which have been designed for use at these new wavelengths. There may also be the opportunity to explore the wavelength dependance of PAG photochemistry which may result from the use of such high energy radiation.

7.2.2 Acid Desorption from Polymer Films

Any appetite in this lab for knowledge about acid desorption from polymer films was entirely sated by the studies described in this thesis. That being said, this technique could still prove useful for screening the new polymers that are being developed for 193 and 157 nm lithography. Realistically, this technique is not a primary tool for evaluation of these new polymers because these materials must meet many other criteria related to image development before issues of acid diffusion and desorption need be considered. However, if a situation arose in which

a certain polymer is giving odd results when imaged, acid desorption studies could reveal if this is related to acid mobility.

The fate of this work may lay in the hands of our collaborators at Shipley Co., manufacturers of resist materials, who have become very interested in the methodology, if not the actual technique. Specifically, the use of an acid sensitive dye in a polymer film can have applications other than studying acid mobility. Current methods for evaluating the thermal stability of PAGs involves differential scanning calorimetry and thermal gravimetric analysis. Data obtained from these techniques can be misleading because they are obtained in the absence of any polymer-PAG interactions which tend to lower thermal stability of a PAG in an actual resist. The oven used for the acid desorption studies is a perfect tool for monitoring the *in situ* thermal decomposition of PAGs, assuming decomposition yields acid. In a similar way, the oven can be employed to evaluate thermal acid generators, which are molecules used in certain photolithographic applications. In a technique more closely related to the acid desorption studies, the oven can be used to explore the process of base desorption from resist films.

7.2.3 Diaryl-α-disulfones and 1,2-di(Arylsulfonyl)hydrazines

Based on the studies on *di-p*-toluene-α-disulfone presented here, most notably their performance at 193 nm, these molecules show some promise for actual use in a resist formulation. However, progress to this end has been hampered by its relative insolubility in typical resist formulations. Work directed towards preparing more soluble diaryl-α-disulfones is currently underway. The use of both diaryl-α-disulfones and 1,2-*di*(arylsulfonyl)hydrazines in actual resists will provide an opportunity to see if the reaction between arylsulfonyl radicals and O_2 to generate sulfonic acids can function effectively in a resist during normal imaging conditions. This will be particularly interesting at 193 and 157 nm, both of which are

absorbed by O_2, necessitating an O_2 free chamber in which to perform resist exposures.

7.2.4 N-Heteroaromatic Salts as PAGs

As mentioned in Section 5.3.2.2.2, the natural progression of the work involving N-heteroaromatic salts as oxidizing agents, led to the idea of using onium salts as oxidizing agents of electron rich radicals for the purposes of acid generation. Unfortunately, this area has already been explored by other researchers in the context of initiators for cationic polymerization and does not appear to be an area that requires more research. One area of this work which still shows promise is the intramolecular photoinduced electron transfer in 1,4-bipyridiniums containing alcohol tethers. Preparation of new molecules with different lengths of tether and which generate different ketyl radicals may result in an improvement in acid generating efficiency. Additionally, studies in aqueous systems, in which high yields of the 1,4-bipyridinium radical cation have been reported, as well as organic solvents, which will solvate the reactive intermediates more strongly than the dicationic starting materials, may reveal conditions under which these systems are more effective PAGs. Studies in aqueous systems are particularly interesting given that they may lead to a more environmentally friendly resist. If any of these systems prove to be effective PAGs, it may be worthwhile to study the analogous reactions of S-heteroaromatic salts because they do not have the issue of photogenerating a base along with the acid.

7.2.5 Sulfonium Salt Photochemistry

Although inducing triplet photochemistry in sulfonium salts proved to be ineffective for achieving high yields of acid generation, alternative means to decrease the recombination reactions of the intermediates involved in the photochemistry of sulfonium salts could yield an effective PAG. The preparation of

sulfonium salts from certain cyclic sulfides may yield molecules which, after bond fragmentation, either adopt conformations which do not allow for recombination or undergo a molecular rearrangement which also does not allow recombination. This is considered to be the most promising area for future work of all those discussed.

7.3 Publications

7.3.1 Publications Resulting From Research Presented in this Thesis

(1) Coenjarts, C.; Cameron, J.; Deschamps, N.; Hambly, D.; Pohlers, G.; Scaiano, J. C.; Sinta, R.; Virdee, S.; Zampini, A. Exploratory Approaches to the Study of Acid Diffusion and Acid Loss from Polymer Films using Absorption and Fluorescence Spectroscopy. *Proc. SPIE.* **1999**, *3678*, 1062-1073.

(2) Coenjarts, C.; Cameron, J. F.; Pohlers, G.; Scaiano, J. C.; Zampini, A. An *In Situ* Method For Measuring Acid Loss from Polymer Films. *J. Appl. Polym. Sci.* **2000**, *78*, 1897-1905.

(3) Coenjarts, C.; Scaiano, J. C. Reaction Pathways Involved in the Quenching of the Photoactivated Aromatic Ketones Xanthone and 1-Azaxanthone by Polyalkylbenzenes. *J. Am. Chem. Soc.* **2000**, *122*, 3635-3641.

(4) Coenjarts, C.; Ortica, F.; Scaiano, J. C.; Liu, H.; Pohlers, G.; Cameron, J.; Zampini, A. Mechanistic Similarities in the Photochemistry of Two Classes of Photoacid Generators: A Laser Flash Photolytic Study. *Proc. SPIE.* **2000**, *3999*, 609-618.

(5) Ortica, F.; Coenjarts, C.; Scaiano, J. C.; Liu, H.; Pohlers, G.; Cameron, J. F. Mechanism of Reaction and Photoacid Generation of N-Oxysuccinimidoarylsulfonate PAGs: a Laser Flash Photolytic Study. *Chem. Mater.* **2001**, *13*, 2297-2304.

(6) Coenjarts, C.; Ortica, F.; Cameron, J.; Pohlers, G.; Zampini, A.; Desilets, D.; Liu, H.; Scaiano, J. C. Mechanism of Reaction and Photoacid Generation of 1,2-di(Arylsulfonyl)hydrazine PAGs: a Laser Flash Photolytic Study. *Chem. Mater.* **2001**, *13*, 2305-2312.

(7) Coenjarts, C.; Boulanger, A.-M.; Cameron, J.; Pohlers, G.; Scaiano, J. C. Intramolecular Triplet Energy Transfer in Sulfonium Salt Photochemistry. *Manuscript in Preparation.*

(8) Coenjarts, C.; Mickelsons, L.; Cameron, J.; Pohlers, G.; Scaiano, J. C. Photoacid Generation via Electron Transfer Reactions of N-Heteroaromatic Salts. *Manuscript in Preparation.*

7.3.2 Other Publication

(9) Ortica, F.; Scaiano, J. C.; Pohlers, G.; Cameron, J. F.; Zampini, A. Laser Flash Photolysis of Two Aromatic N-Oxyimidosulfonate Photoacid Generators. *Chem. Mater.* **2000**, *12*, 414-420